2013-05-01

Understanding Neural Networks in Awake Rat by Resting-State Functional MRI: A Dissertation

Zhifeng Liang
University of Massachusetts Medical School

UNDERSTANDING NEURAL NETWORKS IN AWAKE RAT

BY RESTING-STATE FUNCTIONAL MRI

A Dissertation Presented

By

Zhifeng Liang

Submitted to the Faculty of the
University of Massachusetts Graduate School of Biomedical Sciences, Worcester
in partial fulfillment of the requirements for the degree of

DOCTOR OF PHILOSOPHY

May 1st, 2013

Program in Neuroscience

UNDERSTANDING NEURAL NETWORKS IN AWAKE RAT

BY RESTING-STATE FUNCTIONAL MRI

A Dissertation Presented
By

Zhifeng Liang

The signatures of the Dissertation Defense Committee signify
completion and approval as to style and content of the Dissertation

Nanyin Zhang, Ph.D., Thesis Advisor

Matt Gounis, Ph.D., Member of Committee

Marc Kaufman, Ph.D., Member of Committee

David Kennedy, Ph.D., Member of Committee

Andrew Tapper, Ph.D., Member of Committee

The signature of the Chair of the Committee signifies that the written dissertation meets
the requirements of the Dissertation Committee

Constance Moore, Ph.D., Chair of Committee

The signature of the Dean of the Graduate School of Biomedical Sciences signifies
that the student has met all graduation requirements of the school.

Anthony Carruthers, Ph.D.,
Dean of the Graduate School of Biomedical Sciences

Program in Neuroscience
May 1st, 2013

This dissertation is dedicated to my wife Jinli Ling, my father Mengjin Liang and my mother Yajun Zhu for their love and support.

ACKNOWLEDGEMENTS

First and foremost I would like to thank Dr. Nanyin Zhang for his guidance during my PhD study. I have tremendously benefited from Dr. Zhang's scientific knowledge, technical expertise, research methodology and so much more in the past five years. The research presented in this dissertation would be impossible without his mentorship. I'd also like to thank Dr. Jean King for her kind support to me as well as her leadership in CCNI. It was Dr. King who first introduced me to the research area of neuroimaging in Jan 2009 when I started my first-year rotation in CCNI and continued her support throughout my PhD study.

During my years at CCNI, I have received generous help and support from my current and former colleagues. In particular, Dr. Wei Huang and Dr. Pallavi Rane helped and taught me a lot especially when I first joined CCNI. Other colleagues who offer their help include Ms. Meghan Heffernan and Ms. Kelly Tam for their great research support, Ms Yvette Gonzalez for her administrative support, Dr. Elif Sikoglu, Dr. Ana Liso, Ms. Suzanne Czerniak, Mr. Ryan Rogan, Mr. Zhiwei Ma and Dr. Meina Quan.

Finally I'd like to sincerely thank my dissertation committee members: Dr. Constance Moore, Dr. David Kennedy, Dr. Matt Gounis, Dr. Andrew Tapper and Dr. Marc Kaufman.

ABSTRACT

Resting-state functional magnetic resonance imaging (rs-fMRI) is a non-invasive neuroimaging technique that utilizes spontaneous low-frequency fluctuations of blood-oxygenation-level dependent (BOLD) signals to examine resting-state functional connectivity in the brain. In the past two decades, this technique has been increasingly utilized to investigate properties of large-scale functional neural networks as well as their alterations in various cognitive and disease states. However, much less is known about large-scale functional neural networks of the rodent brain, particularly in the awake state. Therefore, we attempted to unveil local and global functional connectivity in awake rat through a combination of seed-based analysis, independent component analysis and graph-theory analysis. In the current studies, we revealed elementary local networks and their global organization in the awake rat brain. We further systematically compared the functional neural networks in awake and anesthetized states, revealing that the rat brain was locally reorganized while maintaining global topological properties from awake to anesthetized states. Furthermore, specific neural circuitries of the rat brain were examined using resting-state fMRI. First anticorrelated functional connectivity between infralimbic cortex and amygdala were found to be evident with different preprocessing methods (global signal regression, regression of ventricular and white matter signal and no signal regression). Secondly the thalamocortical connectivity was mapped for individual thalamic groups, revealing group-specific functional cortical connections that were generally consistent with known anatomical connections in rat. In conclusion, large-scale neural networks can be robustly and reliably studied using rs-fMRI in awake rat,

and with this technique we established a baseline of local and global neural networks in the awake rat brain as well as their alterations in the anesthetized condition.

TABLE OF CONTENTS

LIST OF TABLES

LIST OF FIGURES

The following figures were modified from journals with permissions:

Figure Number	Publisher	License Number
Fig. 4.7a	John Wiley and Sons	3117140305954
Fig. 4.7b	John Wiley and Sons	3117141139970
Fig. 4.7c	John Wiley and Sons	3117140857681

PREFACE

Part of this dissertation (Chapter I, II, III) has been published as listed below:

1. Liang Z, King J, Zhang N. Intrinsic organization of the anesthetized brain. Journal of Neuroscience. 2012 Jul 25;32(30):10183-91.

2. Liang Z, King J, Zhang N. Anticorrelated resting-state functional connectivity in awake rat brain. Neuroimage. 2012 Jan 16;59(2):1190-9.

3. Liang Z, King J, Zhang N. Uncovering intrinsic Connectional Architecture of functional networks in awake rat brain. Journal of Neuroscience. 2011 Mar 9;31(10):3776-83.

Chapter IV is under revision.

INTRODUCTION

Neural networks and brain mapping

The curiosity to understand ourselves, particularly how our "mind" or "soul" works, is perhaps unique to human nature. From the beginning of human civilizations, philosophers questioned where the "soul" is located, and organs like heart and brain were among the candidates. Over the course of history, the brain became the more plausible candidate for that function. However, the "neural science" was virtually nonexistent until the late 1800s when Camillo Golgi and Santiago Ramón y Cajal observed the first detailed neurons in the brain and the *neuron doctrine* was established.

To understand the relationship between the brain and consciousness, perception and behaviors, it was debated in the early days of neuroscience that whether brain functions were localized in specialized brain regions (localism) or relied on integration of the whole brain (holism). With the advancement of neuroscience, it is apparent now that both extreme localism and holism are inaccurate and scientific facts are perhaps somewhere between. The brain is a formidably complex network of billions of neurons, and most brain functions are carried out by the interaction among several specialized regions, each region in turn comprising of millions or billions of interacting neurons. Therefore, in large brains (such as mammals'), there are neural networks at multiple spatial scales, from local inter-neuronal circuitries (~μm) to macroscopic inter-regional whole-brain networks (~cm). It is the challenge of neuroscience to reveal the properties and functions of these neural networks, and eventually to bridge the gap between the brain and behaviors.

One approach of understanding neural networks is to examine how basic units (neurons, cortical columns or larger neural assemblies) are physically connected. For example, the anatomical neural network of nematode *C. elegans*, consisting of 302 neurons and about 5000 synapses, was reconstructed by electron microscope more than two decades ago (White et al., 1986).Although the success of such mapping is currently limited to the complexity level of *C. elegans*, this approach is being actively pursued in rodent or even human brains with more advanced imaging, genetics and computational methods (Lichtman et al., 2008; Mikula et al., 2012).Together with techniques at larger spatial scales like tracing methods and diffusion tensor imaging (DTI), this type of research can be categorized as studying anatomical neural networks of different spatial scales.

However, it is clear that only knowing the physical connections among neurons or brain regions is not sufficient to understand the brain, as neural networks are inherently dynamic. Therefore, it is crucial to examine the functional relationship among different spatial scales (neurons, neural assemblies or brain regions), or the functional neural networks. At the microscopic level, advancements in electrophysiology, optical imaging, genetics and molecular biology have made it possible to explore the collective dynamics and organizing principles of neuronal networks. For example, local neuronal network of layer 5 pyramidal neurons in rat visual cortex was shown to have highly nonrandom synaptic connectivity, characterized by more bidirectional connections and higher degree of clustering than random networks (Song et al., 2005). Combined with experimental data, theoretical neuroscience has also made significant progress in reconstructing and explaining the dynamics of neuronal networks (Vogels et al., 2005).

However, the brain is massive, consisting of many billions of neurons. It is impossible to formulate or predict repertoires of dynamic behaviors of large-scale neural networks with only the properties of local neuronal network. The emergence of blood-oxygenation-level-dependent (BOLD) functional magnetic resonance imaging (fMRI) more than two decades ago (Ogawa et al., 1990b; Ogawa et al., 1990a; Bandettini et al., 1992; Kwong et al., 1992; Ogawa et al., 1992), has greatly advanced the studies on macroscopic neural networks, with the latest variant of resting-state functional magnetic resonance imaging (rs-fMRI) shifting the paradigm of brain mapping.

The notion of mapping brain activity is not new in the history of neuroscience. More than a century ago in his *The Principles of Psychology* William James mentioned an experiment that measured cerebral blood flow changes when a subject lay on a carefully balanced table and underwent cognitive tasks (Buxton, 2002). This paradigm is unlikely to work based on our current knowledge, but the idea behind this experiment proposed the crucial relationship between local neural activity and blood flow, later extensively studied as part of neurovascular coupling. In the pre-fMRI era, the mainstay of functional neuroimaging was positron emission tomography (PET) which is still used today for its unique features. In neuroimaging with PET, biologically active molecules are labeled with radioactive isotopes and the distribution of those tracers can be mapped in three dimensions. However, due to its radioactive nature, relatively poor spatial and temporal resolution, the popularity of PET was soon bypassed by the relative newcomer, fMRI. The development that lead to fMRI is a truly amazing chain of scientific discoveries. Perhaps few would imagine the physical phenomenon of nuclear magnetic resonance (NMR) could one day lead to the imaging of brain activity when Purcell and

Bloch laid the ground work for NMR in 1946 (Bloch, 1946; Purcell et al., 1946). After being widely used in analytic chemistry, the principles of NMR soon were used to develop the imaging technique of MRI (Lauterbur, 1973).

However, structural or anatomical images of MRI can only reveal structural neural networks at the macroscopic level. Thus efforts were made to reveal the "working" brain, and lead to the first functional human brain mapping experiment using MRI in 1991 which used gadolinium-DTPA as a contrast agent and reported increase of cerebral blood volume (CBV) in primary visual cortex during a visual task (Belliveau et al., 1991). However, a more significant breakthrough was the discovery of the BOLD contrast in the brain (Ogawa et al., 1990b; Ogawa et al., 1990a). It was long known that the magnetic property of hemoglobin depends on the oxygenation state of its heme groups. The weakly diamagnetic oxyhemoglobin turns to paramagnetic deoxyhemoglobin when it loses oxygen (Pauling and Coryell, 1936). The paramagnetic deoxyhemoglobin distorts the microscopic local field and creates phase dispersion of nearby proton spins, thus generated the observation that transverse relaxation time (T_2) of blood water was oxygenation dependent (Thulborn et al., 1982). The key finding of Ogawa et al. was that the signal decrease due to lower oxygenation level (high deoxyhemoglobin concentration) could also be seen not only in intravascular space, but also in extravasular space, indicating that BOLD contrast could be used to detect the oxygenation level in the brain tissue beyond blood vessels. Soon several studies reported similar localized BOLD signal increases in the human brain within a very short period of time (Bandettini et al., 1992; Kwong et al., 1992; Ogawa et al., 1992).

However, as its name suggests, the BOLD effect is directly dependent on blood oxygenation (the amount of deoxyhemoglobin), not neural activity. Thus, besides the magnetic properties of (de)oxyhemoglobin, neurovascular coupling is another vital property of the brain that leads to the success of fMRI. Physiologically, the BOLD effect is known to depend on the three factors: cerebral blood volume (CBV), cerebral blood flow (CBF) and cerebral metabolic rate of oxygen ($CMRO_2$). Therefore, how those three factors respond to neural activation determines the neural basis of BOLD effect. It is relatively well known that CBF increases substantially in activated brain regions (e.g.,(Fox and Raichle, 1986), which brings more oxygen and, in turn, less deoxyhemoglobin (higher BOLD signal). In the same time, increased CBV and $CMRO_2$ have the opposite effect, but the amplitudes of those increases of CBV and $CMRO_2$ are far less than that of CBF. Therefore, the net effect of those three factors is increased BOLD signal in activated brain regions. The detailed mechanism that underlies the neural activity and those three physiological quantities is still under active research, and the quantitative relationship between those three physiological quantities and BOLD signal is still not well understood. However, as Ogawa recently wrote, "Nature has provided quite a few very fortunate situations for BOLD (or vascular)-based fMRI"(Ogawa, 2012).

Resting-state fMRI: techniques

The great success of task-based fMRI has led to extensive mapping of localized brain activation in response to various stimuli or tasks, underscoring the specialization of the brain. However, as mentioned earlier, the brain is naturally a massive network and it

is essential to study neural networks of interacting brain regions. The advent of resting-state fMRI provided a convenient tool for studying large-scale neural networks and thus revolutionized the paradigms of fMRI and neuroscience research.

Biswal et al. first reported spontaneous low frequency (<0.1Hz) fluctuation in BOLD time course during rest, and these low frequency fluctuations (LFF) gave rise to significant correlation between bilateral motor cortex (Biswal et al., 1995). This work stemmed from earlier efforts studying noise structure in the fMRI signal (Biswal et al., 1992; Jezzard et al., 1992; Weisskoff et al., 1992; Biswal et al., 1994) as people realized that the BOLD fMRI signal was very noisy and the amplitude of BOLD increase due to neural activation was comparable to that of noise. Spectral analysis of BOLD time courses during rest revealed peaks at heart and respiratory frequencies as expected. However, the amplitude of BOLD signals at low frequencies (<0.1Hz) was also very prominent but it was at the time poorly understood. Biswal and colleagues found those low frequency fluctuations led to significant correlation between bilateral motor cortex, which was considered as "functional connectivity". However, this finding was not well received, perhaps due to lack of evidence supporting the neural basis of this resting state functional connectivity as well as the difficulty of paradigm shifting from task based to resting state.

The first evidence of the neural origin of low frequency fluctuation, albeit indirect, came from the hypercapnia experiment when human subjects inhaled 5% CO_2 during fMRI sessions (Biswal et al., 1997a). Hypercapnia was frequently used to disrupt the association between cerebral blood flow and brain metabolism as it increases blood flow significantly but not metabolism. It was found that hypercapnia reduced the amplitude of

low frequency fluctuations and the functional connectivity, indicating this resting state connectivity phenomenon was not entirely vascular in origin, but rather had a neural basis. If this phenomenon was entirely vascular origin, the disassociation between cerebral blood flow and brain metabolism by hypercapnia was less likely to significantly lower the functional connectivity. Many more studies followed and supported the hypothesis of neural origin of resting-state functional connectivity, utilizing different approaches. One major category of indirect evidence was to vary neurobiological relevant factors such as anesthetic depth (Lu et al., 2007), lesion of corpus callosum (Quigley et al., 2003), limb deafferentation (Pawela et al., 2010)) and corresponding changes of functional connectivity were observed. Another line of indirect evidence came from the observations of similar spatial patterns between activated networks during task and functional connectivity networks during rest, which was first reported in the very early days of resting state fMRI (Biswal et al., 1995; Biswal et al., 1997b). Those similarities indicated that functional clusters identified in resting-state functional connectivity might function as elementary units in both task and rest conditions.

The ultimate proof for a neural origin of resting state fluctuation and connectivity will require a thorough understanding of the relationship between neural activity and LFF of BOLD signal as well as how the large-scale neural oscillation arises from individual neurononal activity. Spontaneous fluctuations and oscillations are not unique to BOLD signals during rest, and those phenomenons are commonly observed in electrophysiological signals across various temporal and spatial scales e.g., (Leopold et al., 2003) (for a brief review, see Buzsaki and Draguhn, 2004). Therefore, it is natural to examine whether there is a relationship between BOLD fluctuation (and correlation

stemmed from those LFF) and electrophysiological measurements. Lu and colleagues first reported that functional connectivity between bilateral primary somatosensory cortex correlated with power coherence of epidural EEG in anesthetized rats, particularly in δ frequency band (Lu et al., 2007). It should be noted that in Lu et al., fMRI and EEG were conducted separately. A similarly designed study revealed close relation between EEG and BOLD signal even in burst suppression anesthesia state (Liu et al., 2011) in rat. Another rat study utilized simultaneous fMRI and local field potential (LFP) recording in similar regions of primary somatosensory cortex (Pan et al., 2011). That study indicated BOLD spontaneous fluctuation was correlated with LFP across a broad frequency range (1-100Hz) and the peak of correlation between BOLD and LFP signals occurred when BOLD signals were about 4s delayed compared to LFP signals. In a monkey study of simultaneous fMRI and intracortial recording, BOLD time courses were found to be correlated with γ band of local field potential and multi-unit activity, and this correlation was lagged for about 6s likely due to the hemodynamic response of BOLD signal (Shmuel and Leopold, 2008), although the validity of this study was later questioned (Logothetis et al., 2009). Another recent monkey study indicated that the coupling of low-frequency bands, rather than γ band, contributed more to functional connectivity (Wang et al., 2012). Human studies have also reported electrophysiological substrates of resting-state functional connectivity (Laufs et al., 2003; Mantini et al., 2007; Nir et al., 2007; Scheeringa et al., 2008), although mostly only with surface EEG recording due to the limited availablity of conducting invasive recordings such as electrocorticography (ECoG) in human subjects.

As we could learn from the discrepancies in the aforementioned studies, there are still vast unknowns about the neural mechanism of resting-state functional connectivity. Nevertheless, it is a growing consensus that resting-state functional connectivity has neural origin, if raw images are carefully processed (more on this topic later).

Resting-state neural networks can be studied at different spatial levels using a wide range of analysis techniques. However, it is important to first examine the properties of LFF as LFF is the basis for all types of resting-state neural networks. By definition, LFF only concerns signals in the low-frequency range (usually defined as <0.1 or 0.08 Hz) and several methods have been developed to assess the spatial-temporal dynamics of LFF. First, it was long discovered that spontaneous LFF has a characteristic scale-free property, which is expressed as $P \propto 1/f^{\beta}$ (P is power, f is frequency, β is the power-law exponent) (Bullmore et al., 2001). The 1/f shape was noted in the early days of resting-state fMRI according to Biswal's personal recollection (Biswal, 2012) but was not seen in his original paper (Biswal et al., 1995). This scaling property varies in different brain regions and correlates with brain glucose metabolism (He, 2011), and was recently confirmed using improved analysis methods (Ciuciu et al., 2013). Similar scale-free structure was also found in rat (Herman et al., 2011).

Secondly, the amplitude of LFF also contains information of resting-state networks, thus an index of amplitude of LFF (termed ALFF, (Zang et al., 2007)) and its closed related variation of fractional ALFF (fALFF, (Zou et al., 2008)) were developed to detect the intensity of BOLD signal fluctuations in voxels or regions of interest (ROIs). ALFF is simply the integrated sum of the square root of power in the low frequency range, while fALFF is the ratio of ALFF to that of the entire frequency range. By

calculating the ratio, fALFF was believed to improve sensitivity and specificity (Zou et al., 2008).

ALFF and fALFF reflect a local property, the (relative) amplitude of LFF, of resting-state neural networks and they do not concern any relationship with other voxels or ROIs. There are a number of available methods to extract different types of relationship information. One index, regional homogeneity (ReHo), was introduced to evaluate the homogeneity of LFF in a group of neighboring voxels (Zang et al., 2004). Mathematically, ReHo is the Kendall's coefficient of concordance, calculated from time courses of neighboring voxels. It indicates how homogenous the fluctuations of BOLD signals are in small regions, and thus can be viewed as a measure of local functional connectivity. Similarly, homogeneity can also be calculated based on coherence instead of Kendall's coefficient of concordance (Liu et al., 2010).

Although ReHo does provide information about the relation (or similarity) of a neighboring group of voxels, it is still largely a local measurement. A complementary method, seed-based functional connectivity, is able to estimate the "functional connectivity" of one particular seed region with other voxels or regions in the brain (Fox and Raichle, 2007). The common procedure is to calculate the Pearson correlation coefficients between the mean time course of the seed region and time courses of all voxels. The resulting spatial map of correlation coefficients provides the information of how strongly the seed region is "functionally connected" with other brain regions. The seed-based method was used in the first resting-state paper (Biswal et al., 1995), and it is computationally simple yet robust, making it arguably the most popular resting-state method. The major pitfalls of this method are that it requires prior knowledge to choose a

seed region, and it can only provide information regarding one particular seed region each time the analysis is run.

Another commonly used method, independent component analysis (ICA), is more data-driven and does not require defining seed regions (for a technical review, see (Hyvarinen and Oja, 2000)).The basic idea of ICA is to explore nongaussianity of original data and transform the original data into a linear combination of statistically independent (or as independent as possible) components. It was first introduced to fMRI data in the context of task-based fMRI (McKeown et al., 1998), and later was applied in many resting-state fMRI studies with various specific algorithms (e.g., (Allen et al., 2011)). In particular, the availability of group ICA methods (Calhoun et al., 2001; Beckmann and Smith, 2005; Erhardt et al., 2010) has lead to the popularity of ICA, as the original ICA method could only be applied to single subject/data, rendering it much less useful in neuroimaging studies. Because it does not require definitions of seed regions, the ICA method is not restrained by anatomical definition, which is often the case in seed-based analysis. With the ICA method, each component is a spatial map associated with coherent fluctuations within part of the brain, and some components may represent various noises and some may represent resting-state neural networks. This data-driven approach leads to a somewhat arbitrarily defined boundary between noise and "true" neural network components, although this issue could be alleviated by inspection of spatial maps and power spectrum characteristics of time courses associated with each component (Allen et al., 2011). Another potential issue is that the ICA method requires the input of the model order (the number of total components), and naturally, the spatial maps of components vary with different model orders. There are some algorithms such as

Akaike's information criterion and minimum description length criterion (Calhoun et al., 2001) with the potential ability of estimating the model order, but those algorithms are not very reliable on fMRI data. Therefore, it is still largely arbitrary to determine the model order. Depending on the model order, each individual ICA map can have small spatial coverage and be considered a local functioning unit when the model order is large, and the ICA map can have large spatial coverage and be considered a large-scale network when the model order is small. A similarly model-free, but less popular method is voxel-wise clustering based methods (e.g., (van den Heuvel et al., 2008).

The analysis methods discussed above are not able to analyze the organization and dynamics of whole-brain networks. Fortunately, graph theory has provided a theoretical framework for doing so in resting-state fMRI data (for review, see (Bullmore and Bassett, 2010). To utilize tools of graph-theory analysis, the brain needs to be parcellated into nodes (or vertices), and nodes are connected with edges (or connections). Ideally, nodes should be both coherent and independent with each other, which can be difficult to achieve in fMRI studies. In practice, nodes of functional brain images are usually defined as anatomical ROIs, functional ROIs or voxels, each with its own advantages and disadvantages. Voxel is the basic unit of images, and thus could serve as a definition of nodes. But the smoothness in the images (from the data themselves and from image processing) leads to weaker independence of each voxel with its neighboring voxels. In addition, the voxel number of a whole-brain image is fairly large (in the order of 10^4), making the subsequent analysis computationally expensive and statistical testing very difficult due to the massive multiple comparison problem for local graph metrics. If anatomical ROIs are used as nodes, the computational load can be dramatically reduced.

For example, in Automated Anatomical Labeling (AAL) template (Tzourio-Mazoyer et al., 2002), the numbers of anatomical ROIs are reduced to the order of 10^2. The drawbacks are two-fold: first, anatomical ROIs are not necessarily the basic functioning units of the brain and homogeneity within anatomical ROIs might be low; secondly, the sizes of those anatomical nodes usually vary significantly, thus larger nodes have much more voxels than small nodes. The difference of voxel numbers in anatomical nodes could lead to different signal-to-noise ratio, which could be problematic in statistical analysis. Nevertheless, anatomical parcellation is still perhaps the most frequently used method for its simplicity. Similarly, the brain can be parcellated based on functional information. This type of brain templates are generated using data-driven methods such as group ICA (Allen et al., 2011) and voxel-wise clustering (Craddock et al., 2012). Those functional templates are not constrained by anatomical information and could overcome some of the caveats of anatomical parcellation. However, as those templates are data-dependent, the applicability to other datasets might be problematic. Overall, it is not a trivial question to choose the appropriate node definition as nodes are the elementary units of a graph. Not surprisingly, empirical studies have shown that properties of networks are dependent on the brain parcellation schemes (Wang et al., 2009; Zalesky et al., 2010b). Therefore, it is critical to choose an appropriate node definition based on study purpose/hypothesis and data characteristics.

The next crucial step of graph-theoretical analysis is to determine edges of a graph. Just as there are different types of node definition, there are different ways to estimate the edges (Smith et al., 2010). The most simple and popular estimation method in resting-state fMRI is the Pearson correlation based on time courses associated with

nodes. A related method is partial correlation, which is the correlation coefficient between two time courses after controlling the impact of other time courses. Other methods of estimation include non-linear statistics such as coherence, mutual information and lag-based methods such as Granger causality. It is difficult to assess various estimation methods because the "ground truth" of functional connectivity, i.e., the existence of functional connectivity, is usually unknown. However, in a recent comprehensive simulation study, correlation-based methods were found to better detect actual connections compared to other methods in simulated data (Smith et al., 2010).

To finally establish a graph, it is often essential to remove spurious connections by thresholding graphs. One commonly used thresholding method is density thresholding. In this process, a network density is specified and all connections are ranked from strongest to weakest. Connections ranked below the percentile of the previously specified network density are eliminated (value set to zero) and all connections above that threshold are retained (value set to one). To alleviate the problem of setting a single (rather arbitrary) density value, a range of network densities can be specified according to graph properties and network metrics are summarized in that range (e.g., (Liang et al., 2012b). Another type of thresholding methods is local thresholding, as opposed to global thresholding such as density thresholding. One example of local thresholding is to combine the concepts of minimal spanning tree and *k*-nearest neighbor graph (*k*-NNG) to generate a graph with all nodes connected with highest possible connectivity (Alexander-Bloch et al., 2010). This type of local thresholding avoids the problem of disconnectedness of graphs in global thresholding, which can be problematic for calculating certain graph metrics. Naturally the other way to completely eliminate the

above problems (choice of network density and disconnectedness) is to use unthresholded weighted networks, which would require more sophisticated algorithms to compute network metrics (Rubinov and Sporns, 2011).

Finally after the graph (network) is constructed, its graph-theoretical properties can be analyzed through a wide range of network metrics (for a recent review with detailed mathematical definitions as well as interpretations, see (Rubinov and Sporns, 2010). Conceptually there are two major categories of those network metrics: global and local metrics. Global metrics concern properties of the entire network, including the global clustering coefficient, shortest path length, global efficiency and modularity.

At the global scale, the global clustering coefficient measures network segregation, while shortest path length and global efficiency measures network integration. In the context of resting-state connectivity, network segregation indicates the extent of local or specialized processing of the whole-brain network, and network integration indicates how well the whole-brain network integrate information from distributed brain regions. To achieve optimal response to internal and external stimuli, the brain has to be well balanced between segregation and integration, which leads to an important concept of small-world networks (Watts and Strogatz, 1998). A small-world network is a network with higher clustering coefficient than random networks, but still has similar shortest path length of random networks. The index of small-worldness is the ratio of normalized global clustering coefficient and shortest path length (normalized to those two metrics of random networks). Thus, by definition, a small-world network has an index of small-worldness larger than 1. Small-worldness is important as it represents

whole-brain networks balance between two opposing directions: segregation and integration.

Another important global metric is modularity (Newman, 2006). As Newman defined, "the modularity is, up to a multiplicative constant, the number of edges falling within groups minus the expected number in a equivalent network with edges placed at random" (Newman, 2006). Therefore, it measures the extent to which a network can be divided into more densely connected sub-networks (modules), compared to random networks. Functional whole-brain networks are usually modular, indicating that the brain has sub-networks that communicate more within themselves than across different sub-networks.

Another major category of network metrics, local metrics, concerns properties of individual nodes, including degree, local clustering coefficient and various types of node centrality. Degree is the number of connections a node has, and it is the most straightforward and fundamental property of a node. It reflects how well "connected" a node is. The local clustering coefficient measures how well connected a node's neighbors are, indicating the local segregation or specialization. Centrality is one type of metrics that estimate one node's importance in the whole network, including betweenness centrality, closeness centrality and eigenvector centrality (Newman, 2010). Therefore, there are many local network metrics reflecting different aspects of node properties.

Notably, some network metrics are only meaningful when compared to those of random networks. Thus it is critical to choose appropriate random networks for comparison. Usually, theoretical random networks are not comparable to empirical

networks generated from resting-state data due to differences in degree distribution. Instead, a common approach is to randomly rewire the empirical networks to generate random networks, while maintaining degree distributions of empirical networks (Rubinov and Sporns, 2010). One recent study revealed that networks constructed with correlation are inherently more clustered than corresponding random networks with same degree distribution, thus requiring a more sophisticated way to construct appropriate random networks (Zalesky et al., 2012a).

Overall, the graph theory approach is one of the most popular analysis methods for resting-state fMRI data. Utilization of graph theory allows one to examine the global and local topological properties of functional whole-brain networks, and also reveals differences of those properties under different cognitive or pathological conditions.

Besides the above popular analysis methods, there are many other methods available for resting-state fMRI data, including novel statistical approaches to address multiple comparison problems in resting-state analysis (Zalesky et al., 2010a; Zalesky et al., 2012b), and various machine learning techniques (O'Toole et al., 2007). Every technique has its advantages and disadvantages, thus careful consideration must be given to select one or several of techniques that are best suited for the purpose of a study.

One of the biggest obstacles in the early days of resting-state functional connectivity was to convince people that it has neural origin and is not an artifact of noise. It is a particularly difficult task as resting-state functional connectivity stems from low frequency spontaneous fluctuations of BOLD signals, and the BOLD fluctuations naturally have components of various noises. Therefore, it is crucial to examine the true

noise components of spontaneous fluctuation of BOLD signals, and preprocess raw data properly to remove impacts of noises as much as possible. One major category of noises is physiological noise, and it was recognized in the very first resting-state study (Biswal et al., 1995) and reviewed recently (Birn, 2012). Peaks of cardiac and respiratory frequency were apparent in frequency domain of raw resting-state BOLD time course in human studies. Those peaks were also observed in the rat (Majeed et al., 2009), although at higher frequency than human (cardiac~5 Hz, respiratory~1 Hz). The most straightforward way to reduce those physiological noises is to apply a low-pass filter (cutoff frequency 0.1 or 0.08Hz). However, with the sampling rate of most fMRI studies (~0.5Hz) and human noise peaks (cardiac~1Hz and respiratory~0.3Hz), simple low-pass filter would not work very well due to the aliasing of cardiac and respiratory signals into the lower frequency range. This aliasing problem might be less severe in rodent studies as cardiac and respiratory frequencies are much higher, although more studies are needed to verify that. Increasing sampling rate of fMRI without compromising spatial coverage and resolution would alleviate the above aliasing problem. However, major improvements of hardware and software for higher sampling rates are not generally available. Another approach of further reducing confounding cardiac and respiratory effect is to record heart beat and respiration and then to regress out those nuisance variables. This is an approach originally developed for task-based fMRI and later extended to resting-state fMRI (Hu et al., 1995; Glover et al., 2000). The apparent disadvantage of this approach is it requires additional measurements of physiological parameters.

Besides the direct contribution of cardiac and respiratory rhythms, these two also have indirect but still significant contributions. Arterial CO_2 level fluctuations are, in part,

dependent on breathing depth and rate, and those fluctuations are sensed by chemoreceptors in the brain and in turn regulate breathing depth and rate. This feed-back loop leads to low frequency (~0.03 Hz) fluctuations of BOLD signals (Van den Aardweg and Karemaker, 2002; Birn et al., 2006). Therefore, it would not remove all contributions of pulse and respiration if only high frequency (>0.1 or 0.08 Hz) signals are filtered. One study suggested adding end-tidal CO_2 as an additional nuisance variable could explain more variance (Chang and Glover, 2009b). End-tidal CO_2 is the maximum concentration of CO_2 at the end of an exhaled breath.

Another different route of removing physiological noise is regression of signals of "nuisance" brain regions, as those signals are believed to reflect more physiological rather than neural fluctuations. Global signal regression was initially widely used for this purpose (Fox et al., 2005). However, later it was found that global signal regression mathematically mandates the existence of negative correlation, leading to artifactual negative functional connectivity (Murphy et al., 2009). Furthermore, one study in monkeys indicated that local field potential (LFP) correlated with global BOLD signals, suggesting global signals also have neural origin (Scholvinck et al., 2010).Thus global signal regression seems to be inappropriate for the purpose of removing non-neural noise. Signals of white matter and ventricles seem to be safer nuisance regressors as BOLD fluctuations in these regions is less likely to have neural origin. In practice, signals of white matter and ventricles have been shown to increase spatial specificity of functional connectivity. One recent study used additional signals from soft tissues outside the brain as nuisance regressors (Anderson et al., 2011).

In addition to physiological factors, head motion is also known for its confounding effects in resting-state fMRI. However, its importance was only recently recognized after three independent studies reported significant and systematic effects of head motion even when motion is relatively small (Power et al., 2012; Satterthwaite et al., 2012; Van Dijk et al., 2012). For seed-based analysis, higher motion level was associated with increased short-distance connectivity and decreased long-range connectivity (Power et al., 2012; Van Dijk et al., 2012). Motion level was also found to be negatively correlated with modularity and impact ICA and ALFF results (Satterthwaite et al., 2012). Therefore, head motion could affect almost all aspects of resting-state functional connectivity and requires careful considerations, especially in studies where motion level might be related to other variables of interest. To attenuate the effect of head motion, one common approach is to regress out motion parameters. Motion parameters can be 6 translation and rotation parameters from the preprocessing step of realignment as well as their 1^{st} and 2^{nd} order time derivatives. In some cases, motion spikes are also used. One recent study indicated that this traditional approach generated heterogeneous results in a large adolescent dataset (Satterthwaite et al., 2013) depending on the motion levels of individual subjects. Other approaches include "clipping" motion spikes (Carp, 2011; Power et al., 2011; Power et al., 2012). Naturally no techniques are able to completely remove motion artifacts and it is best to always examine results with caution to see if they are motion related.

With all confounding factors in mind, the next question before resting-state fMRI can be safely applied in neuroscience research is whether functional connectivity measured with resting-state fMRI is reliable under the same conditions and in the same

subjects. Fortunately, this assumption has been explicitly examined by test-retest reliability in several studies (Shehzad et al., 2009; Zuo et al., 2010; Braun et al., 2012). These studies indicate that resting-state functional connectivity was consistent in different time points for the same subjects using seed-based analysis (Shehzad et al., 2009), ICA (Zuo et al., 2010) and graph-theory analysis (Braun et al., 2012), respectively. Together with numerous other studies reporting similar resting-state neural networks, it is widely accepted that resting-state fMRI is a reliable tool to investigate large-scale neural networks.

Conventional resting-state functional connectivity can be considered the averaged connectivity across a time period (e.g., 10-15 minutes scan time), because analysis methods like Pearson's correlation estimate one measurement of functional connectivity for the entire time period. However, it is increasingly recognized that functional connectivity is dynamic rather than static as it is well known that neural process occurs at much faster time scales (~ms). One straightforward adaptation of existing methods is to use sliding windows of relatively shorter time periods (~60s) to estimate functional connectivity. Several studies have utilized this approach in conjunction with Pearson's correlation or ICA to reveal the non-stationary property of resting-state functional connectivity (Allen et al., 2012; Hutchison et al., 2012a; Keilholz et al., 2012). Using the combinations of sliding window, ICA and clustering, Allen and colleagues showed functional connectivity of human brains across ICA time courses was time-varying and could be clustered into several distinct states (Allen et al., 2012). The seed-based correlation method revealed similar findings in both rats (Keilholz et al., 2012) and monkeys (Hutchison et al., 2012a). One disadvantage of the sliding window approach is

that noise can lead to more profound effects with much less data points. Therefore, statistical significance should be carefully determined to examine if the dynamic connectivity arises from noise or by chance (Handwerker et al., 2012).

More sophisticated methods include wavelet transform coherence. Wavelet transform coherence is based on continuous wavelet transform and can provide coherence and phase lag information of time series in both time and frequency domains (Torrence and Compo, 1998). Therefore it can be used to track the time-frequency dynamics of resting-state BOLD time courses (Chang and Glover, 2010; Liang et al., 2012a). However, the information (coherence and phase lag in time and frequency domain) extracted by this method is quite complex and therefore difficult to combine individual results. Due to the slow hemodynamic nature of BOLD signal, resting-state fMRI is unlikely to provide precise information of temporal dynamics. However, compared to the current popular analysis methods, much more improvements are expected to further investigate network dynamics on the order of seconds.

Overall, resting-state fMRI is a powerful, robust and reliable non-invasive imaging method that can be used to investigate large-scale neural networks with various analysis techniques focusing on different aspects of neural networks, when original data are carefully processed regarding confounding noises and artifacts.

Resting-state neural networks: from human to rodent

Resting-state fMRI has greatly advanced our knowledge of large-scale functional networks across several species like human, non-human primates and rodents. The

paradigm shift from mapping specific brain regions with task-based fMRI to mapping interacting brain regions with resting-state fMRI has led to more appreciation for the notion that the brain is inherently a network.

Resting-state fMRI was first developed in human, and much more studies have been conducted in humans than all other species combined. At the local network level, converging evidence from different studies and with different analysis methods (seed based, ICA and clustering) have indicated that the human brain has several robust functional systems, including default mode network (DMN), visual networks, sensorimotor networks, frontal networks, salience networks and parietal-frontal networks (van den Heuvel 2010). Among those networks, DMN is perhaps the most well characterized network. Important anatomical structures of DMN include medial prefrontal cortex, posterior cingulated cortex and precuneus. Unlike other resting-state networks, DMN has been shown to have higher neural activity during rest, characterized by higher blood flow and oxygen consumption as measured by PET during rest and increased BOLD signal during rest (compared to task) measured by fMRI (Raichle et al., 2001). Therefore, DMN is a unique network with elevated and synchronized neural activity during rest, while other resting-state networks are only synchronized. Functions of this unique network is indicated in consciousness and internal states (Raichle and Snyder, 2007) and is related to a large number of cognitive and pathological conditions, such as development and ageing, disorders of consciousness and psychiatric diseases (Buckner et al., 2008).

At the global level, the organization principles of the human brain have also been extensively studied using graph-theory analysis. Global functional network has

been found to be a small-world network in several studies (Salvador et al., 2005; Achard et al., 2006; Wang et al., 2009). As mentioned in the previous section, small-worldness is a crucial property for networks like the brain to achieve two conflicting goals: local specialization and global integration. A related network organization principle, modularity, is also evident in human whole-brain functional network (Meunier et al., 2010). Having a modular community structure indicates the human brain can be parcellated into functional modules which connect more densely within than cross modules. Those modules are largely similar to functional systems described above. Not surprisingly, these properties are found to be disrupted in many disease states (Bassett and Bullmore, 2009).

It is very interesting to examine whether the above characteristics of human resting-state neural networks are uniquely human or (in part) conserved in other species, especially in our close relatives, non-human primates, as to study the evolutionary aspect of functional neural networks. Several early studies focused in DMN in non-human primates for its assumed unique roles in internal tasks and consciousness in humans (Rilling et al., 2007; Vincent et al., 2007; Kojima et al., 2009; Mantini et al., 2011). The converging evidence from both resting-state fMRI and PET indicate non-human primates do have at least a structurally similar network of human DMN, with its function still not fully elucidated yet. Other studies indicated complex networks in monkeys across various cognitive states (Moeller et al., 2009) as well as specific networks in cingulate cortex (Hutchison et al., 2012c) and frontal eye fields (Hutchison et al., 2012b). One recent study systematically compared resting-state networks of humans and monkeys, and their results suggest that the most prominent difference between two species is frontal-parietal

networks, with no apparent topological or functional corresponding networks in monkeys (Mantini et al., 2013).

Rodents are the most widely used model animals in biomedical research. However, resting-state networks are much less explored in rodents compared to human studies, leaving a huge gap between our understandings of functional neural networks in the macroscopic and microscopic level. This is in part because anesthesia used in majority of rodent studies may affect results and interpretation of resting-state networks. Rodent resting-state fMRI studies have revealed various intrinsic properties of resting-state networks and influences of cognitive states (e.g., anesthetic depth and types).

Several studies characterized spatial-temporal characteristics of low frequency fluctuations in anesthetized rat brains (Kannurpatti et al., 2008; Majeed et al., 2009). Anesthetized rat brains showed significant low frequency fluctuations in cortex and some subcortical regions, and also exhibited similar noise peaks (cardiac and respiratory) in unfiltered spectrum. These low frequency fluctuations serve as the basis for investigating resting-state connectivity in rodents. In addition, several major resting-state functional networks were identified. The most robust networks across different cognitive states are sensory and motor related networks, such as the somatosensory network, motor network and visual network under anesthetized conditions as well as some subcortical networks (Pawela et al., 2008; Hutchison et al., 2010; Becerra et al., 2011). Additional networks were found in the awake rat brain, such as anterior cingulated/prefrontal networks (Zhang et al., 2010b; Liang et al., 2011). Two studies suggested the possible anatomical analog of default mode network (DMN) in rat, consisting of anterior cingulate cortex, retrosplenial cortex, hippocampus and other cortical regions (Upadhyay et al., 2011; Lu

et al., 2012). However, due to vast anatomical differences between human and rodent brains, it is difficult to evaluate the extent of spatial similarities. Furthermore, future PET studies will be needed to examine if this "DMN" like network in rodent has higher metabolic rate than the rest of the brain, which is the key characteristic of DMN in humans.

Because the majority of rodent resting-state fMRI research utilized various types of anesthesia or sedation, it is critical to examine the effects of anesthesia. Most anesthetic agents have vastly different and fairly complex pharmacological profiles in the central nervous system, acting as antagonists or agonists on many receptors (Alkire et al., 2008). In addition to neural effects, some anesthetic agents have vascular effects, e.g., isoflurane is a strong vasodilator. Therefore, it is expected that different anesthetic agents might differentially influence resting-state neural networks. One study compared rat resting-state networks with three anesthetic agents (α-chloralose, medetomidine and isoflurane), and found both spontaneous fluctuation of BOLD signals and resulting correlation based maps were dependent on anesthetic type (Williams et al., 2010). Another recent study indicated medetomidine was better than isoflurane regarding reliability and specificity of resting-state networks (Kalthoff et al., 2013). In addition, anesthetic depth has been shown to affect functional connectivity strength, generally with higher depth leading to weaker connectivity (Lu et al., 2007; Williams et al., 2010; Liu et al., 2011), although those studies most focused on somatosensory cortex and less is known about other networks.

However, those studies examined effects of anesthesia within various types and depths of anesthesia, missing the vital comparison with resting-state networks in the

conscious state. Thus efforts have been made to establish a resting-state fMRI paradigm in awake rat (Zhang et al., 2010b; Liang et al., 2011), and resting-state networks in isoflurance anesthetized and awake conditions have been comprehensively compared (Liang et al., 2012b). Interestingly, the organizing principles of the rat brain such as small-worldness and modularity were found to be similar between the two conditions. However, the global functional network was reorganized into different modules. Connectional strengths were also found to be differentially affected.

Rodent resting-state fMRI research also has contributed significantly to our understanding of the neural mechanism of resting-state connectivity, which is discussed in the earlier section (Lu et al., 2007; Liu et al., 2011). Other rodent studies addressed issues of physiological noise sources (Kalthoff et al., 2011), dynamic properties (Keilholz et al., 2012) and scale-free structure of low frequency fluctuations (Herman et al., 2011).

The last fifteen years or so has witnessed the huge success of resting-state fMRI from its then little recognized beginning in 1995 (Biswal et al., 1995). Tremendous advancements have been made in both method developments and applications in basic and clinical research. Through this technique, we have gained knowledge about how the brain is functionally organized in local and global networks, and how these networks are altered under various cognitive and pathological conditions. Particularly, rodent resting-state fMRI has great potential to bridge the gap between basic biomedical research and clinical imaging studies, when combined with other invasive methods (such as optogenetics) to manipulate neural activity.

CHAPTER I

Uncovering Intrinsic Connectional Architecture of Functional Networks in Awake Rat Brain

Zhifeng Liang, Jean King and Nanyin Zhang

Center for Comparative Neuroimaging, Department of Psychiatry, University of Massachusetts Medical School, Worcester, Massachusetts 01655

Abstract

Intrinsic connectional architecture of the brain is a crucial element in understanding the governing principle of brain organization. To date, enormous effort has been focused on addressing this issue in humans by combining resting-state functional magnetic resonance imaging (rsfMRI) with other techniques. However, this research area is significantly underexplored in animals, perhaps due to confounding effects of anesthetic agents used in most animal experiments on functional connectivity. To bridge this gap, we have systematically investigated the intrinsic connectional architecture in the rodent brain by using a previously established *awake animal* imaging model. First, group independent component analysis was applied to the rsfMRI data to extract elementary functional clusters of the brain. The connectional relationships between these clusters evaluated by partial correlation analysis were then used to construct a graph of whole-brain neural network. This network exhibited typical features of small-worldness and strong community structures as shown in the human brain. Finally, the whole-brain network was segregated into community structures using a graph-based analysis. The results of this work provided a functional 'atlas' of intrinsic connectional architecture of the rat brain at both intra- and inter-region levels. More importantly, the current work revealed that functional networks in rats are organized in a non-trivial manner and conserved fundamental topological properties as the human brain. Given the high psychopathological relevance of network organization of the brain, this study demonstrated the feasibility to study mechanisms and therapies of multiple neurological and psychiatric diseases through translational research.

Introduction

The effort to understand the connectional architecture of the brain has benefited tremendously from the advent of resting-state functional magnetic resonance imaging (rsfMRI). rsfMRI is a technique that non-invasively measures functional connectivity without external stimulation based on spontaneous low-frequency fluctuations of the fMRI signal (Biswal et al., 1995; Fox and Raichle, 2007). Using this technique, resting-state functional connectivity (RSFC) was consistently revealed in multiple networks of the human brain (Biswal et al., 1995; Fox et al., 2005; Greicius et al., 2007), and was altered by effects of sleep, anesthesia and ageing (Stevens et al., 2008; Horovitz et al., 2009). Recent studies have also delineated significant influences of various pathological conditions on RSFC (Greicius et al., 2007), indicating vital neurobiological and psychopathological relevance (Kennedy et al., 2006; Albert et al., 2009).

Well-documented properties of intra- and inter-regional connectivity make it extremely intriguing to extend the RSFC research at local brain regions to global brain networks. Using graph-based analysis separately identified brain networks sub-serving different functions in humans were found to topologically organize in a non-trivial manner to support efficient information processing (Wang et al., 2010). Graph theoretical approaches in rsfMRI uses anatomically or functionally defined regions of interest (ROIs) as ‘vertices’, and connectivity between ROIs as ‘edges’. These approaches have revealed that the human brain’s networks are characterized by properties of small-world topology, highly connected hub and high modularity (Bassett and Bullmore, 2009). These findings are crucial because: (i) they identified the governing principle of the network organization of the human brain; and (ii) the same methods can be used to examine

alterations of topological configuration of the brain in response to external stimulation or in different pathological conditions (Liu et al., 2008; Bassett and Bullmore, 2009). Therefore, these methods may serve as a potential biomarker of various mental disorders.

To date, the majority of studies on intrinsic connectional organization of the brain are conducted in humans. Systematic investigations of this issue in different animal models have been significantly underexplored (Vincent et al., 2007; Pawela et al., 2008; Schwarz et al., 2009), partially attributed to confounding effects of anesthetic agent used in animal studies on RSFC (Massimini et al., 2005; Lu et al., 2007; Liu et al., 2011). Consequently, it is very important to explore RSFC in *awake animal*s because it can not only provide invaluable information regarding intrinsic connectional architecture of the animal brain and its reconfiguration in response to cognitive and emotional stimuli, but also may provide a unique window to explore comparative functional anatomy between species. Moreover, understanding connectional architecture in animals will allow us to investigate multiple psychiatric and neurological diseases using translational models. Recently, we have successfully demonstrated the feasibility of mapping RSFC in awake rats (Zhang et al., 2010b) based on an *awake animal imaging model* that has been well established in our laboratory (King et al., 2005; Ferris et al., 2006). Using the same animal model here we have characterized the intrinsic network architecture in the awake rat.

Materials and Methods

Animals

Sixteen adult male Long-Evans (LE) rats (350 – 450 g for adult rats) were obtained from Charles River Laboratories. Animals were housed in Plexiglas cages (two per cage) and maintained in ambient temperature (22-24˚C) on a 12-h light:12-h dark schedule. Food and water were provided *ad libitum*. All studies were approved by IACUC Committee of the University of Massachusetts Medical School.

Acclimation procedure

All rats were acclimated to MRI restraint and noise as previously described (King et al., 2005; Ferris et al., 2006). Briefly, rats were anesthetized with isoflurane and secured in Plexiglas stereotaxic head holder using plastic ear-bars. EMLA cream was applied tropically to minimize pain of mechanical restraint. Animals were then placed into black opaque tube 'mock scanner' with tape-recorded scanner noises. Animals were acclimated for eight days, one session per day. The time for exposure was increased from 15 minutes on the first day to 90 minutes on days 6, 7 and 8 with an increment of 15 minutes per day (King et al., 2005).

Animal preparation

Under short-acting isoflurane gas the animal was fitted into a head restrainer with a built-in coil. The head was placed into the cylindrical head-holder with the canines secured over a bite bar, the nose secured with a nose clamp, and ears positioned inside the head-holder with adjustable screws fitted into lateral sleeves. The body of the animal was placed into a body restrainer that allowed unrestricted respiration. After the animal was set up, the isoflurane gas was removed and the restraining system was positioned in the magnet. Animals were fully conscious within 10-15 min.

MR experiments

All experiments were carried out on a Bruker 4.7T/40cm horizontal magnet (Oxford, UK) interfaced with a Biospec Bruker console. A dual ^{1}H radiofrequency (RF) coil configuration (Insight NeuroImaging Systems, Worcester, MA) consisting of a volume coil for exciting MRI signal and a surface coil for receiving MRI signal was used. The volume and surface coils were actively tuned and detuned to prevent mutual coil coupling.

For each session, anatomical images were acquired with a fast spin-echo sequence (RARE) with the following parameters: TR = 2125ms, RARE factor = 8, TE = 50ms, matrix size = 256×256, FOV = 3.2cm×3.2cm, slice number = 18, slice thickness = 1mm. T_2^*-weighted gradient-echo images coving the whole brain were then acquired using the echo-planar imaging (EPI) sequence with following parameters: TR = 1s, TE = 30ms, flip angle = 60°, matrix size = 64×64, FOV = 3.2cm×3.2cm, slice number=18, slice thickness = 1mm. Two hundred EPI volumes were acquired for each run, and six runs were obtained for each session. Rats were in resting state during all imaging sessions.

Pre-processing of imaging data

Imaging data was preprocessed using Medical Image Visualization and Analysis (MIVA, http://ccni.wpi.edu/), Statistical Parametric Mapping (SPM8) software (Wellcome Department of Cognitive Neurology, London, UK) and MATLAB (Mathworks, Inc., Sherborn, MA). All images were first aligned and co-registered with MIVA as previously described (Zhang et al., 2010a). After registration, all functional images were pre-processed with steps of motion correction, spatial smoothing (FWHM =

1mm), and voxel-wise linear detrending and 0.002-0.1Hz band-pass filtering. Data sets with excessive motion (>0.25 mm, 8 runs in total) were discarded, resulting in a total number of 88 runs for subsequent analysis.

Independent component analysis

Group ICA (Calhoun et al., 2001) was performed using GIFT toolbox (http://www.nitrc.org/projects/gift/). The number of components was set at 40 (Hutchison et al., 2010). The infomax algorithm was used to perform spatial ICA and independent components were scaled to z-scores. Time courses of individual components for individual scans were extracted. Among the spatial maps of all 40 components, two were located at *cerebrospinal fluid* (*CSF*) areas and were identified as artifactual components.

Direct connectivity and graph theory analysis

Time courses of 40 components were used in direct connectivity analysis. For each individual RSFC run, the partial correlation coefficient between time courses of each pair of components was calculated, conditioning on time courses of the other 38 components. This step yielded a 40×40 partial correlation matrix for each run. Partial correlation coefficients (r values) were transformed to *z scores* and then averaged across all runs and across all animals. The final partial correlation matrix was generated by transforming the averaged *z scores* back to the r values. Each element of this matrix represented the strength of direct connectivity between two components. We only focused on positive partial correlation coefficients although negative coefficients were also detected. The significance of direct connectivity was calculated by using one sample t-test and thresholded at p-value < 0.01 (n = 88, uncorrected) based on all 88 partial

correlation matrices. The two artifactual components did not show significant connections with other components, and thus were eliminated in further graph-theory analysis. As a result, a 38×38 adjacency matrix A was generated with each element a_{ij} describing the significant direct connection between each two components based on the p-value:

$$a_{ij} = \begin{cases} 1, & \text{if compoent i and j are conncted (i. e. p} < 0.01) \\ 0, & \text{otherwise} \end{cases}$$

Based on this adjacency matrix, the community structure of the rat brain was obtained by using the spectral partitioning method (Newman, 2006). Modularity Q is defined as follows:

$$Q = \frac{1}{4m}\sum_{ij}\left(a_{ij} - \frac{k_i k_j}{2m}\right)\delta(c_i, c_j) \qquad [1]$$

where m is the total number of edges in the network, and k_i and k_j are the degree of each vertex; c_i is the group to which vertex i belongs and $\delta(c_i,c_j)$ is the Kronecker delta symbol.

The partitioning analysis followed the procedure in a previous work (Newman, 2006) and consisted of two steps. In the first step, we obtained a single solution of partitioning by using the spectral approach based on the leading eigenvector of the modularity matrix (Newman, 2006). This step, as pointed out by Newman, gave an excellent guide to the general form that the communities should take. In the second step, we combined the spectral method and the fine-tuning method described in Newman's study to further optimize modularity (Newman, 2006). Considering the fact that the modularity function Q generated by combining the spectral method and the fine-tuning method is degenerate (Good et al., 2010), in the second step we computed a distribution

of Q values and a distribution of partitions by permuting the order of nodes in the adjacency matrix before feeding it into the optimization algorithm. Only the solution consistent over this distribution was reported. The degeneracy of Q goes approximately as 2^k where k is the number of modules (Good et al., 2010). Since k=3 modules were found in the first step, $>2^k$ (20) repetitions were made to form the distribution of Q values and partitions. All analyses in the second step were performed using Brain Connectivity Toolbox (BCT) (Rubinov and Sporns, 2010). After partitioning, components belonging to the same module were displayed in the same colors in the figures.

Clustering coefficient and shortest path length

The averaged local clustering coefficient was calculated as

$$C = \frac{1}{m}\sum_{j=1}^{m}\frac{2E}{V\,(V-1)} \qquad [2]$$

where E_j is the number of edges connecting neighbors of vertex j, and V_j is the number of neighbors of vertex j. Pure random networks with same numbers of nodes and edges were constructed based on Erdős–Rényi model with 100 repetitions. Random networks with the same distribution of degrees as the current rat-brain network were constructed using BCT with 100 repetitions. The averaged minimum path length was calculated as

$$L = \frac{2}{m\times(m-1)}\sum_{j=1}^{m-1}\sum_{k=j+1}^{m} min\_path(j,k) \qquad [3]$$

where *min_path* is the shortest path length between vertices j and k.

Reproducibility of inter-component direct connectivity

To estimate the reliability of inter-component connectivity across animals, we randomly divided data from all animals into two subgroups. The strength of inter-component connectivity (defined as the amplitude of partial correlation coefficient between two components) between the two subgroups was quantitatively compared using the correlation of inter-component connectional strength between the two subgroups. This procedure was repeated 100 times and the correlation value averaged across 100 repetitions was reported.

Results

Elementary clusters of RSFC revealed by group ICA

Group ICA results were obtained from 16 conscious rats. Most components identified were located in specific anatomical regions as displayed in Figure 1.1. Fig. 1.1a showed a component located at anatomically well defined bilateral caudate putamen (CPu). Fig1.1b-e represented functional structures of bilateral hypothalamus, thalamus, hippocampus and somatosensory (SS) cortex, respectively. In addition, functionally related regions also tended to cluster into single components. Fig1.1f showed a component including bilateral prefrontal cortex (PFC) and anterior olfactory nucleus (AON), showing well-known reciprocal functional connections of the olfactory bulbs and other olfactory related areas with the prefrontal cortex in conscious rats (Cinelli et al., 1987). Another olfactory-related component was located at olfactory tubercle (OT) (Fig 1.1g). Fig 1.1h showed a complex component composed of anterior cingulate cortex (ACC),

Figure 1.1. Spatial maps of individual components identified by ICA. (a-h): Examples of ICA components. Left columns are atlas images. Anatomic regions corresponding to individual ICA components are annotated. Middle columns are individual ICA components overlaid on anatomical images in the coronal view. Distances to Bregma (mm) are labeled at the bottom of each image. Right columns are individual ICA components overlaid on anatomical images in the transversal view.

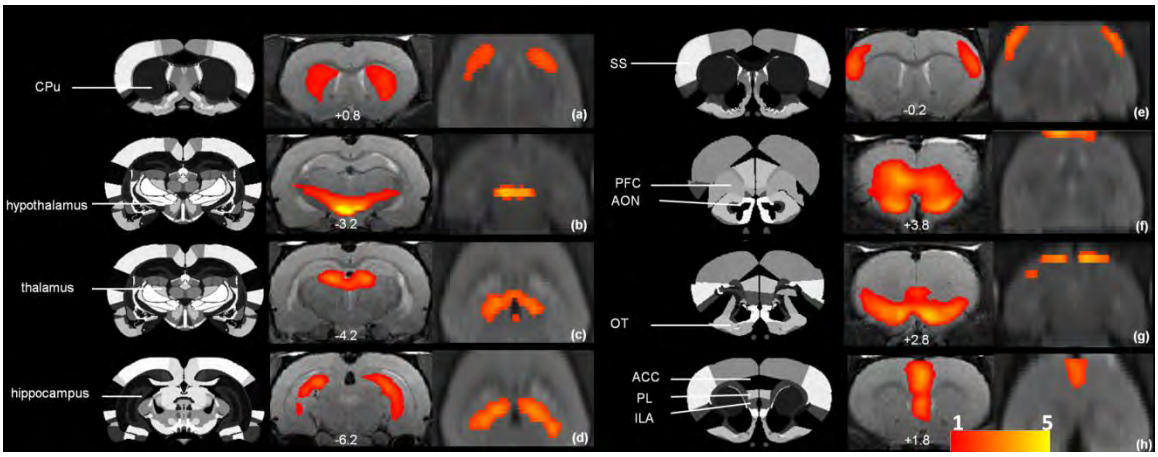
CPu
hypothalamus
thalamus
hippocampus
+0.8
(a)
-3.2
(b)
-4.2
(c)
-6.2
(d)
SS
PFC
AON
OT
ACC
PL
ILA
-0.2
(e)
+3.8
(f)
+2.8
(g)
+1.8
(h)
1
5

prelimbic (PL) and infralimbic (ILA) cortices, together being considered as extended areas of PFC in the rat.

Figure 1.2 showed 38 ICA components (excluding two artifactual components) overlaid on anatomical images, revealing the global clustering pattern of RSFC in the rat brain. Bilateral components were dominant of all ICA components identified (24 out of 38). In cortical regions, bilateral components (13 in total) were also dominant. The numbers of left and right cortical components were approximately equal (5 for left lateral components and 6 for right components).

Direct connectivity between RSFC clusters calculated by partial correlation

To evaluate inter-component connectional relationships, we calculated the direct connectivity between individual components by using partial correlation analysis. The partial correlation coefficient matrix of 40 components averaged across all animals was displayed in Figure 1.3a. Statistical comparison at the group level revealed the pattern of direct connections between different RSFC clusters (one sample t-test, $p < 0.01$). To estimate the reliability of inter-component connectivity across animals, we randomly divided data from all animals into two subgroups. Fig. 1.3b showed a high correlation of inter-component connectional strength between the two subgroups ($r=0.71$, $p<10^{-6}$), suggesting great reproducibility in direct connectivity between RSFC clusters. This result did not change when we repeated the same process for 100 times (averaged correlation coefficient of 100 repetitions $r_{avg} = 0.68$).

Figure 1.2. The spatial pattern of 38 group ICA components (excluding two artifactual components). Individual components are displayed with distinct colors. Distance to Bregma (mm) for each imaging slice is labeled at the bottom of each image.

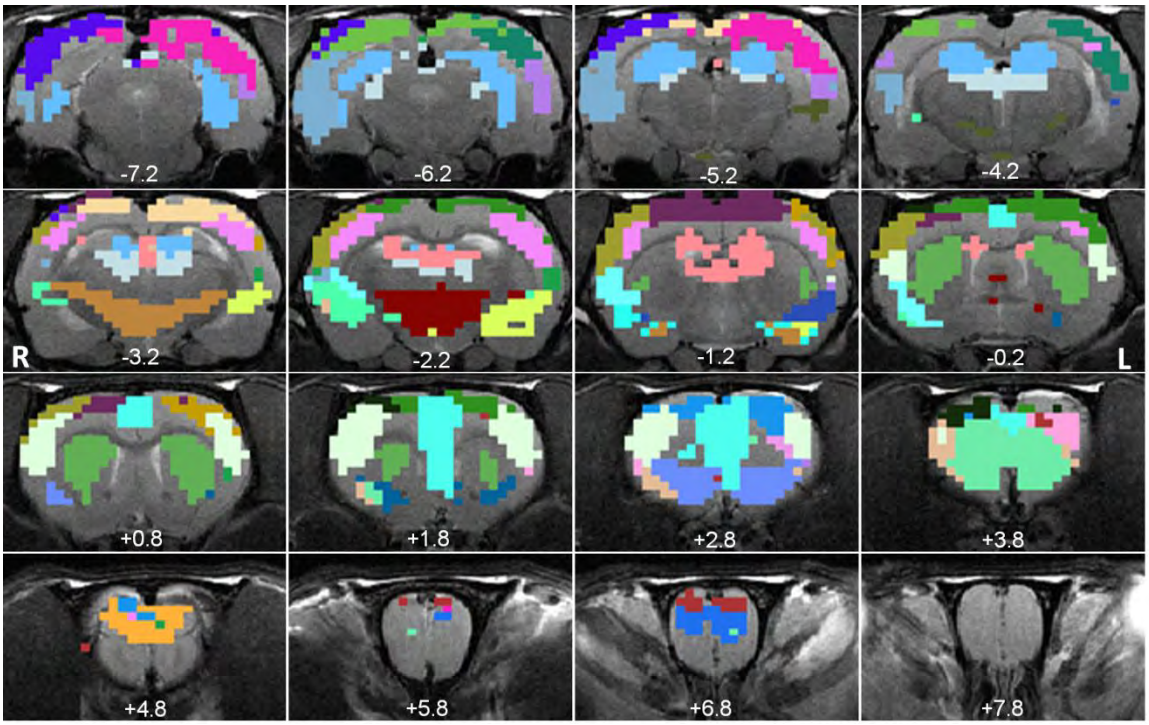
-7.2
-6.2
-5.2
-4.2
R
-3.2
-2.2
-1.2
-0.2
L
+0.8
+1.8
+2.8
+3.8
+4.8
+5.8
+6.8
+7.8

Figure 1.3. Inter-component connectional relationships. (a) The partial correlation coefficient matrix averaged across all rats. Partial correlation coefficients (r values) were first transformed to *z scores* and then averaged across all runs and across all animals. The final partial correlation matrix was generated by transforming the averaged *z scores* back to the r values. All diagonal values were set to zero. (b) Correlation of direct connectional strength (r values) between two randomly divided subgroups. The high correlation coefficient (0.71) suggests that inter-component connections across animals are highly reproducible.

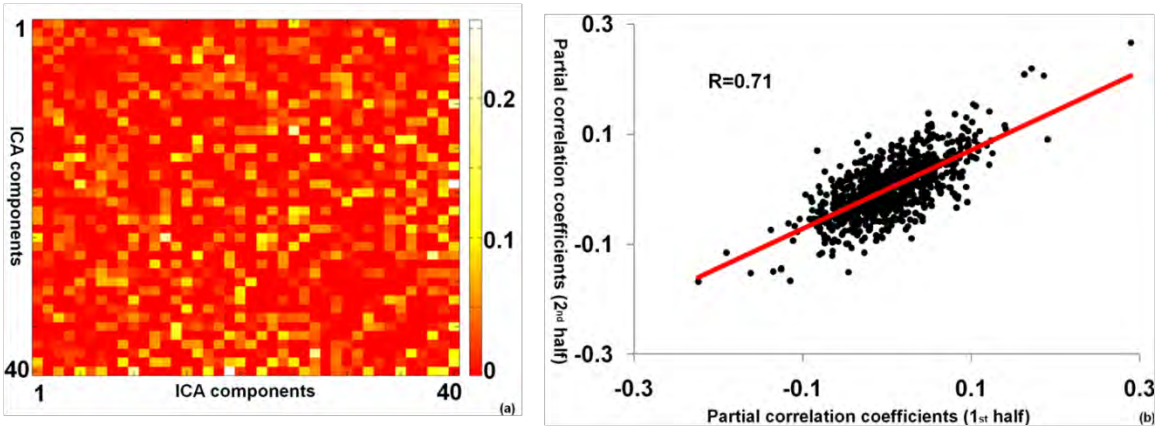
1
40
ICA components
1
ICA components
40
0.2
0.1
0
(a)
0.3
0.1
-0.1
-0.3
R=0.71
Partial correlation coefficients (2nd half)
-0.3
-0.1
0.1
0.3
Partial correlation coefficients (1st half)
(b)

Graph-theory based analysis of the rat brain networks

The graph demonstration of significant direct connections between ICA components was shown in Fig. 1.4a. The total edge number was 78, yielding the connection density of 5.55%.The spectral partitioning algorithm based on the leading eigenvector (Newman, 2006) was applied to this graph (the first step of partitioning, see **Methods**) and revealed that the rat whole-brain network was segregated into three modules to achieve maximum modularity (Q = 0.414, Fig. 1.4). This modularity value was significantly higher than both random networks with same nodes and edges and random networks with same degree distribution ($p<0.01$ for both types of random networks), suggesting a prominent modular structure of intrinsic connectional architecture of the rat brain. Of the three modules, module 1 was dominated by cortical regions including the dorsal olfactory bulb, motor cortex, somatosensory cortex, insular cortex and visual cortex as shown in Fig 1.4b, indicating strong 'direct' communications across the cortical ribbon in the rat (Zhang et al., 2010a). Module 2 included the olfactory system, PFC, ACC, CPu, posterior somatosensory cortex, thalamus, hypothalamus, hippocampus and auditory cortex. This module highlighted the integration of sensory input, cognitive processing and output (Paxinos, 2004). Module 3 consisted of the PFC, insular cortex, amygdala, hypothalamus and auditory cortex. This module might be related to emotion and autonomic regulation in the conscious rat (Paxinos, 2004).

To further maximize the final value of modularity, fine-tuning stages described in Newman's spectral partitioning analysis (Newman, 2006) were included in the 2nd step of the partitioning procedure. Considering that the modularity function Q is degenerate and leads to multiple solutions of graph partitioning (Good et al., 2010), we computed the

Figure 1.4. Segregation of the whole-brain network of the awake rat brain. (a). The global functional network constructed based on significant inter-component connections. Each node represents an ICA component labeled with its corresponding anatomy and the ICA number. Each edge represents a significant connection between two components. Nodes within the same module are displayed in the same color (red, green and yellow). Three modules were obtained by the spectral partitioning algorithm. Abbreviations: B, bilateral; L, left; R, right. ACC, anterior cingulate cortex; AMG, amygdala; AON, anterior olfactory nucleus; CPu, caudate-putamen; INS, insula; NAcc, nucleus accumbens; MO, motor cortex; HC, hippocampus; HY, hypothalamus; OB, olfactory bulb; PFC, prefrontal cortex; Pir, piriform cortex; PTL, parietal cortex; S, septum; SS, somatosensory cortex; TE, temporal cortex; TH, thalamus; VIS, visual cortex. (b-d). Community structures of the whole-brain network revealed by spectral partitioning. (b). The first module is dominated by cortical ribbon. (c) The second module is highlighted by the olfactory pathway and its interaction with PFC, and the integration of other sensory input, cognitive processing and output in cortical and subcortical regions like thalamus and hippocampus. (d) The third module includes regions important for emotional and autonomic functions such as amygdala, insular cortex, PFC and hypothalamus. The same colors are used in (b), (c) and (d) as those in (a). Distance to Bregma (mm) is labeled at the bottom of each image.

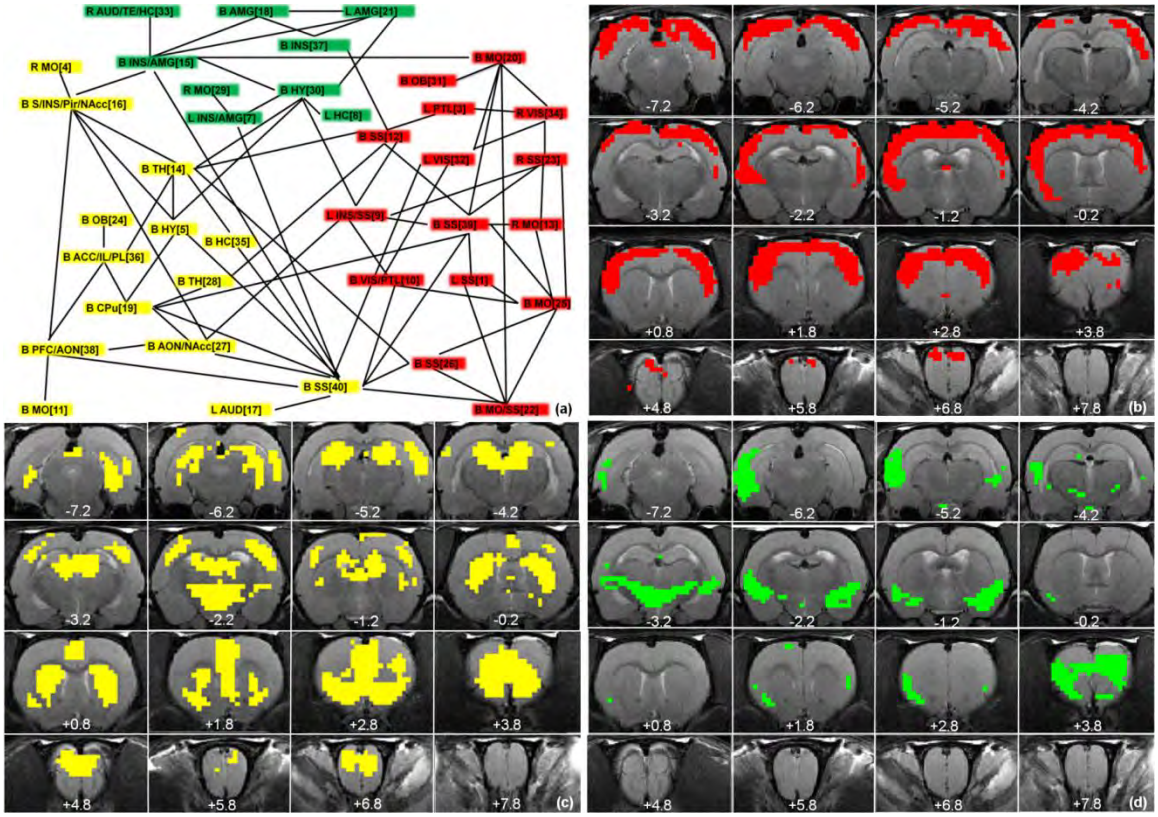
R AUD/TE/HC[33]
B AMG[18]
L AMG[21]
B INS[37]
B INS/AMG[15]
B MO[20]
R MO[4]
B OB[31]
R MO[29]
B HY[30]
B S/INS/Pir/NAcc[16]
L INS/AMG[7]
L HC[8]
L PTL[3]
R VIS[14]
B SS[12]
L VIS[12]
R SS[23]
B TH[14]
B OB[24]
L INS/SS[9]
B S5[39]
R MO[13]
B HY[5]
B HC[35]
B ACC/IL/PL[36]
B TH[28]
B VIS/PTL[10]
L SS[1]
B MO[29]
B CPu[19]
B PFC/AON[38]
B AON/NAcc[27]
B SS[26]
B SS[40]
B MO[11]
L AUD[17]
B MO/SS[22]
(a)
-7.2
-6.2
-5.2
-4.2
-3.2
-2.2
-1.2
-0.2
+0.8
+1.8
+2.8
+3.8
+4.8
+5.8
+6.8
+7.8
(b)
(c)
(d)

distribution of Q values and partitions. The distribution of Q values ranged from 0.392 to 0.429 with the mean value of 0.416, which only slightly improved the Q value of 0.414 obtained in the first step. In all repetitions, the majority yielded 4 modules (12 of 20 repetitions). The major pattern of partitioning showed very high stability. Consistent with the partitioning result from the first step, two modules identical to the 'green' and 'yellow' modules as shown in Fig 1.4 were highly consistent in all 20 partitions with minimal variation. The 'yellow' module was found in all repetitions and the 'green' module was found in 19 of 20 repetitions. However, the 'red' module was less stable and tended to be further divided into two submodules as shown in Figure 1.5. The first submodule was found in 14 of 20 repetitions and the second submodule was found in 13 or 20 repetitions. This reduced stability of the cortical module might indicate higher complexity of cortical network organization.

Furthermore, the connectional architecture of the rat brain showed typical features of small-worldness characterized by high clustering coefficient and short minimum path length. When comparing to pure random networks with the same numbers of nodes and edges, the ratio of clustering coefficient (C/C_{random}) was 1.7 and the ratio of minimum path length (L/L_{random}) is 1.08, indicating a higher level of clustering and a similar minimum path length than pure randomized networks. The ratios of these two metrics compared to a random network with the same distribution of degrees showed similar results, $C/C_{random}=1.5$, and $L/L_{random}=1.02$. These comparisons collectively suggest that the rat brain is a small-world network (Watts and Strogatz, 1998).

Figure 1.5. Community structures dominant in 20 repetitions of the spectral partitioning method combined with the fine-tuning method. Distance to Bregma (mm) is labeled at the bottom of each image. The yellow and green modules are almost identical to those shown in Fig. 1.4, whereas the module of cortical regions is further divided into two sub-modules.

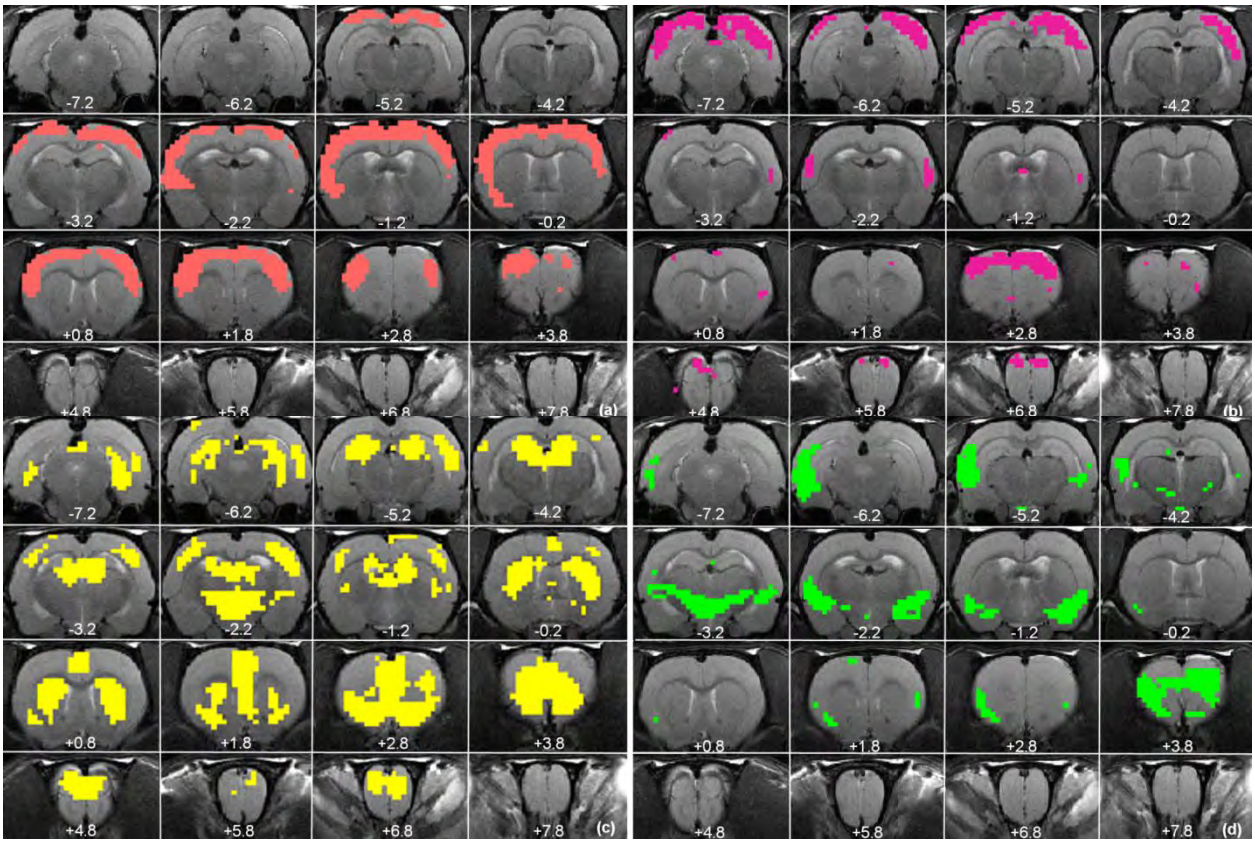
-7.2
-6.2
-5.2
-4.2
-3.2
-2.2
-1.2
-0.2
+0.8
+1.8
+2.8
+3.8
+4.8
+5.8
+6.8
+7.8
(a)
(b)
(c)
(d)

Discussion

In this study, RSFC in awake rats was decomposed into 40 spatial components using group ICA. The direct connectional relationships between these components were evaluated using partial correlation, revealing a complex network linking different regions across the whole brain. This brain network was characterized by the features of small worldness with a large modularity, a large clustering coefficient and a small shortest path length. Furthermore, using a graph-theory approach, the whole-brain network was segregated into community structures.

To our knowledge, this is the first study utilizing group ICA to study RSFC in awake rats. ICA is well established in rsfMRI for decomposing functional clusters in the human brain. However, its application in the rat was rather limited. There is currently only one study that utilized ICA to analyze RSFC of *individual* anesthetized rat without group analysis (Hutchison et al., 2010). Lack of such effort has significantly limited the applicability of rsfMRI particularly in animal models. In the present study, images of all individual rats were aligned to a standard rat atlas, and thus allowed the group results to be obtained using group ICA. In addition, the awake condition avoided confounding effects of anesthesia. We found that the majority of components identified were located in anatomically well-defined regions, indicating a convergence between anatomical parcellation and functional systems. Some components such as bilateral somatosensory, motor, visual and auditory cortices are in excellent consistency with the literature (Peltier et al., 2005; Lu et al., 2007; Liu et al., 2011). Spatial maps of subcortical regions including CPu, thalamus, hypothalamus and hippocampus also well agree with ICA results in individual anesthetized rats (Hutchison et al., 2010), suggesting highly

reproducible patterns of cortical and subcortical clustering across individuals. However, we also observed several less reported yet important clusters. For instance, there were components related to olfactory and executive functions. Olfaction is considered one of the most important sensory inputs in the rodent. Prominent components of olfactory bulb, AON and OT indicated functional significance of olfaction in awake rats. Moreover, PFC and AON were clustered into a single component, suggesting a close association between olfactory and executive functions (Cinelli et al., 1987).

To further evaluate inter-component connectional relationships, we applied partial correlation analysis on time courses of individual ICA components. Partial correlation analysis is an approach for estimating 'direct' statistical association by controlling out correlation mediated by other components. This analysis method essentially eliminated a large portion of connections that were mediated by other nodes with only 'direct' connections left. A recent study that evaluated various network modeling methods indicated that partial correlation performed very well in revealing network connections (Smith et al., 2010). In addition, this analysis could reveal possible long-distance functional integration. Significant amount of direct connection identified in the present study is consistent with anatomical connections in the rat. For instance, direct connection between thalamus and hippocampus observed in the present study has been well documented in the literature using various techniques (Wouterlood et al., 1990; Dolleman-Van Der Weel and Witter, 1996). These two regions and their bi-directional connections are critical components of the anatomical system sub-serving spatial memory (Henry et al., 2004). In addition, connections from the PFC to cingulate cortex and NAcc as shown in our data have been implicated in emotional processing (Hajos et al., 1998).

We also observed that thalamus bridges hippocampus and ACC. In accordance with this result, it was found that nucleus reuniens of the midline thalamus might serve as the link sending projection to the hippocampus from the medial PFC such as ACC (Vertes et al., 2007).

With the global functional network constructed based on inter-component connections (Fig.1.4a), the first question to consider is whether the rat brain exhibits the same network characteristics reported in humans such as small-worldness. Human studies have indicated robust 'small-world' characteristics in both structural and functional connectivity networks. A small-world network is described by a high clustering coefficient and low minimum path length compared to random networks. Small-world networks allow high efficiency of information flow at a low wiring cost for both local (with a high clustering coefficient) and long distance (with a low minimum path length). Although small-worldness represents a crucial feature of brain organization in the human, there is a paucity of information regarding small-world networks in non-human subjects. Previous studies reported similar small-worldness of *anatomical* networks in the macaque visual cortex and cat whole cortex (Hilgetag et al., 2000). However, no study yet specifically addressed this question using functional connectivity in conscious rats. Our network metrics showed that in the rat brain, the whole-brain network is considerably more cliquish than random networks, while retaining approximately the same minimum path length. These results are quantitatively comparable to the human brain and suggest that small-worldness is conserved in the rat functional networks.

In addition to the small-world features, high modularity is also thought to be an important governing principle in brain networks. Several studies consistently reported

that the resting-state brain network in humans exhibited robust community structure (Meunier et al., 2009; Wang et al., 2009). High modularity values of the rat whole-brain network obtained in our study indicated a robust community structure of the global network in the awake rat brain at the resting state. This result indicated that the rat brain shares basic topological characteristics with the human brain.

By utilizing Newman's spectral partitioning method, the rat whole-brain network was segregated into three modules. The first module predominantly extended across the cortical ribbon, indicating a strong inter-cortical communication across the cortex (Zhang et al., 2010a). The second module highlighted the olfactory pathway and its interaction with PFC, and the integration of other sensory input, cognitive processing and output in cortical and subcortical regions. Regions in the third module including PFC, insular cortex, hypothalamus and amygdala are all key components sub-serving emotional and autonomic regulations (Paxinos, 2004). Interestingly, using phMRI Schwarz and others reported very similar results with a module dominated by cortical regions and a second module primarily with subcortical regions (Schwarz et al., 2009). Consistent with the intrinsic modular structure observed in the resting-state human brain, our rat results also showed long-distance interaction within modules.

To address the issue of degeneracy of the modularity function, distributions of Q values and community structures were obtained. The result showed that two of the three modules previously identified (yellow and green modules) were highly consistent across all repetitions with little variation, whereas the community structure of cortical regions was further divided into two sub-modules. We speculate that the relatively lower stability of this module might reflect higher complexity of the organization of cortical networks.

The ‘vertices’ in our graph are ICA components as oppose to individual voxels or anatomically defined ROIs in most other studies. The strategy of using ICA components to construct global networks is based on functionally segregated elements of the brain. Thus, we avoided anatomical restraint of ROI definitions. Recent evidence suggests that different anatomical parcellation schemes had significant influences on network topological properties (Wang et al., 2009) and functionally inaccurate ROIs could severely damage the network estimation (Smith et al., 2010). Therefore, our approach might have significant advantages in constructing the whole brain network compared to anatomical ROI-based approaches. Relative to voxel-by-voxel approaches, our approach is more computationally efficient.

There are several methodological limitations of the present study. First, an unweighted network was used in graph-theory analysis. Exploration on weighted networks should be interesting. Second, although rats were fully awake during RSFC scans, they were briefly anesthetized during setup. The effects of brief anesthesia on later RSFC need further investigation. Third, the ICA components number was arbitrary and other numbers can be used. In addition, negative inter-component partial correlation coefficients (approximately half of all correlation coefficients) were not analyzed but can potentially contain important information regarding neural networks. This information should be taken into consideration in future studies. Furthermore, although inter-component connectivity showed high consistency in the present study, individual variability particularly in topographical properties needs future examination.

Our understanding of the brain function has substantially benefited from preclinical neurobiological investigation in animal models, primarily in rodents. The

present study systematically investigated resting-state functional networks in the awake rat brain. It provided a functional atlas of the intrinsic connectional architecture of the rat brain at both intra- and inter-region levels. More investigations are still needed to further characterize connectional architecture in the rat brain. For example, it is unknown whether functional networks in rats are organized differently at different spatial scales, or whether significant community structure exists within each module. It is also unknown whether the rat brain has the default mode network found in humans and primates (Raichle et al., 2001; Vincent et al., 2007). Nevertheless, the current work revealed that the conscious rat brain conserved topological properties like small-worldness as observed in human. Combined with various invasive procedures, pharmacological interventions and genetic manipulations, it will serve as a prelude to future applications of RSFC in animal models.

Acknowledgement

We thank Dr Wei Huang for her technical assistance. We also thank the reviewers for their insightful comments. This publication was made possible by the NIH Grant Number 1R01 MH067096-02 and 5R01DA021846-02 from the National Institute of Health, and the institutional fund from the University of Massachusetts Medical School. Its contents are solely the responsibility of the authors and do not necessarily represent the official views of the NIH.

CHAPTER II

Intrinsic Organization of the Anesthetized Brain

Zhifeng Liang, Jean King and Nanyin Zhang

Center for Comparative NeuroImaging, Department of Psychiatry, University of Massachusetts Medical School, Worcester, Massachusetts 01655

Abstract

The neural mechanism of unconsciousness has been a major unsolved question in neuroscience despite its vital role in brain states like coma and anesthesia. The existing literature suggests that neural connections, information integration and conscious states are closely related. Indeed, alterations in several important neural circuitries and networks during unconscious conditions have been reported. However, how the whole-brain network is topologically reorganized to support different patterns of information transfer at unconscious states remains unknown. Here we directly compared whole-brain neural networks in an awake and an anesthetized state in rodents. Consistent with our previous report, the awake rat brain was organized in a non-trivial manner and conserved fundamental topological properties as the human brain. Strikingly, these topological features were well maintained in the anesthetized brain. Meanwhile, local neural networks were reorganized with altered local network properties. The connectional strength between brain regions was also considerably different between the awake and anesthetized conditions. Interestingly, we found that long-distance connections were not preferentially reduced in the anesthetized condition, arguing against the hypothesis that loss of long-distance connections is characteristic to unconsciousness. These findings collectively show that the integrity of the whole-brain network can be conserved between widely dissimilar physiologic states while local neural networks can flexibly adapt to new conditions. They also illustrate that the governing principles of intrinsic brain organization might represent fundamental characteristics of the healthy brain. With the unique spatial and temporal scales of rsfMRI, this study has opened a new avenue for understanding the neural mechanism of (un)consciousness.

Introduction

Loss of consciousness is not unusual in life. Anesthetic-induced unconsciousness is particularly interesting given its essential role in modern medicine. Although the molecular mechanisms of various anesthetic agents have been fairly well understood (Alkire et al., 2008; Brown et al., 2011), the system-level neural basis underlying anesthetic-induced unconsciousness is still obscure. In particular, how the whole-brain network is reorganized to support new patterns of information exchange at the anesthetized state remains largely unknown. Given the tight linkage among neural connectivity, information integration and conscious states (Tononi, 2008), investigating this issue is essential for understanding consciousness.

The emerging technique of resting-state functional magnetic resonance imaging (rsfMRI) has been utilized to understand the alterations in neural circuitries and networks at unconscious conditions. Unlike conventional task-based fMRI, rsfMRI does not involve active stimuli but relies on low-frequency intrinsic fluctuations of the fMRI signal to examine functional connectivity (FC). Therefore, rsfMRI is particularly suitable for studies of unconsciousness. With this technique, it has been reported that FC might be correlated with the degree of consciousness from locked-in syndrome, minimally conscious state, vegetative state to brain death (Boly et al., 2009; Cauda et al., 2009; Vanhaudenhuyse et al., 2010). In addition, changes in thalamocortical connectivity and frontoparietal connectivity under anesthetic-induced unconsciousness have been reported in humans (Boveroux et al., 2010; Deshpande et al., 2010; Martuzzi et al., 2010). Furthermore, effort has been made to explore the alteration of FC in several animal

models at anesthetized conditions, though mainly by comparing between different anesthetic depths without the reference of the awake condition (Vincent et al., 2007; Moeller et al., 2009; Wang et al., 2010; Williams et al., 2010; Liu et al., 2011).

Despite these important contributions, it is unclear whether and how the organization of global functional networks is altered during unconsciousness. This issue is critical because it directly addresses the impact of unconsciousness on the *governing principles* of brain network organization. The organizational principles of human brain networks have been extensively studied by neuroimaging techniques in combination with graph-theory analysis. In such analysis, the brain network is modeled as a graph with nodes being individual brain regions and edges being connections between nodes. Various topological properties like clustering coefficient can be evaluated for brain graphs (Rubinov and Sporns, 2010). Accumulating evidence has suggested that the topological architecture of the human brain network is governed by several fundamental principles such like small-worldness and modularity (Bullmore and Bassett, 2010). Importantly, it has been found that topological properties of functional networks are susceptible to various pathological disruptions (Bassett and Bullmore, 2009) such as Alzheimer's disease (Supekar et al., 2008) and schizophrenia (Liu et al., 2008).

We previously reported that the awake rat brain conserved fundamental topological properties as the human brain (King et al., 2005; Zhang et al., 2010b; Liang et al., 2011, 2012a). To further explore the intrinsic organization of the unconscious rat brain, here we have directly compared resting-state neural networks between the awake and anesthetized states. The changes of topology and FC strength of the anesthetized brain networks have been examined.

Materials and Methods:

Animal preparation and MR experiment

Imaging data were acquired in a previous study (Liang et al., 2012a) and re-processed for the purpose of this study. All studies were approved by the IACUC Committee of the University of Massachusetts Medical School. Briefly, 24 adult male Long-Evans (LE) rats (300-400g) were housed in Plexiglas cages (two to a cage) and maintained in ambient temperature (22-24 ˚C) on a 12-h light : 12-h dark schedule. Food and water were provided ad libitum. Rats were acclimated to MRI restraint and noise for seven days before imaging (detailed acclimation procedures were described in our previous publications (King et al., 2005; Zhang et al., 2010b; Liang et al., 2011, 2012a)). On the imaging day, the animal was first briefly anesthetized with isoflurane when it was fit to a head restrainer with a built-in saddle coil. Isoflurane was then discontinued and the restrainer was placed in the scanner. Imaging sessions started approximately 15-20 mins after animals were placed in the magnet. All rats were fully awake during imaging. Among all 24 rats, 16 rats underwent the imaging session at the anesthetized condition at minimum 7 days after they were imaged at the awake condition. In this experiment, the animal preparation procedure was the same as that in the awake imaging experiment. Isoflurane gas (2%) was then delivered to the animal through a nose cone in the magnet to maintain the anesthetized state. The body temperature of the animal was monitored and maintained at 37°C ± 0.5°C by using a feedback controlling heating pad.

All experiments were carried out on a Bruker 4.7T/40cm horizontal magnet (Oxford, UK) interfaced with a Biospec Bruker console. A dual 1H radiofrequency (RF) coil configuration (Insight NeuroImaging Systems, Worcester, MA) consisting of a volume coil for exciting the water proton spins and a surface coil for receiving the MRI signal was used. The volume and surface coils were actively tuned and detuned to prevent mutual coil coupling. For each session, anatomical images were acquired by using a fast spin-echo sequence (RARE) with the following parameters: TR = 2125ms, RARE factor = 8, TE = 50ms, matrix size = 256×256, FOV = 3.2cm×3.2cm, slice number = 18, slice thickness = 1mm. Gradient-echo images covering the whole brain were then acquired using the echo-planar imaging (EPI) sequence with the following parameters: TR = 1s, TE = 30ms, flip angle = 60°, matrix size = 64×64, FOV = 3.2cm×3.2cm, slice number = 18, slice thickness = 1mm. Two hundred volumes were acquired for each run, and six runs were obtained for each session.

Data preprocessing

All images were co-registered to a fully segmented rat atlas, and were then subject to motion correction with SPM8 (http://www.fil.ion.ucl.ac.uk/spm/), spatial smoothing (FWHM = 1mm), regression of motion parameters and the signals of white matter and ventricles, and 0.002-0.1Hz band-pass filtering. Scans with excessive motion (>0.25 mm) were discarded.

Construction of whole-brain resting-state functional network

The rat brain was parcellated into 114 anatomical ROIs (57 regions for each hemisphere) using MIVA (http://ccni.wpi.edu/, Figure 2.1). Anatomical definitions were

based on the Swanson atlas (Swanson, 2004).The complete list of all anatomical ROIs was included in Table 2.1. Based on this parcellation scheme, a regionally averaged time course for each ROI was generated by averaging the time courses of all voxels within the ROI. FC was evaluated by Pearson correlation between the time courses of each pair of ROIs. Correlation coefficients (i.e. r values) were transformed to z scores by using Fisher's z transformation and averaged across all runs for each subject. Averaged z scores were then transformed back to r values. As a result, a 114×114 matrix of correlation coefficients was generated for each subject and each element of this matrix represented the strength of FC between two ROIs. To examine the reliability of FC, matrices of the awake and anesthetized conditions were randomly split into two subgroups, respectively, and averaged within each subgroup. The correlation between the FC strength of all functional connections between the two subgroups (i.e. the correlation between the corresponding elements of the two matrices) was then calculated for each condition. This process was repeated 1000 times to generate a measure of reliability. The result revealed high reliability in both awake (mean$\pm$SD = 0.93$\pm$0.01) and anesthetized (mean$\pm$SD = 0.90$\pm$0.02) conditions.

Graph theory analysis of the whole-brain network

In a brain graph, a node represented an anatomical ROI and an edge represented the connectional strength between two ROIs. All brain graphs were visualized by Pajek (http://pajek.imfm.si/doku.php). Matrices of Individual subjects generated in the previous

Figure 2.1. Parcellation scheme of the rat brain. Colored regions represent anatomically parcellated ROIs overlaid on anatomical images. Distance to Bregma (mm) is labeled at the bottom of each slice.

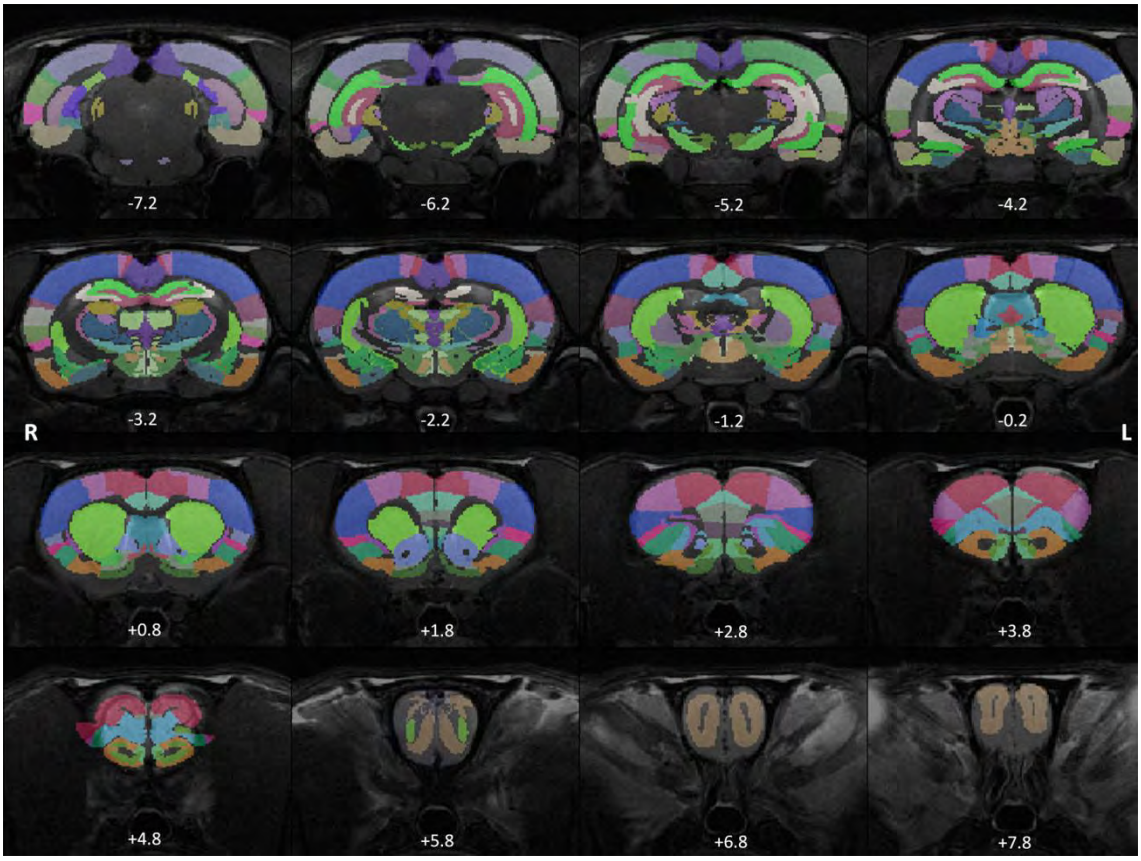
-7.2
-6.2
-5.2
-4.2
-3.2
-2.2
-1.2
-0.2
R
L
+0.8
+1.8
+2.8
+3.8
+4.8
+5.8
+6.8
+7.8

Table 2.1. List of ROIs. From left: the first column lists the number of the anatomical-functional system to which each ROI is affiliated (see Table 2.3); the second column lists the number of each ROI (the same number used in Figure 2.5); the third column lists the abbreviation of each ROI; the fourth column lists the full name of each ROI.

Anatomical-functional system	ROI(left, right)	abbreviation	full name
1	1, 58	AON	anterior olfactory nucleus
1	2, 59	MOB	main olfactory bulb
1	3, 60	PIR	piriform area
1	4, 61	ILA	infralimbic area
1	5, 62	TR	postpiriform transition area
1	6, 63	MOp	primary somatomotor area
1	7, 64	MOs	secondary somatomotor areas
1	8, 65	GU	gustatory area
1	9, 66	VISC	visceral area
1	10, 67	TT	tenia tecta
1	11, 68	SSp	primary somatosensory area
1	12, 69	SSs	supplemental somatosensory area
1	13, 70	AUD	auditory areas
1	14, 71	VIS	visual areas
2	15, 72	PTL	parietal region
2	16, 73	TeV	ventral temporal association areas
2	17, 74	PL	prelimbic area
2	18, 75	ORB	orbital area
2	19, 76	ACA	anterior cingulate area
2	20, 77	AI	agranular insular area
2	21, 78	ECT	ectorhinal area

2	22, 79	RSP	retrosplenial area
3	23, 80	ENT	entorhinal area
3	24, 81	PAR	parasubiculum
3	25, 82	POST	postsubiculum
3	26, 83	PRE	presubiculum
3	27, 84	SUB	subiculum
4	28, 85	CA1	field CA1
4	29, 86	DG	dentate gyrus
4	30, 87	CA3	field CA3
5	31, 88	COA	cortical amygdalar nucleus
5	32, 89	AMG	amygdala
6	33, 90	ACB	nucleus accumbens
6	34, 91	CP	caudoputamen
6	35, 92	OT	olfactory tubercle
6	36, 93	FS	striatal fundus
6	37, 94	LSX	lateral septal complex
7	38, 95	BST	bed nuclei stria terminalis
7	39, 96	MSC	medial septal complex
7	40, 97	GP	globus pallidus
7	41, 98	SI	substantia innominata
8	42, 99	MG	medial geniculate complex
8	43, 100	ATN	anterior nuclei, dorsal thalamus
8	44, 101	VENT	ventral nuclei, dorsal thalamus
8	45, 102	LAT	lateral nuclei, dorsal thalamus

8	46, 103	MED	medial nuclei, dorsal thalamus
8	47, 104	MTN	midline group, dorsal thalamus
8	48, 105	LG	lateral geniculate complex
8	49, 106	RT	reticular nucleus thalamus
8	50, 107	ZI	zona incerta
9	51, 108	MEZ	medial zone of hypothalamus
9	52, 109	LZ	lateral zone of hypothalamus
9	53, 110	PVZ	periventricular zone of hypothalamus
0	54, 111	SNr	substantia nigra
0	55, 112	VTA	ventral tegmental area
0	56, 113	TRN	tegmental reticular nucleus, pontine gray
0	57, 114	CLA	claustrum

step were subject to density-based thresholding, similar to the procedure used by Zhang et. al. (Zhang et al., 2011). Network density was defined by the ratio of existing edges to the maximal number of all possible edges in the network. A range of network densities were selected based on the following criteria: 1) The lower boundary was selected to ensure the averaged degree was not smaller than 2×log(N), where N was the total number of nodes (i.e. N=114). This lower boundary guaranteed that the resulting networks were estimable networks (Watts and Strogatz, 1998). The upper boundary was selected to ensure that mean small-worldness (see the definition of small-worldness below) of the awake brain was not smaller than 1.5. This upper boundary ensured that thresholded networks were biologically plausible in the sense of being small-world networks and had as few spurious edges as possible. As a result, the network density of each brain graph was thresholded in the range from 9% to 26% with a step size of 1%. At each threshold in this range, correlation coefficients of each matrix were first sorted from high numbers to low numbers. A binary matrix was then obtained by retaining the highest correlation coefficients and setting their values to 1, and the correlation coefficients of the rest of the matrix were set to 0. The portion of the correlation coefficients retained was equal to the threshold chosen (e.g. 9%). The averaged size of the largest connected networks ranged from 99.3 (at 9% density) to 112.5 (at 26% density) nodes for the awake condition, and from 101.2 (at 9% density) to 113.5 (at 26% density) nodes for the anesthetized condition.

The local clustering coefficient c was defined as follows:

$$c = \frac{2E_j}{V_j(V_j-1)},$$

where E_j is the number of edges connecting the neighbors of node j, and V_j is the number of neighbors of node j. The global clustering coefficient C is the average of local clustering coefficients of all nodes within the network:

$$C = \frac{1}{m}\sum_{j=1}^{m} c,$$

where m is the total number of nodes of the network. Mean shortest path length was defined as the harmonic mean of the shortest path length between all possible pairs of nodes:

$$L = \frac{2}{m\times(m-1)} \frac{1}{\sum_{j=1}^{m-1}\sum_{k=j+1}^{m} 1/_{\min\_\mathrm{path}(i,j)}},$$

where *min_path* is the shortest path length between nodes *i* and *j*. The harmonic mean was used to address the issue of infinite path length between disconnected nodes. Global clustering coefficient and mean shortest path length was normalized to the corresponding metrics of random networks (see below for details about random networks). Small-worldness was defined as the ratio of normalized global clustering coefficient to normalized mean shortest path length.

Betweeness centrality of a node υ was defined as follows:

$$B(v) = \frac{1}{(m-1)\times(m-2)}\sum_{s\neq v\neq t} \sigma_{st(v)},$$

where $\sigma_{st(v)}$ = 1 if the shortest path between node *s* and *t* passes through node υ, otherwise it was 0.

Modularity was defined as follows:

$$Q = \frac{1}{4m}\sum_{ij}\left(a_{ij} - \frac{k_i k_j}{2m}\right)\delta(c_i, c_j),$$

where k_i and k_j were the degree of nodes i and j, respectively; c_i was the group to which node i belongs, and $\delta(c_i,c_j)$ was the Kronecker delta symbol. For each network, Newman's algorithm (Newman, 2006) implemented in the Brain connectivity toolbox (https://sites.google.com/a/brain-connectivity-toolbox.net/bct/) was repeated 100 times and the modularity (Q) calculated for each repetition was then averaged. Modularity values were normalized to the corresponding values of random networks.

It has been reported that modularity-based network partition algorithms are complicated by the issue of degeneracy (Good et al., 2010). To avoid this problem and identify consistent community structures of the whole-brain functional network, the within-module connectivity likelihood method was adopted in the present study (Rubinov and Sporns, 2011). In the connectivity likelihood matrix, the value of each matrix entry measured how likely both nodes (i.e. the column and row of this entry) were within the same module in all network partitions. Specifically, a matrix entry was assigned to 1 for each network partition if both nodes belonged to the same module and 0 otherwise. These matrices were then averaged across all partition repetitions, all network densities and then all subjects to generate the final connectivity likelihood matrix. This approach has been utilized to reconstruct consistent community structures across a large number of network partitions (Rubinov and Sporns, 2011). In the current study the likelihood matrix is based on the total partition numbers of 100 repetitions for each network × 18 network densities for each subject × the total number of subjects in each condition. The final community structure was created by thresholding the averaged within-module connectivity likelihood

matrix at 0.75 for both conditions, meaning that if the likelihood for two nodes belonging to the same module was above 0.75, they were considered in the same module.

To normalize network metrics of the awake and anesthetized conditions, each empirical network was randomized to generate 100 random networks with the same degree distribution. Network metrics (global clustering coefficient, mean shortest path length and modularity) of random networks were then calculated. Finally, all empirical metrics were normalized to the corresponding metrics of random networks.

The area-under-the-curve (AUC) method was utilized to summarize the results of aforementioned network metrics across the range of network density.

Statistics

The statistical analysis of network metrics was performed with nonparametric permutation test (Nichols and Holmes, 2002). First, the difference between the means of the two conditions was calculated as the actual group difference. Second, the combined pool of the two conditions was resampled into two new groups. The mean of these two re-sampled groups was then calculated. This process was repeated for 50000 times to generate a null distribution of the difference of the group mean. The p-value of the actual group difference was calculated as the percentile in the null distribution. For local network metrics (i.e. local clustering coefficient and betweeness centrality), false discovery rate (FDR) correction was additionally performed to correct for multiple comparisons. P values < 0.05 after FDR correction was considered statistically significant.

Connectional strength

The connectional strength was compared between the corresponding connections at the awake and anesthetized conditions with the same permutation test. P value < 0.05 after FDR correction was deemed statistically significant.

Physical distance

The physical distance between two anatomical ROIs was defined as the Euclidean distance between the two ROIs' centers of mass. Coordinates of ROIs were obtained from the parcellated anatomical template. Mean connectivity strength was plotted against the physical distance, binned at 1mm, for both conditions.

Results

The brain network was reorganized under the same governing principles at the anesthetized state.

Although anesthesia can dramatically impact numerous brain functions, it is unknown whether the global functional neural network remained organized under similar principles. Here we compared four global network topological metrics (*global clustering coefficient, mean shortest path length, small-worldness and modularity*) between the awake and anesthetized conditions. Strikingly, all four metrics showed no statistically significant difference between the two conditions (Figure 2.2). Similar global clustering coefficients (p=0.18) indicated a close level of "cliquishness" between brain regions; and similar mean shortest path length (p=0.34) implied indistinguishable communication efficiency. Small-worldness, measured by the ratio of the first two metrics, was also not

Figure 2.2. Consistent global topological features including a) global clustering coefficients ($p = 0.18$), b) mean shortest path lengths ($p = 0.34$), c) small-worldness ($p=0.25$), and d) modularity ($p=0.32$) during the awake and anesthetized states. Error bars indicated S.E.M. The difference between the awake and anesthetized states was evaluated by using nonparametric permutation test. Statistical significance was thresholded at $p<0.05$.

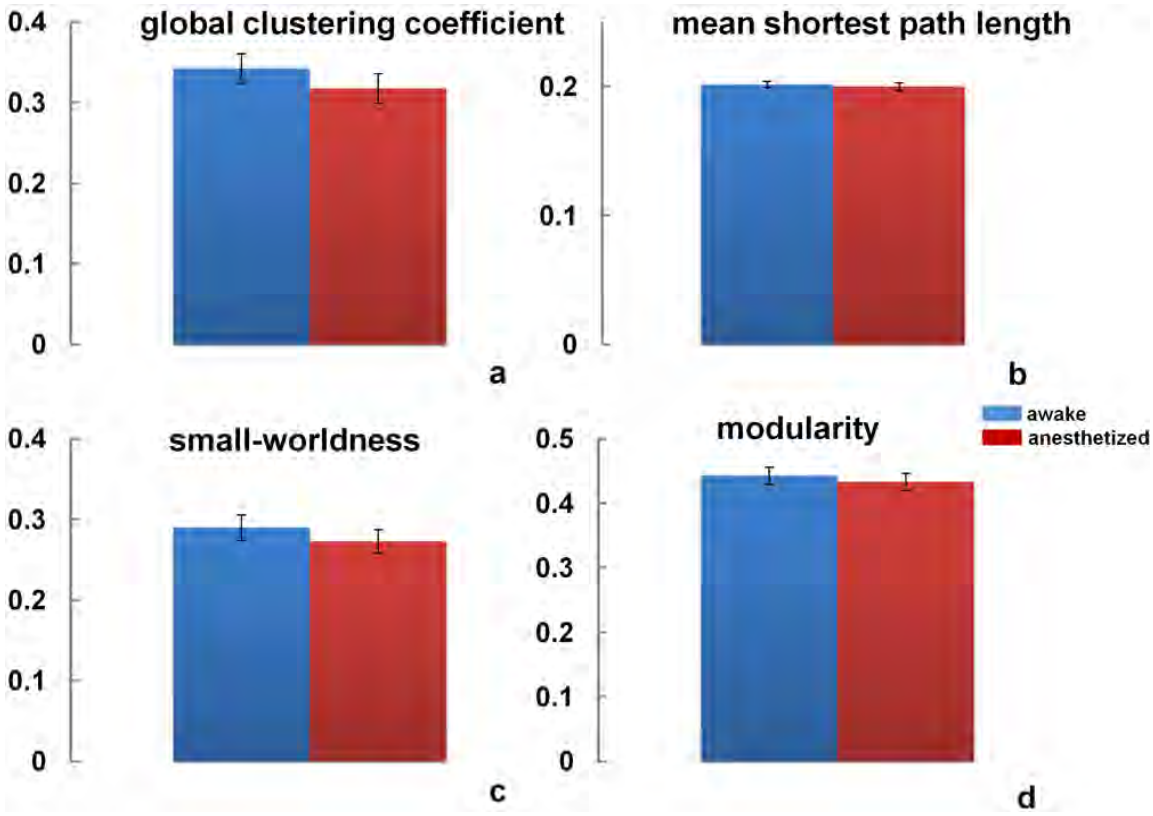
global clustering coefficient
0.4
0.3
0.2
0.1
0
a
mean shortest path length
0.2
0.1
0
b
awake
anesthetized
small-worldness
0.4
0.3
0.2
0.1
0
c
modularity
0.5
0.4
0.3
0.2
0.1
0
d

significantly different between the two conditions ($p=0.25$). Lastly, comparing modularity between the awake and anesthetized conditions revealed a similar level of modular organization (p value=0.32). These results collectively demonstrated that the global neural network at the anesthetized state was topologically organized under the same governing principles as the awake state.

In spite of similar global topological properties, local topological metrics such as *local clustering coefficient* and *betweeness centrality* demonstrated pronounced changes in specific brain areas (Table 2.2, $p<0.05$, FDR corrected). In particular, regions of the basal ganglia including nucleus accumbens and septal nuclei showed significantly reduced local clustering coefficients in the anesthetized condition. Also, several thalamic nuclei showed decreased betweeness centrality (Table 2.2), indicating impaired information relay in the thalamus in the anesthetized rat brain.

Additional changes in local connectivity were examined through the measure of community structure. By utilizing the within-module connectivity likelihood method (see Methods), it is possible to reveal consistent modules across different network densities and subjects in the awake and anesthetized conditions, respectively (Rubinov and Sporns, 2011). Figure 2.3a showed that the awake rat brain was primarily comprised of a "frontal module" (red), a "sensory-motor module" (light blue), a "thalamo-hypothalamo module" (green), a “thalamo-hippocampal-posterior cortices” module (dark blue), a “bilateral retrosplenial cortex” module and an “amygdala complex" module. By contrast, the anesthetized rat brain was considerably re-organized in community structure. The cortex

Table 2.2. Altered local network metrics in the awake and anesthetized rat brain. Crosses indicate significantly decreased local network metrics in the anesthetized rat brain. L: left, R: right.

	ROI	L	R
local clustering coefficient	ACB	×	×
	AON	×	
	MSC	×	×
	LSX	×	×
	TT	×	×
betweeness centrality	LAT	×	
	MTN	×	
	LG	×	

Figure 2.3. Community structures in the (a) awake and (b) anesthetized conditions. ROIs with the same color are within the same module. ROIs without the annotation of L or R suggest the modules include bilateral sides. L: left, R: right, A: anterior, P: posterior, V: ventral, D: dorsal.

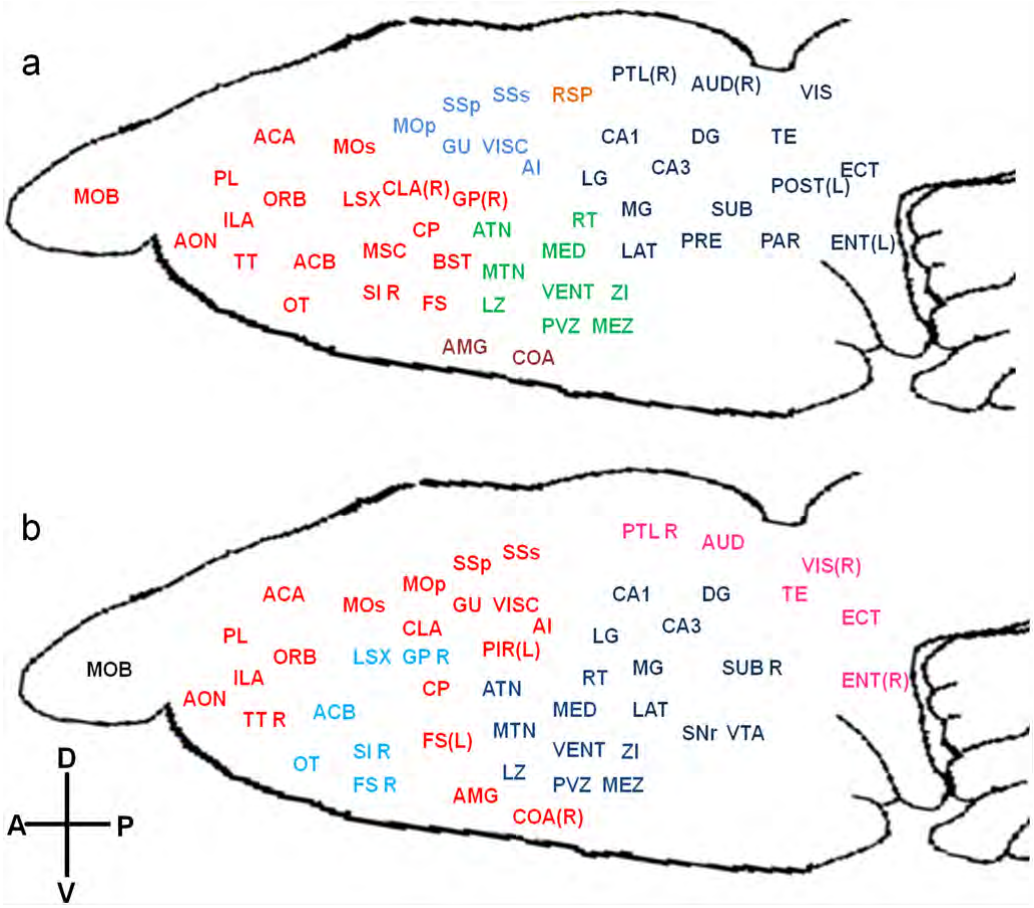
a
PTL(R)
AUD(R)
VIS
SSp
SSs
RSP
MOp
ACA
MOs
GU
VISC
CA1
DG
TE
AI
LG
CA3
ECT
POST(L)
MOB
PL
ORB
LSX
CLA(R)
GP(R)
MG
SUB
ILA
RT
CP
ATN
AON
MED
LAT
PRE
PAR
ENT(L)
TT
ACB
MSC
BST
MTN
SI R
VENT
ZI
OT
FS
LZ
PVZ
MEZ
AMG
COA
b
PTL R
AUD
SSp
SSs
VIS(R)
MOp
ACA
MOs
GU
VISC
CA1
DG
TE
CLA
AI
CA3
ECT
PL
LG
ORB
LSX
GP R
PIR(L)
MOB
RT
MG
SUB R
ILA
ENT(R)
CP
ATN
AON
MED
LAT
TT R
ACB
MTN
SNr
VTA
FS(L)
VENT
ZI
SI R
OT
LZ
FS R
PVZ
MEZ
AMG
COA(R)
D
A
P
V

was mainly divided into an anterior module and a posterior module, and subcortical areas were reorganized into a hypothalamo-thalamo-hippocampal module and a basal ganglia module. Notably, unlike the awake brain in which cortical or subcortical regions frequently mingled together into a single community structure, cortex and subcortex tended to be isolated in separate communities at the anesthetized state. For example, all thalamic nuclei, the hypothalamus and the hippocampus were clustered in one module without much involvement of cortex in the anesthetized condition (Fig 2.3b, dark blue), whereas part of thalamus and the whole hippocampus were in the same community with posterior cortical regions at the awake condition (Fig 2.3a, dark blue). The same scenario also occurred in the "frontal" module of the awake brain which included the frontal cortex and basal ganglia, whereas they were separated into different modules in the anesthetized brain (Fig 2.3b, light blue). These results collectively indicated that the cortical-subcortical communication was significantly compromised in the anesthetized condition.

Alterations in FC strength at specific anatomical locations

The distributions of connectivity strength of all functional connections across the whole brain in both awake and anesthetized conditions were shown in Figure 2.4. Consistent with previous studies (Peltier et al., 2005; Boveroux et al., 2010; Martuzzi et al., 2010), the connectivity strength on average was significantly lower in the anesthetized condition (two sample t-test, p value<1e-10). Specific anatomical

Figure 2.4. Histograms of functional connectivity strength in (a) awake and (b) anesthetized conditions. The connectivity strength was on average significantly weaker in the anesthetized condition (two-sample t-test, $p<10^{-10}$).

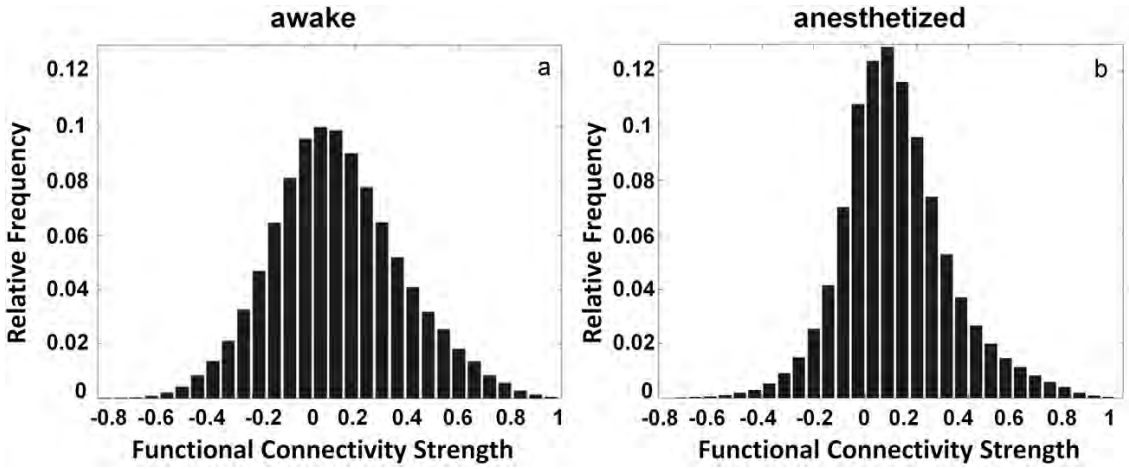
awake
a
Relative Frequency
0.12
0.1
0.08
0.06
0.04
0.02
0
-0.8 -0.6 -0.4 -0.2 0 0.2 0.4 0.6 0.8 1
Functional Connectivity Strength
anesthetized
b
Relative Frequency
0.12
0.1
0.08
0.06
0.04
0.02
0
-0.8 -0.6 -0.4 -0.2 0 0.2 0.4 0.6 0.8 1
Functional Connectivity Strength

information of significantly changed FC was further revealed by individually comparing the corresponding connections between the two conditions (p value<0.05, FDR corrected, Figure 2.5). To better conceptualize the complex pattern of altered FC, ROIs of the whole brain were divided into nine major functional-anatomical groups based on the Swanson Atlas (Swanson, 2004) (Table 2.3), and altered FC within and between these groups was displayed in brain graphs (Figure 2.6). To preserve the quantitative information, the weight of the edge between two groups was proportional to the percentage of the total number of significantly changed connections between the two groups (p value < 0.05 with FDR correction) relative to the total number of all possible connections between the two groups. The node size was proportional to the percentage of the total number of significantly changed connections within the group relative to the total number of all possible connections within the group. The results showed that FC was profoundly weakened in striatum, pallidum, thalamus and cortices, albeit considerably strengthened in hippocampus, amygdala and hypothalamus in the anesthetized condition.

Recently, Boveroux et. al. has reported a selective decrease of thalamo-cortical connectivity in high-order associative networks compared to low-level sensory-motor networks at the anesthetized condition (Boveroux et al., 2010). In the present study, we specifically compared the thalamo-cortical connectivity strength in associative networks (i.e. between associative cortices and thalamic nuclei related to associative cortices) and sensory-motor networks (i.e. between sensory-motor cortices and thalamic nuclei related to sensory-motor cortices) between the awake and anesthetized conditions. As expected, thalamo-cortical connectivity strength in both types of networks were reduced under

Figure 2.5. (a) Significantly changed functional connectivity ($p<0.05$, FDR corrected) displayed in the dorsal view of the rat brain. Each node represents an anatomical region listed in Table 2.1. Red (blue) lines indicate connections with significantly stronger (weaker) connectivity in the awake condition. The size of each node is proportional to the number of altered connections for this node. (b) Matrix representation of (a). Red (blue) elements are connections with significantly stronger (weaker) connectivity strength in the awake condition. The numbers of columns and rows are the ROI numbers listed in the second column of Table 2.1.

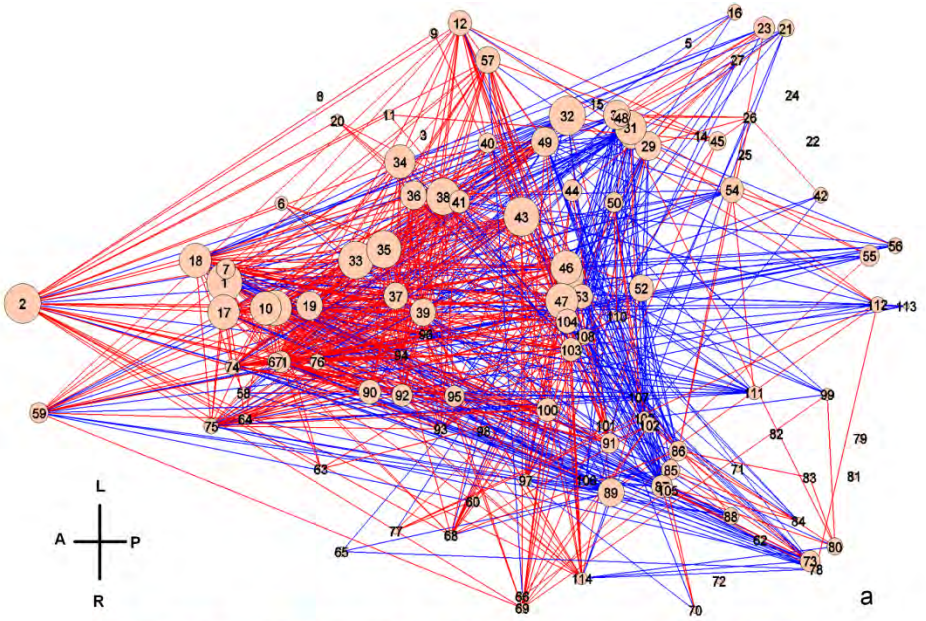
L
A
P
R
a

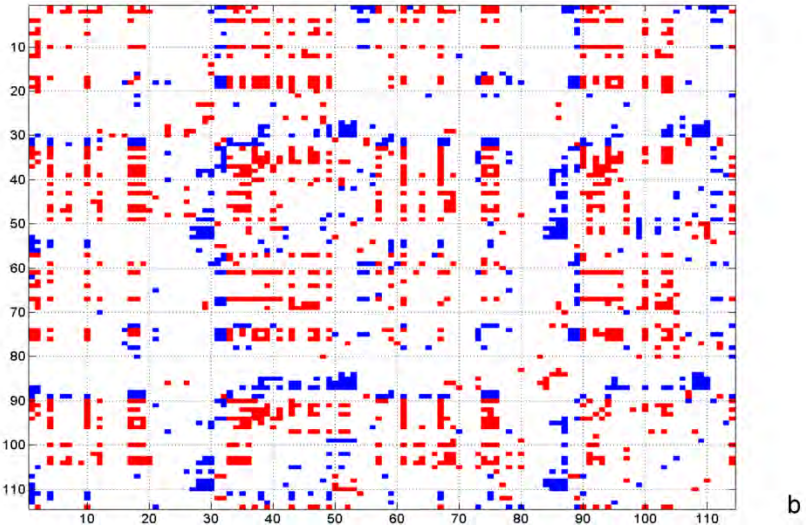
10
20
30
40
50
60
70
80
90
100
110
b

Table 2.3. List of nine major anatomical-functional systems. From left: the first column lists the number of each system (the same number indicated in the leftmost column of Table 2.1); the second column lists the abbreviation of each system used in Figure 2.6; and the third column lists the full name of each system.

Group number	Abbreviation in Figure 2.3	Anatomical-functional system
1	sensorymotor	sensory-motor
2	polymodal	polymodal association
3	RH	retrohippocampal regions
4	HP	hippocampus
5	AMG	amygdala complex
6	striatum	striatum
7	pallidum	pallidum
8	thalamus	thalamus
9	hypothalamus	hypothalamus
0		not included

Figure 2.6. Significantly (a) decreased and (b) increased functional connectivity during the anesthetized state. ROIs of the whole brain were divided into nine major functional-anatomical groups (Table 2.3) based on the Swanson Atlas (Swanson, 2004). The weight of edges in both graphs was proportional to the percentage of the total number of significantly changed connections relative to the total number of all possible connections between the two groups. The node size was proportional to the percentage of the total number of significantly changed connections within the group divided by the total number of all possible connections within the group. A, anterior, P, posterior, V, ventral, D, dorsal.

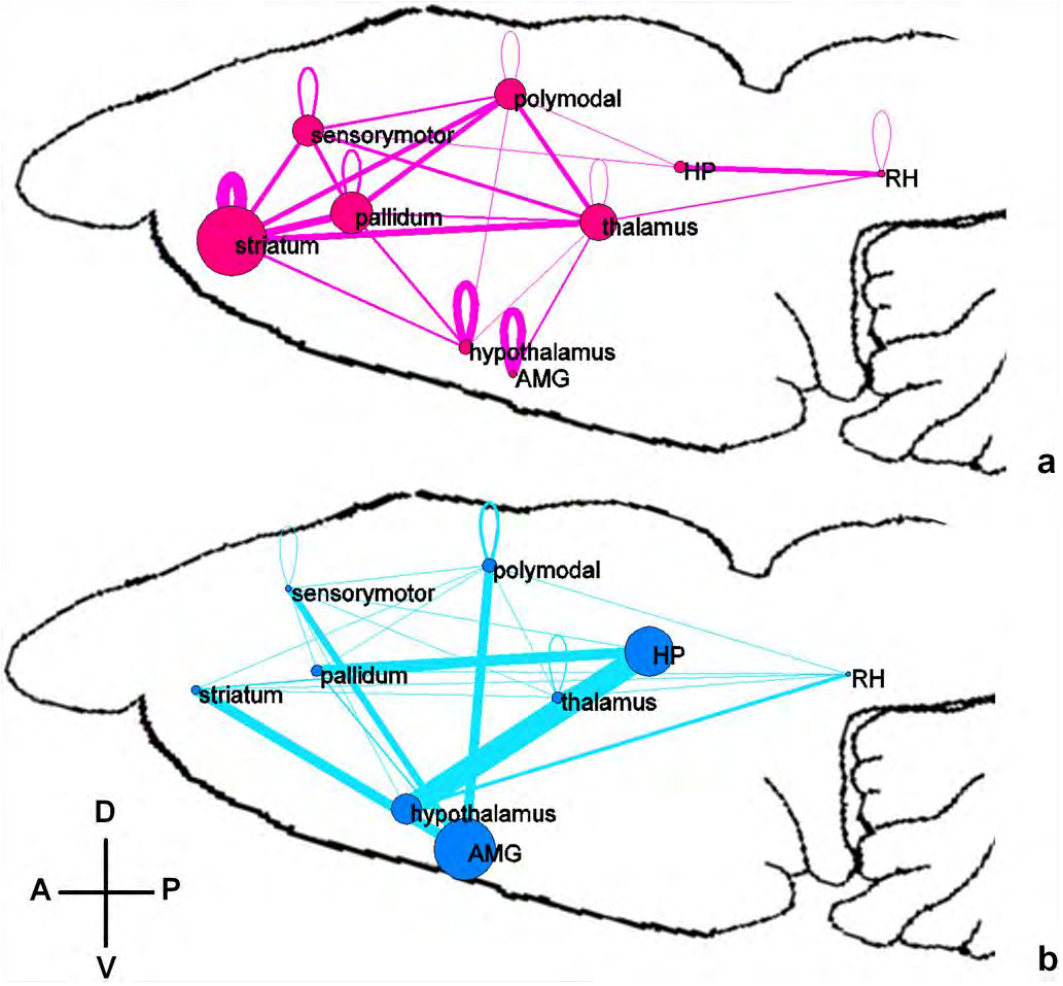
polymodal
sensorymotor
HP
RH
pallidum
thalamus
striatum
hypothalamus
AMG
a
polymodal
sensorymotor
HP
pallidum
striatum
thalamus
RH
hypothalamus
AMG
D
A
P
V
b

anesthesia (Figure 2.7, p value<0.0001). More importantly, there was a significant interaction effect (p value=0.022) between the category of thalamic nuclei (i.e. related to associative or sensory-motor cortices) and awake/anesthetized conditions. Thus, this result clear indicates that thalamo-cortical connectivity in associative networks was more affected than that in low-level sensory-motor networks under anesthesia.

The relationship between the strength and physical distance of functional connections

It has been long hypothesized that anesthesia affects the information integration of neural networks by reducing long-distance functional connections (Alkire et al., 2008). To elucidate this issue, we examined the relationship between the physical distance and connectivity strength across all functional connections. Figure 2.8 demonstrated that FC strength nonlinearly decreased as the physical distance between two ROIs increased for both awake and anesthetized conditions (Figure 2.8, insert). However, in the long-distance range (>10mm), the connectivity strength appeared to "rebound", and this trend was even more pronounced in the anesthetized condition. In contrast, the strength of short-distance connections was decreased at the anesthetized condition. Taken together, our results suggest that long-distance connections were not preferentially reduced at the anesthetized condition.

Discussion

In the present study we have examined changes in whole-brain neural networks in anesthetized rats. Our results suggested that functional neural networks were reorganized

Figure 2.7. Connectivity strength changes in thalamo-cortical connections between the awake and anesthetized conditions. The thalamus was segregated into seven nuclei. Among these nuclei, MG, LG and VENT are related to low-level sensory-motor cortices. ATN, LAT, MED and MTN are related to high-level associative cortices (Swanson, 2004). Sensory-motor: FC between sensory-motor cortices and thalamic nuclei related to sensory-motor cortices. Associative: FC between associative cortices and thalamic nuclei related to associative cortices. ANOVA analysis: Factors: thalamic nuclei (sensory-motor/associative), condition (awake/anesthetized). P_nuclei = 0.2, p_condition <0.0001, p_interaction = 0.022.

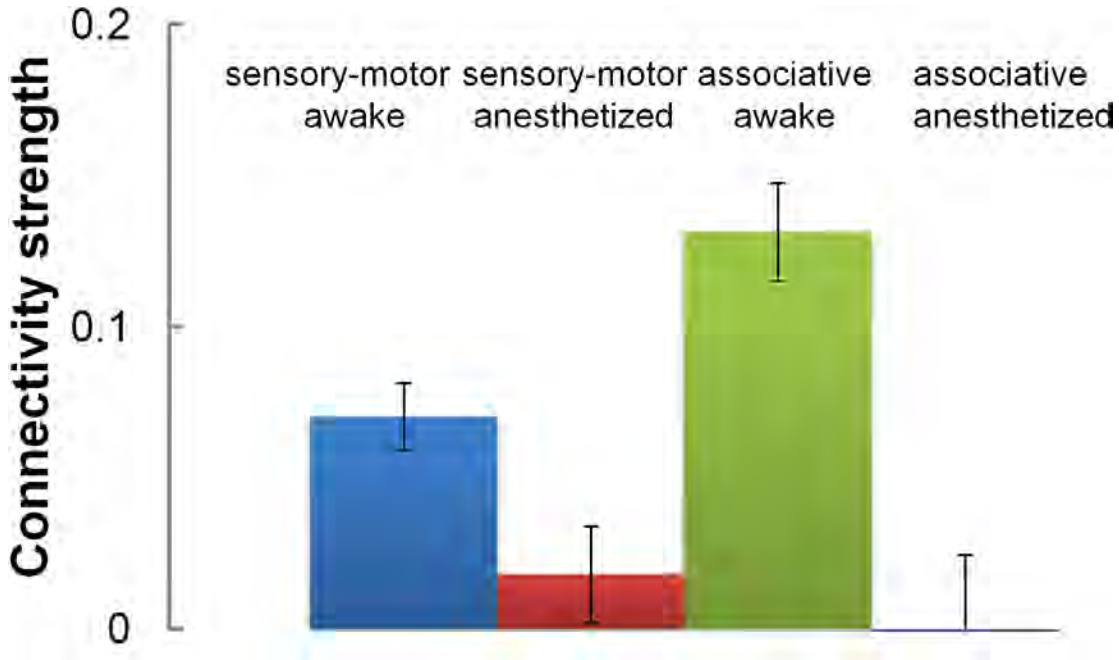
Connectivity strength
0.2
0.1
0
sensory-motor awake
sensory-motor anesthetized
associative awake
associative anesthetized

Figure 2.8. Connectivity strength as a function of physical distance. Anesthesia does not preferentially reduce long-distance functional connections. Bars are S.E.M. Insert, scatter plots of functional connectivity strength versus physical distance. Left panel: awake state, right panel: anesthetized state. X axis, physical distance of the functional connection (mm); Y axis, connectivity strength.

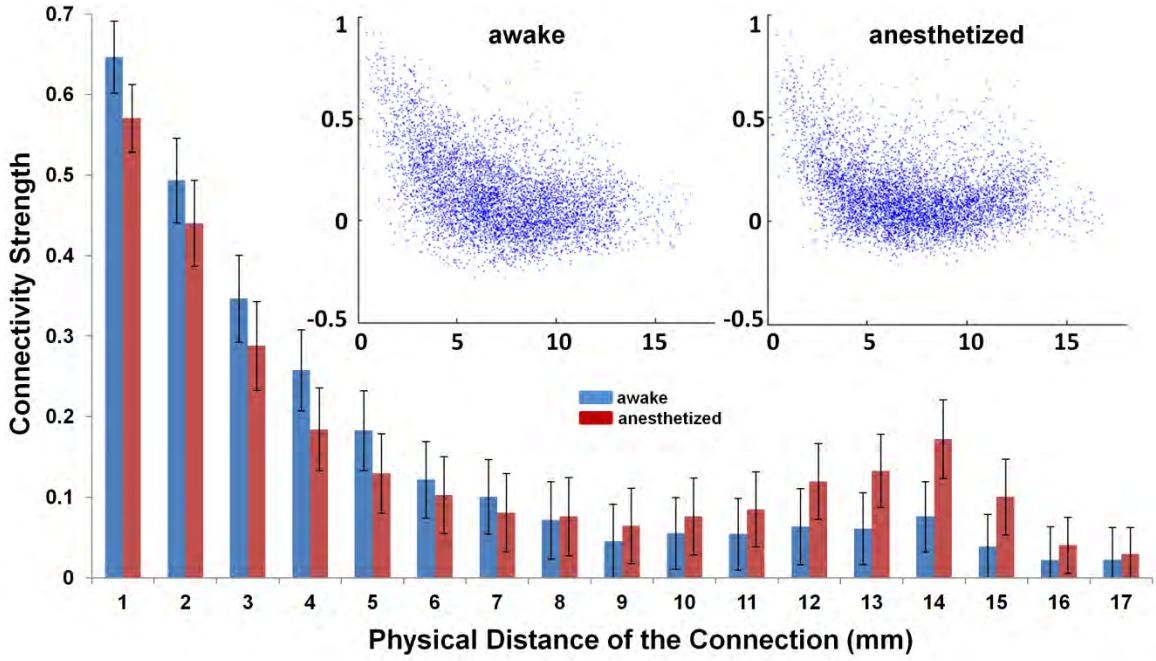
awake
anesthetized
awake
anesthetized
Connectivity Strength
Physical Distance of the Connection (mm)

from the awake to anesthetized state, and this reorganization was governed by the same topological principles. One remarkable finding was that although the connectivity strength was on average decreased in the anesthetized condition, long-distance connections were not preferentially reduced. To our knowledge, this is the first study to examine the reconfiguration of the architecture of large-scale resting-state neural networks in the anesthetized state by directly comparing topological features and connectivity strength between the awake and anesthetized brains in animals.

Perhaps the most important finding of the present study is the preservation of global topological characteristics of the whole-brain neural network in the anesthetized state. Among all global network metrics calculated, only global clustering coefficients showed a marginal but statistically insignificant decrease ($p=0.18$). Mean shortest path length was even slightly shorter in the anesthetized condition, suggesting the overall information integration capacity was not impaired in the anesthetized rat brain. Likewise, small-worldness and modularity did not show any changes between the two states, again indicating a similar level of modular organization. Numerous human rsfMRI studies have showed altered topological features of the global network (e.g. global clustering coefficient) in various neurological and psychiatric diseases (Bassett and Bullmore, 2009), implying that the architecture of the brain network might be sensitive to pathological disruptions. Given the profound impact of anesthesia on brain functions, it is striking that the anesthetized brain was able to maintain intact global organization. However, this result was indeed consistent with a previous human EEG study, in which global scale-free organization was found to be preserved across consciousness, anesthesia and

recovery states (Lee et al., 2010). Therefore, this conclusion is very likely not limited to the specific spatial and temporal scales of the rsfMRI technique. An important implication of this finding is that, unlike disrupted global networks in pathological conditions, the brain is able to maintain intact topological structures under pharmacologically induced unconsciousness. This property might be related to the ability of the brain to quickly recover from the unconscious state to the conscious state once the anesthetic is discontinued. It may also suggest that the governing principles of intrinsic brain organization might be fundamental characteristics of the healthy brain.

Despite similar global network topology, local neural networks were considerably re-organized in the anesthetized rat brain. For instance, local clustering coefficients of the nucleus accumbens and septal nuclei were significantly reduced by anesthesia, suggesting those regions were less connected to their neighboring regions in the anesthetized condition. Interestingly, these two regions were reported to enhance anesthetic effects when they were pharmacologically inactivated (Ma et al., 2002; Ma and Leung, 2006). In addition, a rat study reported reduced glutamate and *aspartate* levels in the nucleus accumbens during sleep (Lena et al., 2005). These results and the findings in the present study collectively underscore the importance of the nucleus accumbens and septal nuclei in anesthetic-induced unconsciousness. Furthermore, several thalamic nuclei showed a significant reduction in betweeness centrality, indicating reduced information relay in the thalamus in the anesthetized rat brain. Consistent with the report by Boveroux et. al. (Boveroux et al., 2010), we also observed a preferential reduction in high-level thalamo-cortical connectivity relative to low-level thalamo-cortical connectivity under anesthesia

(Figure 2.7). Taken together, these findings well agree with the extensive literature regarding the role of thalamus in anesthesia and (un)consciousness (Nallasamy and Tsao, 2011). Moreover, detailed community structure considerably differed even at a similar global modularity (Q) value. Consistent with our previous study (Liang et al., 2011), modules in the awake brain were more likely to contain both cortical and sub-cortical regions, whereas modules in the anesthetized brain tend to include only cortical or only subcortical regions, implying compromised communications between the cortex and subcortex. Taken together, these results clearly suggested that although the global organizational principles were not changed at the anesthetized state, the brain networks are locally reorganized to support new patterns of information integration among neuronal groups.

It has been repeatedly reported that anesthesia can change FC strength between brain regions (Peltier et al., 2005; Boveroux et al., 2010; Martuzzi et al., 2010; Stamatakis et al., 2010). For instance, our previous study reported decreased anticorrelated FC between the infralimbic cortex and amygdala in anesthetized rodents (Liang et al., 2012a). Additionally, Liu and colleagues found that FC decreased as the anesthetic depth increased (Liu et al., 2011). Consistent with these results, in the present study we found that the connectivity strength was on average weaker in the anesthetized condition. When individually comparing the corresponding functional connections between the awake and anesthetized states, most significantly changed connections were weaker in connectivity strength at the anesthetized condition, and these connections were spatially distributed throughout cortical and subcortical areas (Figure 2.5). Therefore, our

data indicated that the effect of anesthesia was widespread across the whole brain. However, it has to be noted that anesthesia did not uniformly affect all brain regions and functional connections. In fact, the basal ganglia area including the striatum and pallidum showed the largest decrease in FC strength. By contrast, a number of functional connections showed increased connectivity strength in the anesthetized state particularly in hippocampus, hypothalamus and amygdala. These brain regions and connections are relatively less studied regarding their roles in anesthesia. Interestingly, all these regions are part of the limbic system which generally subserves the functions of emotion, memory and homeostatic regulation. Therefore, it can be hypothesized that anesthesia, or perhaps unconsciousness in a more general case, can lead to hyper-synchrony in this part of the limbic system.

Another interesting aspect of connectional strength is its relation with the physical distance of the functional connection. It has been suggested that the disruption of long-distance functional connections, in particular fronto-parietal connections, contributes to unconsciousness (Laureys and Schiff, 2011). However, in the present study we observed that long-distance functional connections were not particularly diminished at the anesthetic-induced unconscious state, rather, the short-distance connections showed obvious reductions (Figure 2.8). This result suggests that the disruption of long-distance connectivity is not necessarily a general mechanism of unconsciousness. However, it does not exclude the possibility that certain long-distance connections might play a key role in maintaining consciousness. Further studies are necessary to identify these potentially vital long-distance connections.

There are several methodological limitations in the present study. First, different levels of motion can affect network metrics as well as the connectional strength (Power et al., 2012; Satterthwaite et al., 2012; Van Dijk et al., 2012). This issue was particularly troublesome when the awake condition had higher motion level than the anesthetized condition. However, a stringent motion control was applied in our study to address this problem. Scans with head displacement more than 0.25mm (i.e. half voxel size) were discarded, and all scans were motion corrected and motion parameters were regressed out. It should be noted that even with the rigorous control of motion, the influence of motion on FC may still persist (Power et al., 2012; Satterthwaite et al., 2012; Van Dijk et al., 2012). To further examine this issue, global network metrics were recalculated from a subset of data with the smallest motion at the awake condition (movement<0.125mm). The motion level in this sub-dataset did not significantly differ from the anesthetized condition (p values >0.1). Results were in excellent agreement with those calculated from the whole dataset. Also, a very similar relationship between connectional strength and physical distance was obtained in this subset of data. Therefore, it is unlikely that different levels of motion can account for the changes between the two conditions observed in the present study. Second, the anesthetic agent used (i.e. isoflurane) is a vasodilator. The vasodilatory effect might have significant effects on the fMRI signal. However, Liu and colleagues (Liu et al., 2011) reported a strong neurovascular coupling in isoflurane-anesthetized rats, suggesting resting-state FC measured by rsfMRI in isoflurane anesthetized rats was mostly of neural origin. Third, only one type of

anesthetic agent was used at one dosage in the present study. Whether these results can be generalized to other anesthetic agents and/or different dosages needs to be confirmed.

The explicit neural mechanism underlying anesthetic-induced unconsciousness is likely to be extremely complex and manifests at various spatial and temporal scales. Here our results show that the integrity of the whole-brain network can be conserved in a wide physiologic range from awake to anesthetized states while local neural networks can flexibly adapt in new conditions. They also illustrate that the governing principles of intrinsic brain organization might represent fundamental characteristics of the healthy brain. With the unique spatial and temporal scale provided by rsfMRI, this study has opened a new avenue for investigating the neural mechanism underlying anesthetic-induced unconsciousness. Considering that all unconscious states share many the same endpoints in brain functions such as amnesia, analgesia, immobility and attenuation of autonomic responses to noxious stimulation (Paul G. Barash, 2009), our results may help to decipher other unconscious states such as coma.

Acknowledgement:

We thank Ms. Meghan Heffernan and Suzanne Czerniak for their discussions. This publication was made possible by the institutional fund from the University of Massachusetts Medical School and the NIH Grant Number 5R01DA021846-02 from the National Institute of Health.

CHAPTER III

Anticorrelated Resting-state Functional Connectivity in Awake Rat Brain

Zhifeng Liang, Jean King and Nanyin Zhang

Center for Comparative Neuroimaging, Department of Psychiatry,

University of Massachusetts Medical School, Worcester, Massachusetts

Abstract

Resting-state functional connectivity (RSFC) measured by functional magnetic resonance imaging has played an essential role in understanding neural circuitry and brain diseases. The vast majority of RSFC studies have been focused on positive RSFC, whereas our understanding about its conceptual counterpart—negative RSFC (i.e. anticorrelation)—remains elusive. To date, anticorrelated RSFC has yet been observed without the commonly used preprocessing step of global signal correction. However, this step can induce *artifactual* anticorrelation (Murphy et al., 2009), making it difficult to determine whether the observed anticorrelation in humans is a processing artifact (Fox et al., 2005). In this report we demonstrated robust anticorrelated RSFC in a well characterized frontolimbic circuit between the infralimbic cortex (IL) and amygdala in the awake rat. This anticorrelation was anatomically specific, highly reproducible and independent of preprocessing methods. Interestingly, this anticorrelated relationship was absent in anesthetized rats even with global signal regression, further supporting its functional significance. Establishing negative RSFC independent of data preprocessing methods will significantly enhance the applicability of RSFC in better understanding neural circuitries and brain networks. In addition, combining the neurobiological data of the IL-amygdala circuit in rodents, the finding of the present study will enable further investigation of the neurobiological basis underlying anticorrelation.

Introduction

Resting-state functional connectivity (RSFC) has been intensively and extensively studied using functional magnetic resonance imaging (fMRI) (Biswal et al., 1995). Resting-state fMRI (rsfMRI) measures spatial patterns of functional connectivity across the brain by detecting temporal correlations of low-frequency spontaneous fluctuations of the blood-oxygenation-level dependent (BOLD) signal. Using this technique, RSFC was consistently revealed in multiple networks in humans (Biswal et al., 1995; Lowe et al., 1998; Hampson et al., 2002; Greicius et al., 2003) and animals (Vincent et al., 2007; Zhang et al., 2010b; Liang et al., 2011), and was sensitive to effects like sleep, anesthesia and aging (Stevens et al., 2008; Horovitz et al., 2009). Additionally, altered RSFC was found in multiple pathological conditions (Greicius et al., 2007), indicating its vital neurobiological and psychopathological relevance (Kennedy et al., 2006; Albert et al., 2009). Taken together, it has been strongly suggested that RSFC plays a very important role in brain function.

Conceptually, temporal correlations of spontaneous BOLD fluctuations between functionally connected brain regions should include both positive and negative values. More importantly, positive and negative correlations in RSFC are most likely related to distinct neurophysiologic substrates underlying functional connections. To date, predominant efforts have been spent investigating positive RSFC, whereas negative correlation (i.e. anticorrelation) has been much less studied.

Anticorrelation was first reported between the default mode network (DMN) and task-positive network (TPN) in the human (Fox et al., 2005). This temporally inverse

correlation in spontaneous BOLD fluctuations was initially interpreted as competition or functional segregation for opposite goals between neural networks. Further, the strength of this anticorrelation was associated with response time in cognitive functions (Kelly et al., 2008) and performance in working memory tasks (Hampson et al., 2010). However, these interpretations were complicated by one commonly used fMRI preprocessing procedure–global signal regression (Murphy et al., 2009). This procedure was used to remove global physiological noise in resting-state functional images, and thus improved the spatial specificity of RSFC (Fox et al., 2009; Scholvinck et al., 2010). However, Murphy *et. al.* in their recent study pointed out that global signal removal can induce artifactual anticorrelation. This is because removal of the global signal ensures that the sum of correlation coefficients across all voxels within the whole brain must approach zero, and thus this procedure mandated anticorrelation (Murphy et al., 2009). Although several preprocessing methods were proposed subsequently in hope to overcome the limitation of global signal regression, contradicting results were obtained (Chang and Glover, 2009a; Anderson et al., 2011). For instance, it was reported that anticorrelation between DMN and TPN was present with or without model-based physiological noise correction (Chang and Glover, 2009a) and this anticorrelation was not static (Chang and Glover, 2010). Anderson and colleagues, however, reported the absence of anticorrelation between DMN and TPN using phase-shifted soft tissue regression (Anderson et al., 2011).

The ambiguity of anticorrelated RSFC has become a major obstacle to further understanding its neurophysiologic mechanism and has significantly limited its applicability. Therefore, validating the existence of anticorrelation that is independent of preprocessing methods is of critical importance particularly considering the possibility

that negative RSFC might represent a group of functional connections with a distinct neurophysiologic mechanism and thus could be crucial for better understanding of neural circuitries and brain diseases. In order to achieve this goal, identifying a neural circuit with robust negative RSFC is a crucial step.

Well-documented reports of the neural circuit between infralimbic cortex (IL) and amygdala in the rat (Pape and Pare, 2010) have shed light on the aforementioned issue. This frontolimbic circuit has been extensively studied in several aspects: Anatomically, IL and amygdala share dense reciprocal interconnections (Russchen, 1982b, a; Sesack et al., 1989; McDonald, 1998). Functionally, neurobiological evidence indicates that IL plays a role of inhibitory regulation of the amygdala (Rosenkranz and Grace, 2001). Specifically, IL sends glutamatergic projections to intercalated cells of the amygdala (Berretta et al., 2005; Amano et al., 2010). Intercalated interneurons in turn send GABAergic projections to central amygdala nucleus, thus enabling IL to exert inhibitory modulation on amygdala. Additionally, electrophysiological studies indicate that the stimulation of IL area suppresses the basolateral amygdala activity (Rosenkranz and Grace, 2001; Likhtik et al., 2005), and decreases the responsiveness of central amygdala (Quirk and Gehlert, 2003; Quirk et al., 2003). Based on these findings, we hypothesize that anticorrelated RSFC should be present within the IL-amygdala circuit. To test this hypothesis, in the current study we have systematically examined the temporal relationship of spontaneous BOLD fluctuations between IL and amygdala using rsfMRI in awake and isoflurane-anesthetized rats (Zhang et al., 2010b; Liang et al., 2011). We reported robust anticorrelated RSFC within the IL-amygdala circuit regardless of global signal regression in awake rats. This anticorrelation, however, disappeared in

anesthetized rats even with global signal regression. Time-frequency dynamics of this negative functional connectivity were also examined using wavelet analysis.

Materials and Methods

Animals

Twenty four adult male Long-Evans (LE) rats (300 – 400 g) were obtained from Charles River Laboratories. Animals were housed in Plexiglas cages and maintained in ambient temperature (22-24 °C) on a reversed 12-h light:12-h dark cycle. Food and water were provided *ad libitum*. All studies were approved by IACUC Committee of the University of Massachusetts Medical School.

Acclimation procedure

Rats were acclimated to MRI restraint and noise as described in our previous studies (King et al., 2005). Briefly, rats were anesthetized with isoflurane and secured in Plexiglas stereotaxic head holders using plastic ear-bars. EMLA cream was applied topically to minimize pain of mechanical restraint. Animals were then placed into a black opaque tube 'mock scanner' with tape-recorded scanner noises. Animals were acclimated for eight days, one session per day. The time of exposure was increased from 15 minutes on the first day to 90 minutes on days 6, 7 and 8, with an increment of 15 minutes per day.

Animal preparation

Animal was briefly anesthetized using isoflurane and fitted into a head restrainer with a built-in coil. The head was placed into the cylindrical head-holder with the canines secured over a bite bar, the nose secured with a nose clamp, and ear bars positioned inside the head-holder with adjustable screws fitted into lateral sleeves. The body of the animal was then placed into a body restrainer. After this setup procedure was completed, the isoflurane was removed and the restraining system was positioned in the magnet for imaging under awake condition.

Rats (16 of the 24) underwent the imaging session in the anesthetized condition at minimal 7 days after being imaged at the awake condition. The animal preparation procedure was the same as in the awake condition. Isoflurane gas (2%) was then delivered to the animal through a nose cone in the magnet to maintain the anesthetized state. The body temperature of the animal was monitored and maintained at 37°C ± 0.5°C using a feedback controlled heating pad. Imaging sessions started at least 15-20 mins after animals were placed in the magnet.

MR experiments

All experiments were carried out on a Bruker 4.7T/40cm horizontal magnet (Oxford, UK) interfaced with a Biospec Bruker console. A dual ^{1}H radiofrequency (RF) coil configuration (Insight NeuroImaging Systems, Worcester, MA) consisting of a volume coil for exciting the water proton spins and a surface coil for receiving MRI signal was used. The volume and surface coils were actively tuned and detuned to prevent mutual coil coupling.

For each session, anatomical images were acquired using a fast spin-echo sequence (RARE) with the following parameters: TR = 2125ms, RARE factor = 8, TE = 50ms, matrix size = 256×256, FOV = 3.2cm×3.2cm, slice number = 18, slice thickness = 1mm. Gradient-echo images covering the whole brain were then acquired using the echo-planar imaging (EPI) sequence with the following parameters: TR = 1s, TE = 30ms, flip angle = 60°, matrix size = 64×64, FOV = 3.2cm×3.2cm, slice number=18, slice thickness = 1mm. Two hundred volumes were acquired for each run, and six runs were obtained for each session.

Pre-processing of imaging data

Part of the raw rsfMRI data (16 out of 24 rats) were from a previous study (Liang et al., 2011) and reprocessed for the purpose of the present study. Data from the other 8 (out of 24) rats were acquired for the present study.

Imaging data was preprocessed using Medical Image Visualization and Analysis (MIVA, http://ccni.wpi.edu/), Statistical Parametric Mapping (SPM8) software (Wellcome Department of Cognitive Neurology, London, UK) and MATLAB (Mathworks, Inc., Sherborn, MA). All images were first aligned and co-registered to a fully segmented standard rat atlas in MIVA (Zhang et al., 2010b; Liang et al., 2011). The registration procedure provided the coordinates of each seed ROI in the image space. In this study two seed regions of interest, bilateral IL and bilateral amygdala, as well as a control seed region, unilateral (right) motor cortex, were selected (as shown in Figure 3.1). After registration, all functional images were pre-processed with steps of motion correction, spatial smoothing (FWHM = 1mm), voxel-wise linear detrending and 0.002-

0.1Hz band-pass filtering. Data sets with excessive motion (>0.5 mm, 17 runs in total) were discarded. The time course for each individual voxel was further corrected for head movement by regression on the six motion parameters (translations and rotations) estimated in the procedure of motion correction. The global signal was estimated by averaging the time courses of all voxels inside the whole-brain mask. The ventricle and white matter signal was estimated by averaging the time courses of all voxels inside the ventricle and white matter.

Functional connectivity analysis

Functional connectivity was evaluated using seed-based correlational analysis on a voxel-by-voxel basis (Zhang et al., 2010b). Regionally averaged time courses from all voxels inside the seed regions were used as reference time courses. Pearson cross-correlation coefficients between reference time courses and the time course of each individual voxel were calculated. This correlational analysis was carried out for each run. Correlation coefficients were transformed using Fisher's z transformation and then averaged across runs and animals. Subsequently, the averaged z values were transformed back to r values, yielding a mean correlation map for each seed. RSFC maps were displayed by thresholding the correlation coefficient at 0.21 and a cluster size of 10 voxels (equivalent to uncorrected $p<0.001$) (Forman et al., 1995). The reliability of functional connectivity was examined through inter-subject reproducibility. Animals were randomly divided into two subgroups and functional connectivity maps were separately created for each group. The strength of functional connectivity was quantitatively compared on the voxel-by-voxel basis between the two subgroups.

Figure 3.1. Seed ROI definitions. Three seed ROIs were used in the present study: bilateral infralimbic cortex (IL), bilateral amygdala and unilateral (right) motor cortex. All ROIs were defined based on a fully segmented standard rat atlas in MIVA and overlaid on anatomical images (Zhang et al., 2010b; Liang et al., 2011). Distances to Bregma (mm) are labeled at the bottom of each image.

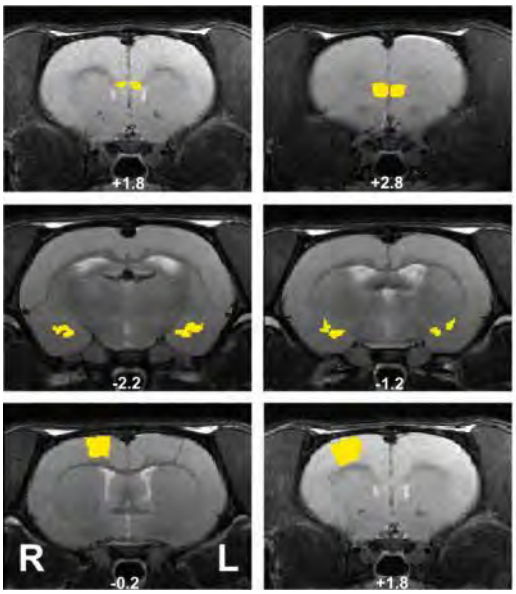

Bilateral IL

Bilateral Amygdala

Right Motor Cortex

Wavelet analysis

Wavelet transform coherence (WTC) was previously utilized for analyzing dynamic changes between rsfMRI time series (Chang and Glover, 2010). This approach was used in the present study to investigate the dynamics of the anticorrelated relationship between time courses of IL and amygdala. Briefly, the continuous wavelet transform of a time series (x_n, n=1,2…N) with equal time step Δt was defined as:

$$W^X(n,s) = \sqrt{\frac{\Delta t}{s}} \sum_{n=1}^{N} x_n \psi^0 \left[(n - n) \left(\frac{\Delta t}{s} \right) \right] \qquad [1]$$

where n is the time index, s is the time scale, and ψ^0 is the Morlet wavelet as follows:

$$\psi_0(\eta) = \pi^{-1/4} e^{i\omega_0 \eta} e^{-\frac{1}{2}\eta^2} \qquad [2]$$

where ω_0 is dimensionless time and set at 6, η is dimensionless frequency. The wavelet power was defined as $|W^X(n,s)|^2$. Similarly, the cross wavelet transform (XWT) for two time series is defined as

$$W^{XY}(n,s) = W^X(n,s) W^{Y*}(n,s) \qquad [3]$$

Where * denotes complex conjugation. XWT evaluates the common power of two time series in time frequency space. To evaluate the coherence of cross wavelet transform, cross wavelet coherence was calculated as follows:

$$R_n^2(s) = \frac{\left| S(s^{-1} W_n^{XY}(s)) \right|^2}{S(s^{-1} \left| W_n^X(s) \right|^2) \cdot S(s^{-1} \left| W_n^Y(s) \right|^2)} \qquad [4]$$

Cross wavelet coherence can be seen as local "correlation coefficients" in time frequency space. The statistical significance was determined using Monte Carlo methods. Wavelet

transform coherence and cross-wavelet transform were implemented with a matlab toolbox provided by Grinsted et. al. (http://www.pol.ac.uk/home/research/waveletcoherence/), and detailed information could be found in Ref. (Grinsted et al., 2004).

Results

Anticorrelated relationship between amygdala and infralimbic cortex

Figure 3.2 showed the RSFC maps from the seed of IL. Anticorrelated functional connectivity between IL and amygdala was evident without any global signal correction (referred to as "uncorrected" hereafter) (Fig 3.2a). Interestingly, negative RSFC from IL was only observed in amygdala while positive RSFC was widely spread across cortical and subcortical areas. With the correction of the global signal (Fig 3.2c), the spatial location of anticorrelation remained in amygdala. In addition, anticorrelation was also observed in some other regions such as hypothalamus (HT) after global signal regression. By contrast, the wide spread positive RSFC seen in the uncorrected map was greatly confined to more anatomically specific regions including anterior cingulate cortex (ACC), septum, caudate-putamen (CPU), neuclus accumbens (NAcc), and dorsal lateral prefrontal cortex (dlPFC). These results were consistent with the previous literature suggesting that global signal regression significantly improved the spatial specificity of positive RSFC (Fox et al., 2009). The RSFC map obtained after removing the white matter and ventricle signal (Fig. 3.2b) showed an intermediate pattern between the uncorrected map (Fig. 3.2a) and the map corrected for the global signal (Fig. 3.2c), also consistent with the results in human studies (Fox et al., 2009).

Figure 3.2. IL RSFC maps. (a) The IL RSFC map in the awake condition without correction of any global signal. (b) The IL RSFC map in the awake condition with correction of the ventricle and white matter signal. (c) The IL RSFC map in the awake condition with correction of the global signal. (d) The IL RSFC map in the anesthetized condition with correction of the global signal. Data from all maps were corrected for six movement parameters. All maps were overlaid on anatomical images. Distances to Bregma (mm) are labeled at the bottom of each image.

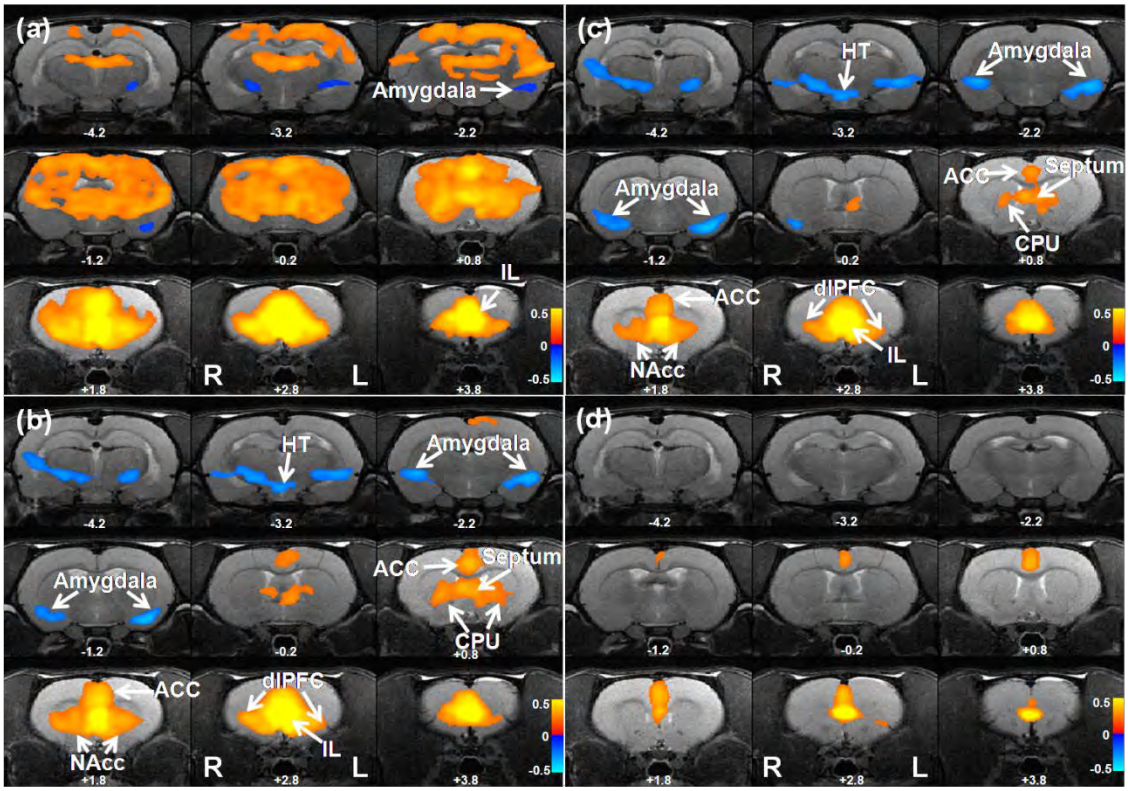
(a)
Amygdala
-4.2
-3.2
-2.2
-1.2
-0.2
+0.8
IL
0.5
0
-0.5
R
L
+1.8
+2.8
+3.8
(c)
HT
Amygdala
ACC
Septum
CPU
dlPFC
NAcc
(b)
(d)

The reciprocal anticorrelated relationship between the amygdala and IL can be observed in the RSFC maps from the amygdala as shown in Figure 3.3. Negative RSFC was clearly observed in IL in the uncorrected map (Fig. 3.3a). Similarly, corrections of the ventricle and white matter signal (Fig. 3.3b) as well as the global signal (Fig. 3.3c) significantly improved the spatial specificity of positive RSFC between amygdala and HT, as well as between amygdala and hippocampus. The anticorrelation between amygdala and IL remained largely the same. Additionally, some other regions such like CPU also showed an anticorrelated relationship with amygdala after global signal removal. Figure 3.2 and 3.3 collectively showed high anatomical specificity of the reciprocal anticorrelated relationship between the amygdala and IL.

Absence of anticorrelation in anesthetized rats

Considering that one major function of the IL-amygdala circuitry is regulating affective behaviors, it can be expected that anesthesia will disrupt the functional connectivity within the IL-amygdala circuit. Indeed, our data showed that the anticorrelated relationship between IL and amygdala observed in awake rats was completely abolished in isoflurane-anesthetized rats even with the global signal correction as shown in both Fig 3.2d and Fig 3.3d. This remarkable difference indicated that: i) the anticorrelated relationship observed in awake rats was not induced by preprocessing methods because the same preprocessing methods were applied to both awake and anesthetized rats data, and ii) the anticorrelation between amygdala and IL has important functional relevance that is impacted by anesthesia.

Figure 3.3. Amygdala RSFC maps. (a) The Amygdala RSFC map in the awake condition without correction of any global signal. (b) The Amygdala RSFC map in the awake condition with correction of the ventricle and white matter signal. (c) The Amygdala RSFC map in the awake condition with correction of the global signal. (d) The Amygdala RSFC map in the anesthetized condition with correction of the global signal. Data from all maps were corrected for six movement parameters. All maps were overlaid on anatomical images. Distances to Bregma (mm) are labeled at the bottom of each image.

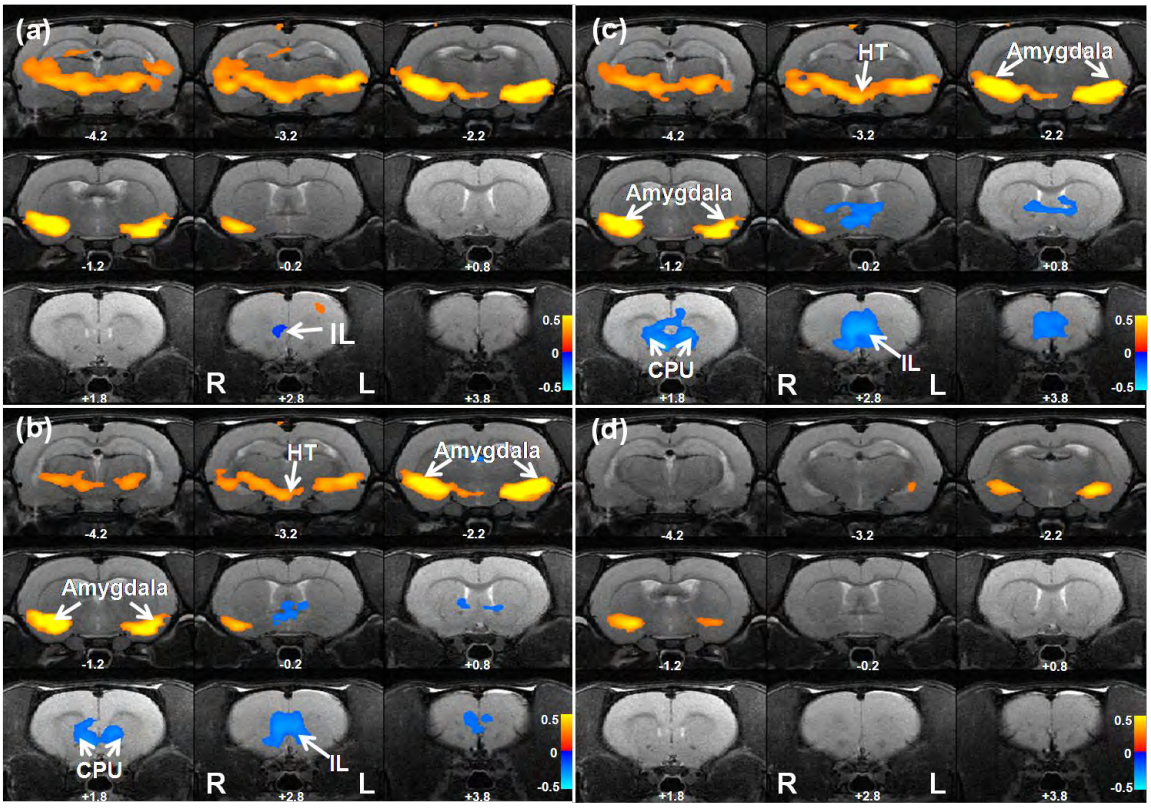
(a)
-4.2
-3.2
-2.2
-1.2
-0.2
+0.8
IL
R
L
+1.8
+2.8
+3.8
0.5
0
-0.5
(c)
HT
Amygdala
Amygdala
CPU
IL
(b)
HT
Amygdala
Amygdala
CPU
IL
(d)

RSFC maps of unilateral motor cortex

In order to examine the specificity of the anticorrelation between amygdala and IL, a control seed region unilateral motor cortex was also selected. Figure 3.4 demonstrated the RSFC maps of unilateral (right) motor cortex in awake (Fig. 3.4a) and anesthetized (Fig. 3.4b) rats, respectively. Both maps were obtained after the global signal regression. In awake rats, we observed strong functional connections between right and the left motor cortices, whereas this bilateral connection was less apparent in anesthetized rats. This result is consistent with the notion that anesthesia reduced the strength of RSFC (Liu et al., 2011). More importantly, no anticorrelated RSFC was observed in either awake or anesthetized group, suggesting that the anticorrelated relationship observed between IL and amygdala was specific to the frontolimbic circuit as oppose to a general effect.

Distributions of correlation coefficients of RSFC between IL and amygdala

It was previously reported that global signal regression dramatically changed the distribution of computed correlation coefficients in RSFC maps: (i) artifactual negative correlations were induced, and (ii) the distribution became approximately normal with a mean correlation value close to zero (Fox et al., 2009). In the present study, we independently extracted regional mean time courses from amygdala and IL for each run, with or without global signal regression, and calculated their temporal correlation coefficients. Figure 3.5 showed the histograms of correlation coefficients before (Fig. 3.5a) and after (Fig. 3.5b) global signal regression. The distribution of correlation

Figure 3.4. RSFC maps from unilateral (right) motor cortex in (a) the awake condition and (b) the anesthetized condition. Both maps were obtained after global signal regression. Distances to Bregma (mm) are labeled at the bottom of each image.

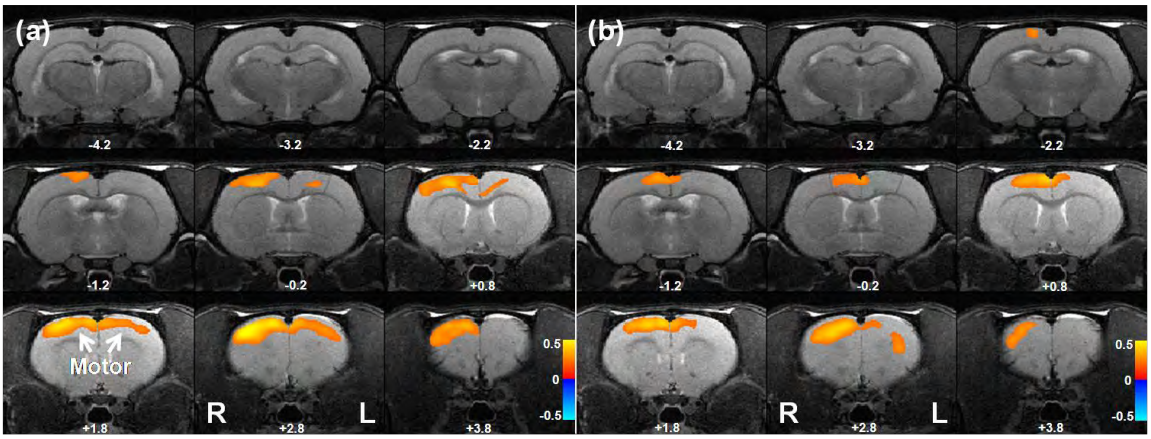
(a)
-4.2
-3.2
-2.2
-1.2
-0.2
+0.8
Motor
R
L
+1.8
+2.8
+3.8
0.5
0
-0.5
(b)
-4.2
-3.2
-2.2
-1.2
-0.2
+0.8
R
L
+1.8
+2.8
+3.8
0.5
0
-0.5

coefficients indeed shifted towards a Gaussian shape with global signal regression (Fig 3.5b). Nevertheless, the majority of correlation coefficients was in the negative range regardless of global signal regression (Fig. 3.5a, mean correlation coefficient = -0.20, Fig. 3.5b, mean correlation coefficient = -0.37).

Reliability of anticorrelation between amygdala and infralimbic cortex

To test the reliability of the anticorrelated relationship between spontaneous BOLD fluctuations in amygdala and IL, data from all animals were randomly divided into two subgroups and a RSFC map, with the seed of IL, was individually obtained for each subgroup. Figure 3.6a and 3.6b showed the RSFC maps from the two subgroups, demonstrating excellent consistency. Quantitatively, the computed correlation coefficients between the two RSFC maps well agree with each other on a voxel-by-voxel basis (Fig. 3.6c, $r = 0.58$, $p < 10^{-5}$). Similar results can be obtained from the seed of amygdala (data not shown). These results suggest that the anticorrelated relationship between amygdala and IL observed in awake rats was highly reliable.

Time-frequency dynamics of anticorrelation between amygdala and infralimbic cortex

WTC was utilized to investigate time-frequency dynamics of the anticorrelated relationship between amygdala and IL, with and without global signal regression. We observed a strong anti-phase relationship in cross-wavelet power and wavelet transform coherence between the time courses of IL and amygdala (Figure 3.7 showed one

Figure 3.5. Histograms of correlation coefficients between regional mean time courses of IL and amygdala (a) without and (b) with global signal regression.

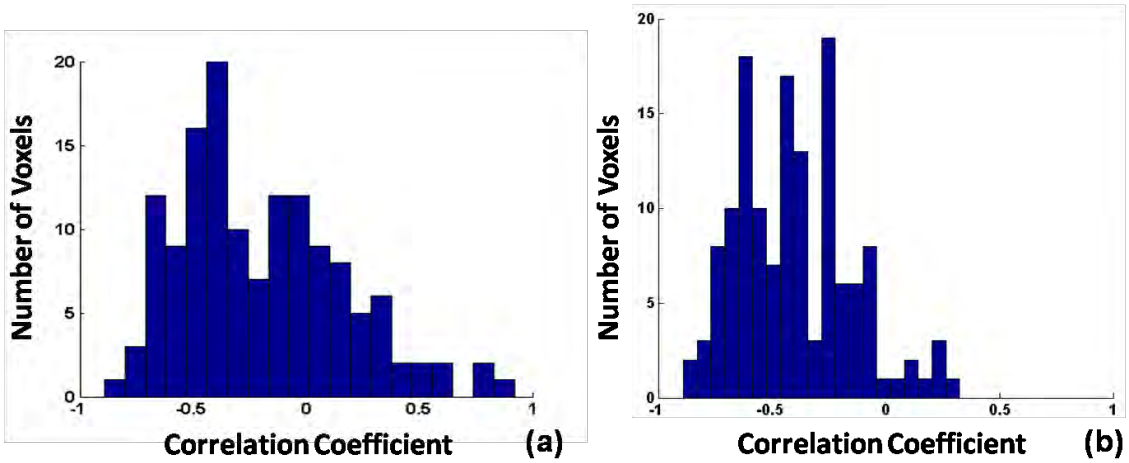
Number of Voxels
Correlation Coefficient
(a)
Number of Voxels
Correlation Coefficient
(b)

Figure 3.6. Reproducibility of anticorrelation between IL and amygdala. Data from all animals were randomly divided into two subgroups. (a) The IL RSFC map generated from one subgroup with global signal regression. (b) The IL RSFC map generated from the other subgroup with global signal regression. Distances to Bregma (mm) are labeled at the bottom of each image. (c) The voxel-to-voxel correlation of the RSFC strength between the two subgroups.

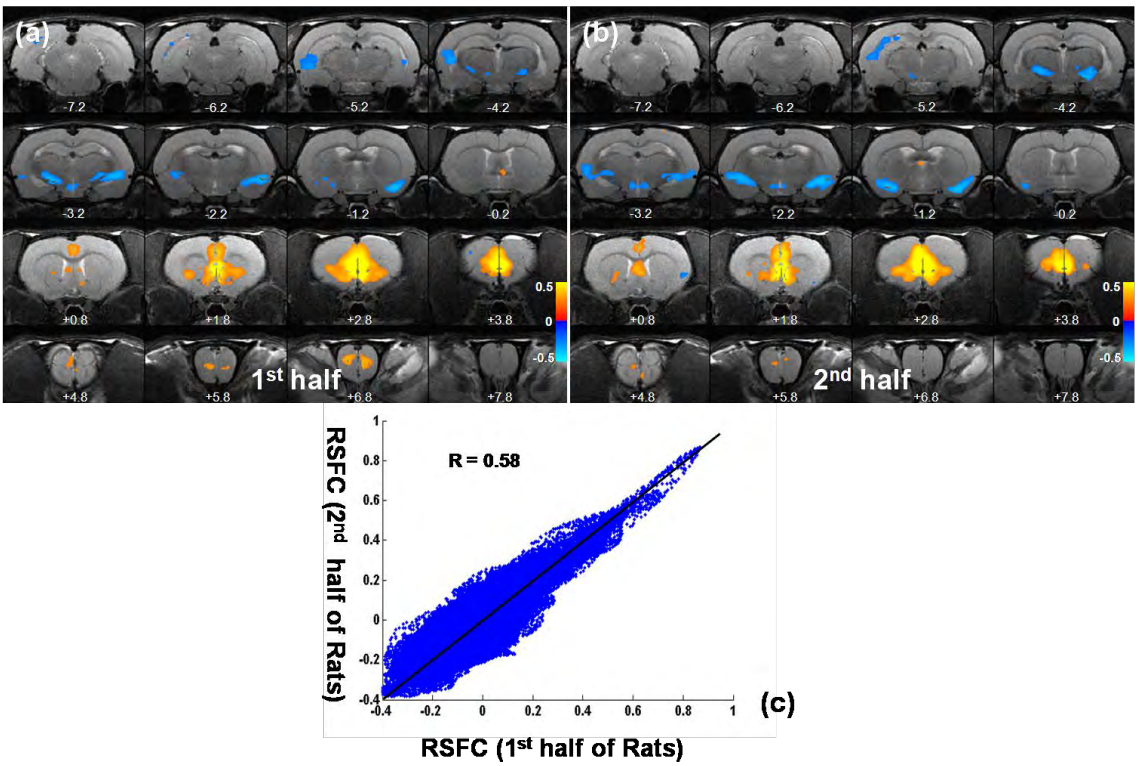
(a)
-7.2
-6.2
-5.2
-4.2
-3.2
-2.2
-1.2
-0.2
+0.8
+1.8
+2.8
+3.8
+4.8
+5.8
+6.8
+7.8
0.5
0
-0.5
1st half
(b)
2nd half
R = 0.58
RSFC (2nd half of Rats)
RSFC (1st half of Rats)
(c)

example), and this anti-phase relationship was relatively consistent throughout the whole scan. In addition, the anti-phase relationship was evident without global signal regression.

Discussion

In the present study we have characterized the anticorrelated temporal relationship between spontaneous BOLD fluctuations in IL and amygdala in awake rats. To the best of our knowledge, this is the first study investigating negative RSFC in animals. Independent of preprocessing methods, we observed robust anticorrelation within this anatomically well-defined frontolimbic circuit. In addition, this anticorrelation was highly reliable as reflected from its high reproducibility between two randomly divided subgroups. Moreover, this anticorrelation was between two distinct and distant anatomical regions, and contained high anatomical specificity. Furthermore, the anticorrelated relationship between the two regions was absent in anesthetized rats even with global signal regression. Taken together, data of the present study have provided strong evidence validating the existence of anticorrelated RSFC.

The influence of global signal regression

Although the presence of anticorrelation was independent of global signal regression, it was noticeable that global signal regression indeed affected the spatial pattern of RSFC maps and the distribution of correlation coefficients. Consistent with previous reports (Fox et al., 2009), global signal removal significantly improved the spatial specificity of positive RSFC. Interestingly, global signal regression enlarged areas

Figure 3.7. Wavelet transform coherence analysis revealed anti-phase relationship between IL and amygdala. (a) Cross wavelet power of IL and amygdala time series from one representative RSFC run. (b) Cross wavelet coherence of IL and amygdala time series from the same RSFC run. Time series in (a) and (b) were not corrected for the global signal. (c) Cross wavelet power of IL and amygdala time series from the same RSFC run after global signal regression. (d) Cross wavelet coherence of IL and amygdala time series after global signal regression. X axis represents time (sec) and Y axis represents period.

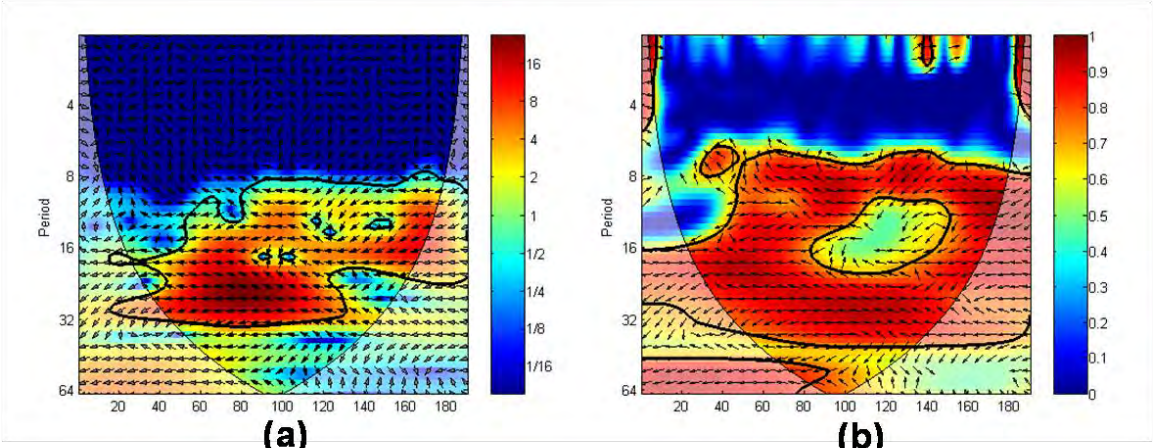
Period
4
8
16
32
64
20 40 60 80 100 120 140 160 180
16
8
4
2
1
1/2
1/4
1/8
1/16
1
0.9
0.8
0.7
0.6
0.5
0.4
0.3
0.2
0.1
0
(a)
(b)
Without correction

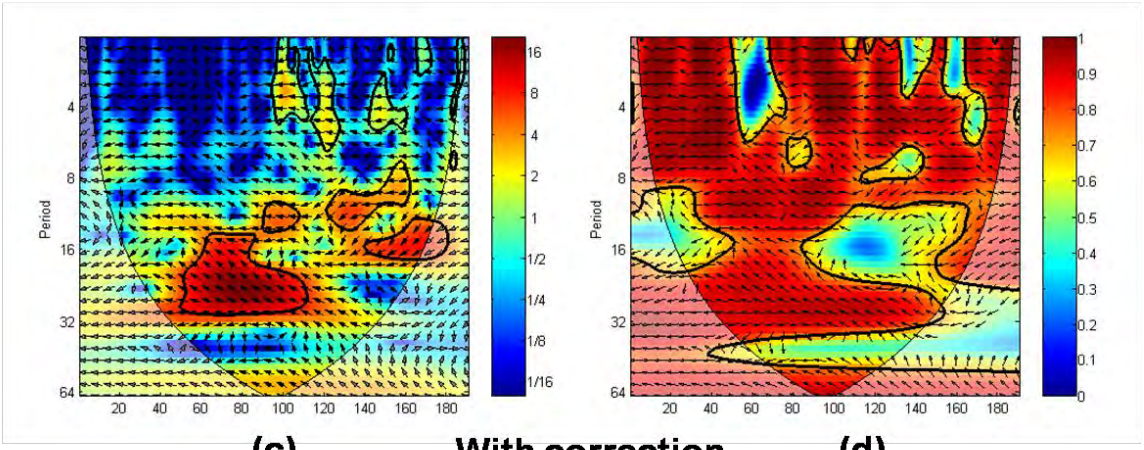
Period
4
8
16
32
64
20 40 60 80 100 120 140 160 180
16
8
4
2
1
1/2
1/4
1/8
1/16
1
0.9
0.8
0.7
0.6
0.5
0.4
0.3
0.2
0.1
0
(c)
With correction
(d)

of negative RSFC. Compared to uncorrected maps, additional regions such as hypothalamus (HT) showed anticorrelated relationship with IL (Fig. 3.2c), and CPU showed anticorrelated relationship with amygdala (Fig. 3.3c). Although the origin of these enlarged anticorrelated areas after global signal removal was not clear, we speculate that it could result from the propagation effect of indirect connectivity. It is well known that amygdala and HT are tightly connected as part of the *amygdala-hypothalamic*-pituitary-adrenal axis which is responsible for the autonomic stress/fear body response. This functional connection resulted in positive correlations between BOLD fluctuations in amygdala and HT as shown in Figs. 3.3b and 3.3c. Since IL and amygdala contained an anticorrelated relationship in their BOLD fluctuations, it can be predicted that this anticorrelated relationship would propagate to areas that were positively correlated to amygdala such as HT. This propagation effect, being masked by the global signal in uncorrected maps, became detectable after the global signal was removed. Similar argument can be used to explain the anticorrelation between amygdala and CPU appeared after global signal regression. However, it has to be noted that we cannot rule out the possibility that IL and HT are directly connected with an anticorrelated relationship. Further experiments are needed to resolve this issue.

The distribution of correlation coefficients between IL and amygdala was also altered by global signal regression, shifting to an approximately normal distribution centered at about CC=-0.37. However, it did not change the sign of the majority of correlation values. Taken together, although global signal regression indeed affected the resultant RSFC maps as expected (Murphy et al., 2009), it was clearly not attributing to the anticorrelated RSFC observed between IL and amygdala.

Impact of Anesthesia

The anticorrelated relationship between IL and amygdala was absent in the anesthetized condition. Accumulating evidence has suggested that anesthesia profoundly affects RSFC. For instance, Lu and colleagues demonstrated a dose-dependent decrease of cross-hemispheric functional connectivity in □-chloralose-anesthetized rats (Lu et al., 2007). Similarly, Liu et. al. found that intrinsic BOLD fluctuations and functional connectivity in the resting rat were strongly dependent on anesthesia depth (Liu et al., 2011). In human subjects, functional connectivity in the motor cortices was completely ablated with deep anesthesia (Peltier et al., 2005). Taken together, these results suggest that anesthesia significantly weakens RSFC relative to the awake condition. In the present study, anesthesia weakened the positive RSFC between left and right motor cortex (Fig. 3.4), and completely abolished the negative RSFC between IL and amygdala regardless of preprocessing procedures (Fig. 3.2d and Fig. 3.3d). These results were in line with previous animal imaging studies indicating that anesthesia reduces the amplitude of RSFC (Liu et al., 2011). More importantly, distinct difference between awake and anesthetized rats further ruled out the possibility that the anticorrelation observed at the awake condition was a processing artifact because the same preprocessing procedures were applied to both conditions. Furthermore, our data demonstrated that RSFC might serve as a sensitive marker for the functionality of brain circuitry given the fact that the IL-amygdala circuit is critically involved in affective behaviors that are impacted by anesthesia. This result also provided important evidence supporting the advantage of measuring RSFC in awake animals particularly in studies of neural

circuitries subserving cognitive and emotional functions (Zhang et al., 2010b; Liang et al., 2011).

Possible Neural Mechanism

The anatomy and function of the IL-amygdala circuit have been well studied using various methods. These studies may shed light on understanding the neural mechanism underlying the negative RSFC within this circuit. It is well known that the IL-amygdala circuitry is implicated in affective behaviors such as fear conditioning and extinction in rodents (LeDoux, 2000), as well as in emotion regulation in humans and nonhuman primates (Phelps et al., 2004; Phelps and LeDoux, 2005). In addition, malfunction in this circuit has been found to be tightly linked to mood and anxiety disorders (Shin et al., 2004). Anatomically, IL and amygdala share dense reciprocal connections (Russchen, 1982b, a; Sesack et al., 1989; McDonald, 1998). These physical connections provide the anatomical basis of the observed anticorrelated RSFC between the two regions. More importantly, there is substantial evidence suggesting IL could exert inhibitory regulation on amygdala. For instance, electrical stimulation of IL reduces responsiveness of central nucleus output neurons in the amygdala to basolateral amygdala (BLA) stimulation (Quirk and Gehlert, 2003), and chemical stimulation of IL activate cFos in the ITC neurons which are known to inhibit central nucleus output neurons (Pare and Smith, 1993). These results collectively suggest that the anticorrelated relationship between amygdala and IL observed in the present study could arise from an inhibitory interaction between them.

Time-frequency dynamics

One recent human study examined the anticorrelation between DMN and TPN by employing WTC and found that the anticorrelation between these two networks was not static (Chang and Glover, 2010). In the present study, wavelet analysis revealed a more stable anti-phase relationship between spontaneous BOLD fluctuations from IL and amygdala in awake rats. This difference may suggest a stronger anticorrelated relationship over time in rats and may also explain why it can be observed even in the mask of the global signal.

The influence of motion

In the present study, effects of movement in rats was minimized by using (i) motion correction; (ii) discarding data sets with excessive movement (> 0.5 mm, 17 sessions in total); and (iii) regressing out motion correction covariates. However, we did notice that movement of awake rats was significantly larger than that of anesthetized rats. There is the possibility that the difference in anticorrelation between awake and anesthetized rats was due to different levels of movement during data acquisition. To rule out this possibility, data from awake rats with minimal movement (< 0.125 mm, i.e. ¼ voxel size) were selected (33 sessions in total, 27.3% of the whole data set). In this subgroup, movement in awake rats was not significantly different from anesthetized rats (two-sample t-test, $p = 0.19$). Figure 3.8 showed that strong anticorrelated RSFC between amygdala and IL was persistent in this subgroup. This result suggests that the

anticorrelated RSFC observed in the present study cannot be attributed to the factor of movement.

Limitations and Future implications

Although the current study has shown for the first time robust fMRI anticorrelation in a system with known inhibitory connections, it cannot resolve the debate on the origin of anticorrelations in humans. There are important differences between the rat and human results which prohibit this extension. First, the rat anticorrelations are present even prior to global regression, but the human anticorrelations are not. Second, the rat anticorrelations are between two specific anatomic regions with known strong anatomical connections, the human anticorrelations are between two wide-spread networks. Nevertheless, the finding of this study makes it possible to uncover the neurophysiologic basis of anticorrelated RSFC when combining with other techniques such as neuron recordings. Since anticorrelated RSFC represents a group of functional connections with distinct neurophysiologic features, it can tremendously contribute to studies of neural circuitries and brain networks. More importantly, given the vital role that RSFC plays in regulating brain function at normal and pathological conditions, the results of the present study can help test the hypothesis that negative RSFC might serve as an important biomarker to evaluate the functionality of neural circuits at normal and

Figure 3.8. IL RSFC maps from a subgroup of awake rats with movement smaller than 0.125mm (a) without and (b) with global signal regression. Movement in this subgroup was similar to that in anesthetized rats (two sample t-test, $p = 0.19$).

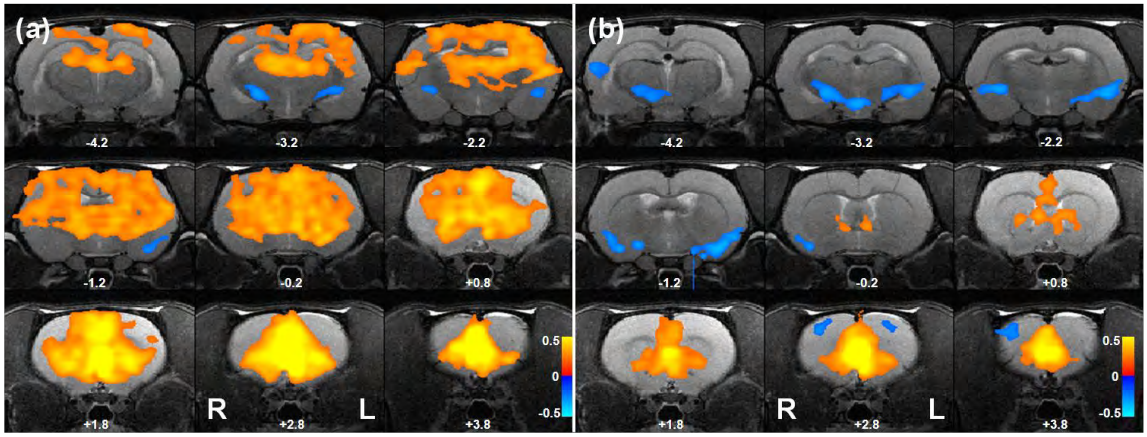
(a)
-4.2
-3.2
-2.2
-1.2
-0.2
+0.8
+1.8
R
+2.8
L
+3.8
0.5
0
-0.5
(b)
-4.2
-3.2
-2.2
-1.2
-0.2
+0.8
+1.8
R
+2.8
L
+3.8
0.5
0
-0.5

pathological conditions. Therefore, the present study has opened a new avenue to further expanding the applicability of rsfMRI.

Acknowledgement

We thank Dr Wei Huang and Ms Meghan Heffernan for their technical assistance. We also would like to thank anonymous reviewers for their insightful comments. This publication was made possible by the NIH Grant Number 1R01 MH067096-02 (PI: Jean King, PhD) and 5R01DA021846-02 (PI: Jean King, PhD) from the National Institute of Health, and the institutional fund from the University of Massachusetts Medical School. Its contents are solely the responsibility of the authors and do not necessarily represent the official views of the NIH.

CHAPTER IV

Mapping Thalamocortical Networks in the Rat Brain using Resting-State Functional Connectivity

Zhifeng Liang[1], Tao Li[2], Jean King[1] and Nanyin Zhang[1]

[1]Center for Comparative Neuroimaging, Department of Psychiatry, University of Massachusetts Medical School, Worcester, Massachusetts 01655, USA

[2]The Mental Health Center and the Psychiatric Laboratory, West China Hospital, Sichuan University, Chengdu, Sichuan 610041, China

Abstract

Thalamocortical connectivity plays a vital role in brain function. Anatomical and functional aspects of thalamocortical networks have been extensively studied in animals by numerous invasive techniques. Non-invasively mapping thalamocortical networks in humans has also been demonstrated by utilizing resting-state functional magnetic resonance imaging (rsfMRI). However, success in simultaneously imaging multiple thalamocortical networks in animals is rather limited. This is largely due to profound impact of anesthesia used in most animal experiments on functional connectivity measurement. Here we have employed an awake animal imaging approach to systematically map thalamocortical connectivity for multiple thalamic nuclei in rats. Seed-based correlational analysis demonstrated robust functional connectivity for each thalamic nucleus in the cortex, and the cortical connectivity profiles revealed were in excellent accordance with the known thalamocortical connectional relationship. In addition, partial correlation analysis was utilized to further improve the spatial specificity of thalamocortical connectivity. Functional connectivity maps generated by partial correlation were in remarkable agreement with the results from literature tracing studies. Taken together, these findings have provided important evidence supporting the validity of rsfMRI measurement in awake animals. More importantly, the present study has made it possible to non-invasively investigate the function, neuroplasticity and mutual interactions of thalamocortical networks in animal models.

Introduction

The thalamus and cerebral cortex are connected through well-organized connections. Studies have long revealed that the thalamus acts as the "gateway" for almost all extrinsic and intrinsic information before they reach the cortex via thalamocortical connections (Guillery and Sherman, 2002). More recently, research has suggested that the thalamus plays many significant roles that extend beyond the relay function. For instance, it has been shown that the interactions between the lateral geniculate (LG) nucleus—a thalamic nucleus that transmits visual information—is actively involved in information processing (Schmid et al., 2010), binocular rivalry (Haynes et al., 2005; Wunderlich et al., 2005), visual attention (O'Connor et al., 2002), perception and cognition (Saalmann and Kastner, 2009). In addition, the function of thalamus is critical to the states of wakefulness, sleep and consciousness (Alkire et al., 2008; Poulet et al., 2012). Furthermore, it has been reported that thalamocortical connectivity is essential for the establishment of oscillatory brain waves (Jones, 2001). Also importantly, abnormal thalamocortical connectivity has been observed in multiple brain disorders like schizophrenia (Welsh et al., 2010; Woodward et al., 2012), suggesting its vital psychopathological relevance.

Given the critical importance of thalamocortical networks, numerous studies have examined the anatomical and functional aspects of thalamocortical connectivity through a wide range of invasive techniques such as retrograde/anterograde tracing and electrophysiological methods (Krettek and Price, 1977; Van Groen and Wyss, 1995;

Vertes and Hoover, 2008). These studies have identified characteristic connectional patterns for separate thalamic nucleus groups (Swanson, 2004). Specifically, thalamocortical connections related to primary sensory and motor cortices are relatively simple and well organized. For instance, LG nucleus is predominantly connected to the visual system; medial geniculate (MG) nucleus is essentially connected to the auditory system; and ventral group of dorsal thalamus (VENT) is primarily linked to the sensorimotor system. Interestingly, these thalamocortical connectivity patterns are well preserved in multiple species from rodents to humans (Jones, 2007). In contrast, thalamic nuclei connected to higher-tier association cortices can have more complex connectivity patterns with possible overlapping cortical projections. For example, medial group of dorsal thalamus (MED) has connections to the prefrontal cortex and cingulate; midline group of dorsal thalamus (MTN) and anterior group of dorsal thalamus (ATN) both contain connections to the prefrontal cortex, cingulate and hippocampal formation; MTN is also connected to subcortical regions like lateral septal complex (LSX); and lateral group of dorsal thalamus (LAT) projects to association cortices in parietal, temporal and occipital regions. A summary of the thalamocortical connectional relationship is shown in the diagram in SI Figure 1.

Most techniques for studying thalamocortical connections suffer from invasiveness and inability to systematically trace connectivity across multiple thalamocortical networks. Non-invasively and simultaneously examining functional connectivity between separate thalamic nuclei and their corresponding cortices has posed a significant challenge, albeit this ability can be extremely important in further understanding the characteristic functions of individual thalamocortical networks as well

as their mutual interactions. To bridge this gap, Zhang and colleagues (Zhang et al., 2008; Zhang et al., 2010a) have successfully demonstrated the feasibility of mapping the thalamocortical networks in humans by utilizing an emerging brain mapping technique of resting-state functional magnetic resonance imaging (rs-fMRI). rs-fMRI measures functional connectivity between brain regions based on synchronized spontaneous fluctuations of the rsfMRI signal (Biswal et al., 1995). With this technique, the thalamocortical connectivity patterns revealed well agreed with the known anatomical connectivity relationship (Zhang et al., 2008; Zhang et al., 2010a). However, success in this research topic in animals is rather limited (Pawela et al., 2008). This can largely be attributed to the profound impact of anesthesia used in most animal experiments on the measurement of resting-state functional connectivity (Lu et al., 2007; Liu et al., 2011; Liang et al., 2012b). Indeed, our recent study showed that thalamocortical connectivity and local network organizations of the rat brain can be significantly altered by using routine anesthetizing procedures (Liang et al., 2012a). Consequently, the confounding effects of anesthesia have significantly hindered the exploration of thalamocortical networks in animals by using rsfMRI.

In the present study we have employed a previously established awake animal rsfMRI approach to map thalamocortical connectivity in rats. This imaging method can avoid the confounding effects of anesthesia on rsfMRI measurement. To examine whether specific thalamocortical connectional relationship in rodents can be reliably revealed by this approach, anatomically defined thalamic nucleus groups were used as separate seed regions of interest (ROIs) to generate the corresponding functional connectivity maps. Resulting functional connectivity in the cortex has demonstrated high

spatial specificity and is in excellent accordance with the known thalamocortical connectional relationship.

Materials and Methods

Animal Preparation and MR Experiment

rsfMRI data collected at the identical condition from several previous studies (Zhang et al., 2010b; Liang et al., 2011, 2012a) were pooled and re-analyzed for the purpose of the present study. Detailed descriptions of the experimental procedures can be found in aforementioned studies. Briefly, 42 adult male Long-Evans rats were acclimated to MRI restraint and noise for seven days to minimize the stress induced by imaging as described before (Zhang et al., 2010b; Liang et al., 2011, 2012a). During the experimental setup, the rat was briefly anesthetized by isoflurane (2%) and the head was secured into a head restrainer with a build-in coil, and the body was fit into a body restrainer. After the setup was completed, isoflurane was removed and the whole system was positioned in magnet. Rats were all fully awake during imaging sessions. In order to compare the thalamocortical connectivity at the awake and anesthetized conditions, 16 of 42 rats underwent the imaging session at the anesthetized condition at minimum 7 days after they were imaged at the awake condition. In this experiment, the animal preparation procedure was the same as that in the awake imaging experiment. Isoflurane gas (2%) was then delivered to the animal through a nose cone in the magnet to maintain the anesthetized state. The body temperature of the animal was monitored and maintained at

37°C ± 0.5°C by using a feedback controlling heating pad. All studies were approved by IACUC of the University of Massachusetts Medical School.

All MRI experiments were conducted on a Bruker 4.7 T magnet. A dual 1H radiofrequency (RF) coil configuration (Insight NeuroImaging Systems, Worcester, MA) consisting of a volume coil for exciting the water proton spins and a surface coil for receiving MRI signal was used; the volume and surface coils were actively tuned and detuned to prevent mutual coil coupling. This dual-coil configuration allows for sufficient RF field homogeneity in the rat brain for RF transmission, while preserving the advantage of higher signal-to-noise ratio (SNR) provided by the smaller reception coil. For each MRI session, RARE sequence was used to acquire anatomical images with the following parameters: TR = 2125ms, TE = 50ms, matrix size = 256×256, FOV = 3.2×3.2cm2, slice number = 18, slice thickness = 1mm, RARE factor = 8. Gradient-echo images were then acquired using the echo-planar imaging (EPI) sequence with the following parameters: TR = 1s, TE = 30ms, flip angle = 60°, matrix size = 64×64, FOV = 3.2cm×3.2cm, slice number=18, slice thickness = 1mm. Two hundred volumes were acquired for each scan, and six to nine scans were obtained for each session.

rsfMRI Data Analysis

rsfMRI images of all rats were first co-registered to a fully segmented rat atlas based on anatomical images by using Medical Image Visualization and Analysis (MIVA, http://ccni.wpi.edu/). Preprocessing steps included motion correction with SPM8 (http://www.fil.ion.ucl.ac.uk/spm/), spatial smoothing (FWHM = 1mm), regression of

motion parameters and the signals of white matter and ventricles to eliminate the contributions of physiologic noise to the rsfMRI signal, and 0.002-0.1Hz band-pass filtering. Scans with excessive motion (>0.25 mm) were discarded.

To accommodate the spatial resolution of rsMRI, the thalamus was partitioned into eight thalamic nuclei ROIs and seven of them were selected as seeds for functional connectivity analysis (Figure 4.1) with one ROI (reticular nucleus of thalamus) excluded due to its little cortical connections reported in the literature (Swanson, 2004). The total number of voxels in EPI images that fit into the ROI of each individual thalamic nucleus was LG: 15, MG: 17, VENT: 79, LAT: 34, MED: 26, MTN: 26, and ATN: 30. This calculation was based on our segmented atlas template that was resampled to the spatial resolution of EPI images (0.5x0.5x1mm3). Anatomical definitions were based on the Swanson atlas (Swanson, 2004). Detailed anatomical information of all seed ROIs can be found in SI Table 4.1.

Functional connectivity was evaluated using seed-based correlational analysis on a voxel-by-voxel basis (Zhang et al., 2010b; Liang et al., 2012a). Time courses from all voxels within individual seed regions were averaged and used as reference time courses. Pearson cross-correlation coefficients between these reference time courses and the time course of each individual voxel were then calculated. Correlation coefficients (i.e. r values) were transformed to z scores using Fisher's z transformation. This correlational analysis was carried out for each scan. To assess the reproducibility of functional connectivity maps, rats were randomly split into two subgroups for each (awake or

Figure 4.1. ROI definitions of thalamic nucleus groups. Spatial maps of seven thalamic nucleus groups were displayed in different colors overlaid on anatomical images. Distance to bregma (in mm) is labeled at the bottom of each slice. L, left, R, right.

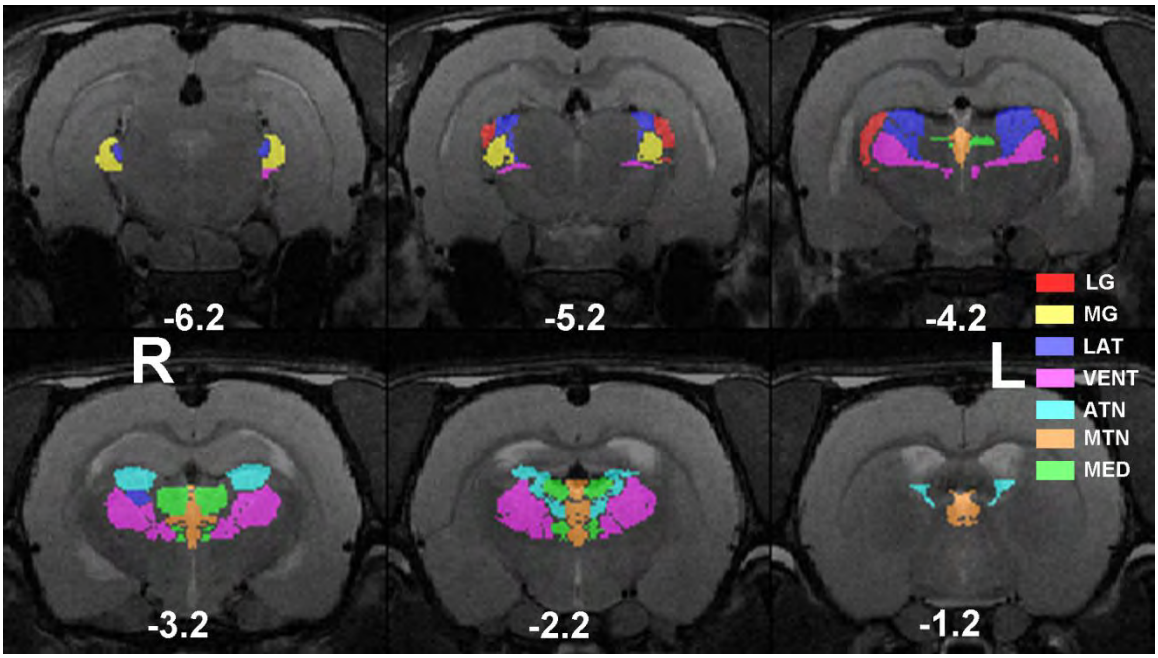
-6.2
-5.2
-4.2
R
L
LG
MG
LAT
VENT
ATN
MTN
MED
-3.2
-2.2
-1.2

anesthetized) condition. A thalamocortical connectivity map was generated for each seed in each subgroup. The correlation coefficient of z scores between individual corresponding voxels from two subgroups was then calculated. This process was repeated for 100 times. Averaged correlation coefficients from 100 repetitions provided a measure of reproducibility of functional connectivity maps.

Statistics

For each seed ROI, a linear mixed-effect model was calculated using the lme4 package in the R environment (http://www.r-project.org, version 2.15.1) with the random effect of rats and the fixed effect of z scores. The p value of the fixed effect for each voxel was then calculated by using the Markov chain Monte Carlo (MCMC) method with 10000 samples (implemented in the languageR package in R). Maps were thresholded at p value < 0.05, corrected for multiple comparisons with the False Discovery Rate (FDR) criteria. Maps of t values were displayed.

Winner-take-all approach

To simultaneously display multiple thalamocortical networks for all seven ROIs, a winner-take-all approach was utilized. For each voxel that showed significant connectivity with at least one seed ROI (i.e. $p<0.05$, FDR corrected), it was assigned to the ROI with the highest z score in all seven thalamic nucleus connectivity maps. Winning voxels that did not pass the statistical threshold were not displayed.

Results

Cortical connectivity of individual thalamic nucleus groups

The connectivity profiles of individual seeds were generated by the correlational analysis of the rsfMRI signal in rats. All seven thalamic nucleus groups were broadly divided into two categories: nucleus groups related to sensory-motor cortices and nucleus groups related to polymodal association cortices. Sensory-motor related thalamic nucleus groups (Figure 4.1) included LG (visual), MG (auditory) and VENT (somatosensory and motor).

In awake rats, the LG connectivity map showed robust functional connectivity with the visual cortex (Figure 4.2a). Other subcortical and cortical brain regions revealed in the functional connectivity map included part of thalamus, hypothalamus, hippocampus and temporal cortex. In the MG connectivity map shown in Figure 4.2b, connectivity with the auditory cortex was clearly observed. In addition, part of hippocampus and thalamus appeared to connect to MG. With respect to VENT, the connectivity map revealed prominent cortical connectivity in somatomotor, somatosensory and anterior cingulate cortices, as shown in Figure 4.2c. Strong subcortical connections were also evident in caudate-putamen (CPu).

Four thalamic nucleus groups are related to polymodal association cortices (Figure 4.1): LAT, MED, MTN and ATN. In awake rats, widespread cortical connections were observed in the LAT connectivity map (Figure 4.3a), prominently involving somatosensory, motor, anterior cingulate and insular cortices. In addition, the LAT connectivity map also showed functional connectivity with subcortical regions such as

Figure 4.2. Functional connectivity maps of sensory-motor related thalamic groups. a) Map of LG connectivity. b) Map of MG connectivity. c) Map of VENT connectivity. All maps were thresholded at p value<0.05, FDR corrected and t values were color coded and displayed. Distance to bregma (in mm) is labeled at the bottom of each slice. L, left, R, right.

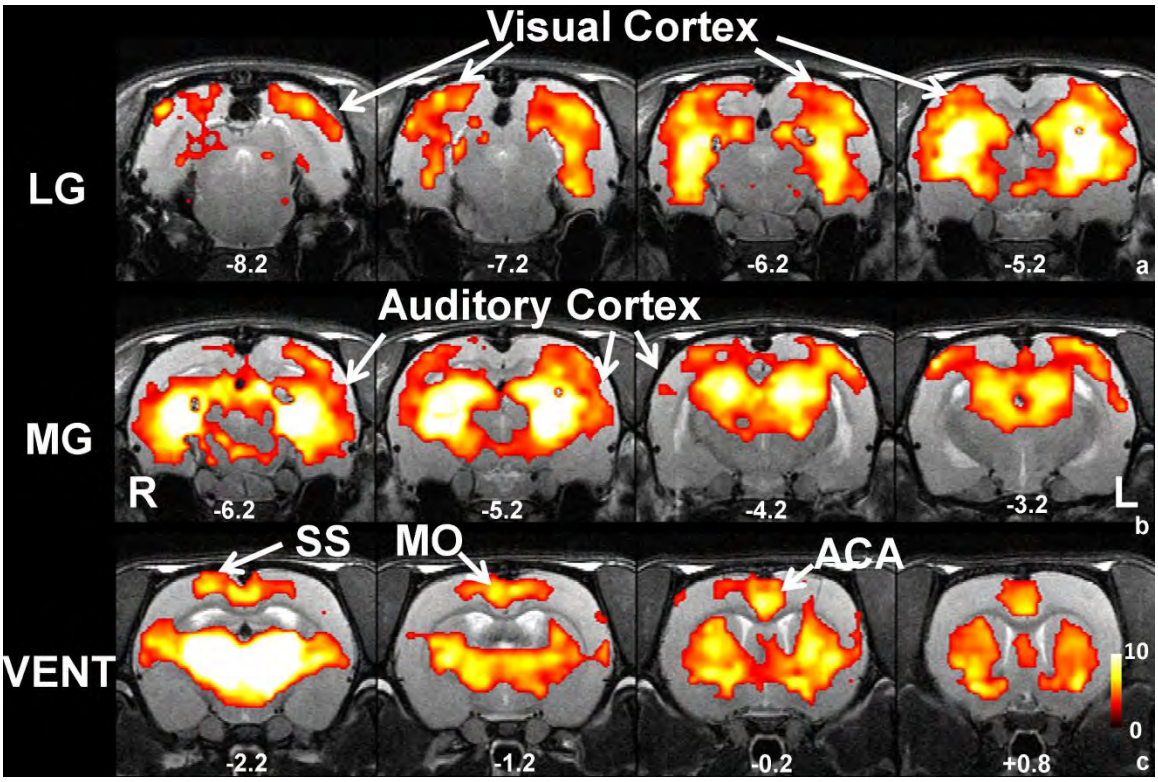
Visual Cortex
LG
-8.2
-7.2
-6.2
-5.2
a
Auditory Cortex
MG
R
-6.2
-5.2
-4.2
-3.2
L
b
SS
MO
ACA
VENT
-2.2
-1.2
-0.2
+0.8
10
0
c

CPu (Figure 4.3a). The other three thalamic groups, MED, MTN and ATN, all showed very similar connectivity profiles, mostly with the prefrontal cortex, cingulate and CPu (Figure 4.3b, c, d).

The sagittal and axial views of the connectivity maps for all seven thalamic nuclei groups in awake rats were shown in SI Figure 4.2. The cortical connectivity patterns for all seven thalamic nuclei in the anesthetized rat were shown in SI Figure 4.3. The results indicated that the thalamocortical connectivity was significantly compromised in all thalamocortical networks at the anesthetized condition. These results were also consistent with the finding in our previous publication (Figure 7 in Liang et al., 2012b).

To estimate the reproducibility of functional connectivity maps, voxel-wise correlation between two randomly divided subgroups was calculated for individual nuclei and repeated for 100 times. Averaged correlation coefficients across 100 repetitions were highly significant for all seeds in awake rats (CCaverage = 0.74, 0.82, 0.80, 0.81, 0.82, 0.82 and 0.80 for LG, MG, VENT, ATN, LAT, MED and MTN, respectively, $p<10^{-7}$ for all seeds). In anesthetized rats, averaged correlation coefficients were also high but tended to be lower than those in awake rats (CCaverage= 0.65, 0.63, 0.73, 0.71, 0.72, 0.72 and 0.71 for LG, MG, VENT, ATN, LAT, MED and MTN, respectively). Two representative examples of voxel-wise correlations between two randomly divided subgroups in awake and anesthetized rats were shown in Figure 4.4.

Multiple thalamocortical networks revealed by the winner-take-all approach

Figure 4.3. Functional connectivity maps of poly-modal association cortices related thalamic groups. a) LAT connectivity map. b) MED connectivity map. c) MTN connectivity map. d) ATN connectivity map. All maps were thresholded at p value<0.05, FDR corrected and t values were color coded and displayed. Distance to bregma (in mm) is labeled at the bottom of each slice. L, left, R, right.

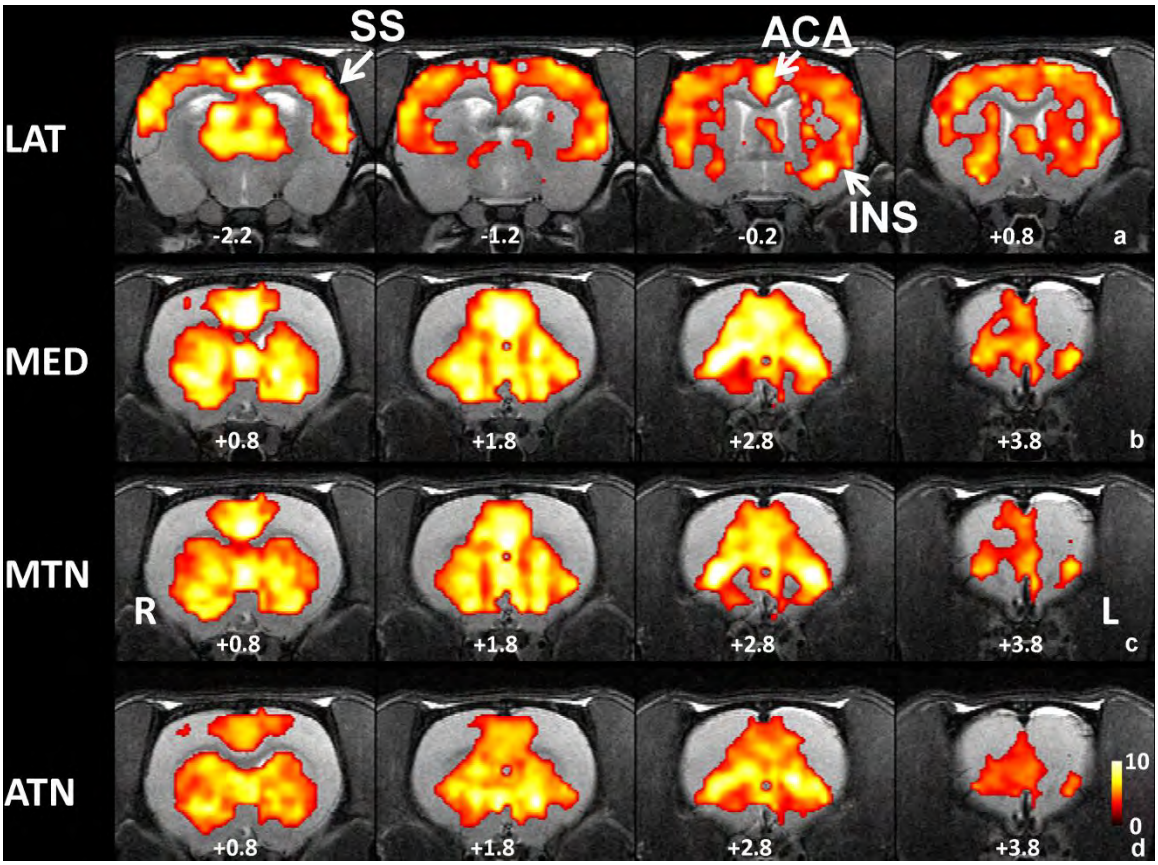
SS
ACA
INS
LAT
MED
MTN
ATN
-2.2
-1.2
-0.2
+0.8
a
+0.8
+1.8
+2.8
+3.8
b
R
L
+0.8
+1.8
+2.8
+3.8
c
10
0
+0.8
+1.8
+2.8
+3.8
d

Figure 4.4. Two representative examples of voxel-wise resting-state functional connectivity (RSFC) correlations between two randomly divided subgroups in awake and anesthetized rats.

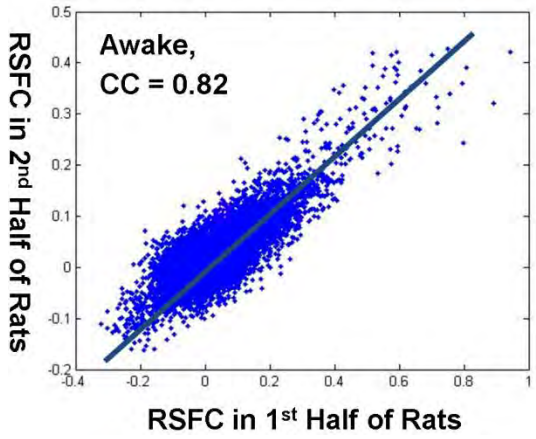
Awake,
CC = 0.82
RSFC in 2nd Half of Rats
RSFC in 1st Half of Rats

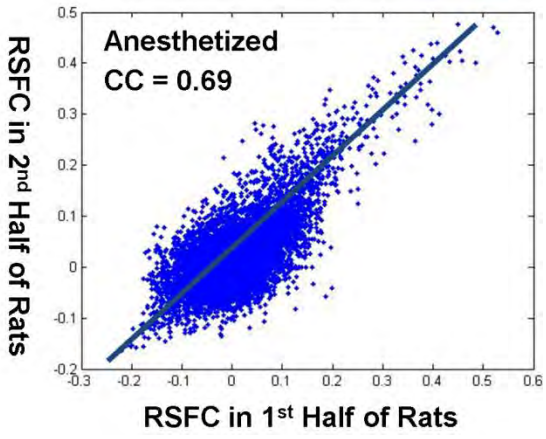
Anesthetized
CC = 0.69
RSFC in 2nd Half of Rats
RSFC in 1st Half of Rats

Multiple thalamocortical networks measured by resting-state functional connectivity in awake rats were simultaneously displayed by using the whole-brain winner-take-all approach (Figure 4.5, see Methods for details). The map clearly showed highly organized cortical connectivity patterns for individual thalamic nucleus groups that were in excellent accordance with the known anatomical connectivity relationship. For example, dominant LG connectivity was observed in the visual cortex (labeled in red); and MG connectivity was mostly in the auditory cortex (labeled in yellow). In addition, LAT showed robust connectivity in somatosensory cortex (labeled in blue). Interestingly, MED, MTN and ATN showed differential connectivity patterns in the winner-take-all map, and these patterns also agreed with their anatomical connections (Krettek and Price, 1977; Van Groen and Wyss, 1995; Vertes and Hoover, 2008). Specifically, dominant MED cortical connectivity was seen in the prefrontal cortex and cingulate (labeled in green). MTN connectivity (labeled in brown) was evident in subcortical regions of lateral septal complex (LSX).

Improved spatial specificity of cortical connectivity with partial correlation

Functional connectivity maps of MED, MTN and ATN revealed by full correlation analysis (Figures 4.3b, c and d) showed almost identical profiles in the prefrontal regions. It is likely that similar cortical connectional patterns among these nucleus groups resulted from indirect connectivity to the cortex mediated by inter-nucleus connections. To examine this possibility, we further inspected inter-nucleus

Figure 4.5. Multiple thalamocortical networks revealed by the winner-take-all map approach. The color of each voxel was labeled as the color of the winning thalamic nucleus seed. Colors of all thalamic nucleus seeds are identical to those in Figure 1. Distance to bregma (in mm) is labeled at the bottom of each slice. L, left, R, right.

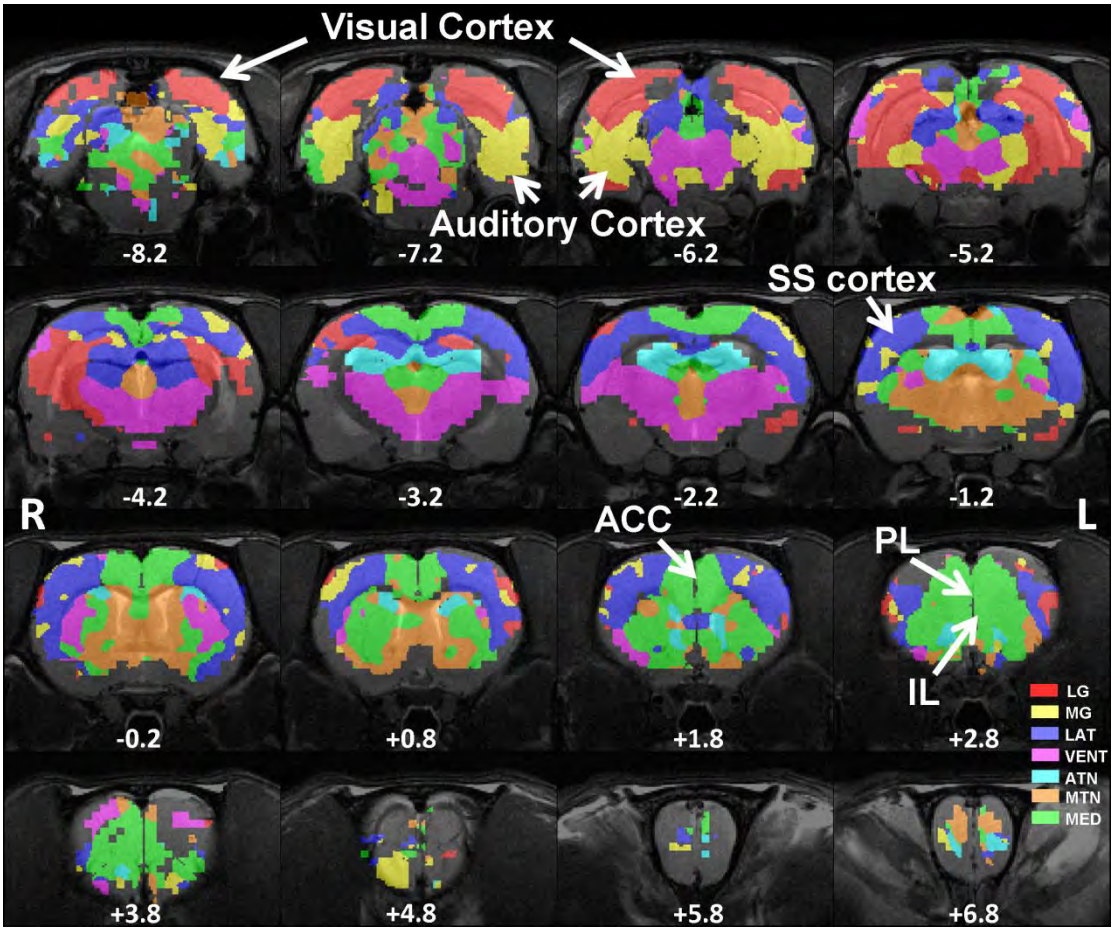
Visual Cortex
Auditory Cortex
SS cortex
ACC
PL
IL
R
L
-8.2
-7.2
-6.2
-5.2
-4.2
-3.2
-2.2
-1.2
-0.2
+0.8
+1.8
+2.8
+3.8
+4.8
+5.8
+6.8
LG
MG
LAT
VENT
ATN
MTN
MED

connectivity between all nucleus groups. The result indicated that these three thalamic nucleus groups indeed had very high mutual connectivity among themselves. Mean connectivity strength (estimated by r values) between MED-MTN, MED-ATN and MTN-ATN were 0.66, 0.50 and 0.38 respectively, while the mean connectivity of these three nucleus groups with the other four nucleus groups were considerably lower (MED: 0.26, MTN: 0.18, ATN: 0.26). Therefore, strong inter-nucleus connections among MED, MTN and ATN could mediate indirect connectivity to the cortex, resulting in apparently similar cortical connectivity patterns among these three nucleus groups. For the purpose of differentiating the connectivity pattern for MTN, MED and ATN, the method of partial correlation was utilized. For each of the three nucleus groups, the time courses of the other two nucleus groups were used as covariates when evaluating its specific functional connectivity. Similar to the full correlation analysis, partial correlation coefficients (i.e. r values) were transformed to z scores using Fisher's z transformation. The same statistical analysis and threshold were applied. The resulting maps showed distinct connectivity patterns for each seed (Figure 4.6). MED retained the characteristic functional connectivity with prefrontal regions including infralimbic (IL), prelimic (PL), anterior cingulate and orbital frontal cortices. Interestingly, its connectivity pattern obtained by partial correlation analysis was consistent with the pattern in the winner-take-all map (Figure 5, labeled in green). Also similar to the pattern in the winner-take-all map, MTN connectivity was dominant in subcortical areas including LSX (Figure 5, labeled in brown). In contrast, the ATN showed a distinct pattern with its specific connectivity in retrohippocampal regions—a more posterior part of the brain.

Figure 4.6. Functional connectivity maps of MED, MTN and ATN generated by partial correlation analysis. The functional connectivity map of one nucleus group was obtained by controlling for the rsfMRI signals of the other two nucleus groups. a) MED connectivity map. b) MTN connectivity map. c) ATN connectivity map. All maps were thresholded at p value<0.05, FDR corrected and t values were color coded and displayed. Distance to bregma (in mm) is labeled at the bottom of each slice. L, left, R, right.

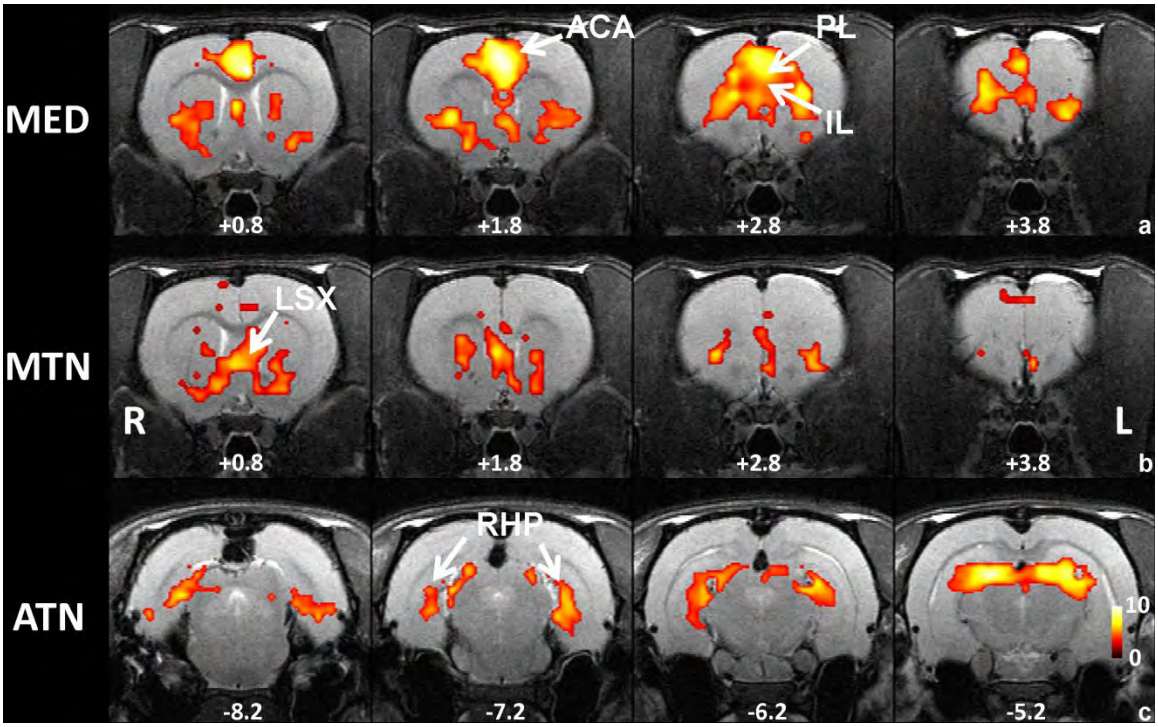
MED
MTN
ATN
ACA
PL
IL
LSX
RHP
R
L
+0.8
+1.8
+2.8
+3.8
-8.2
-7.2
-6.2
-5.2
a
b
c
10
0

To further examine the validity of connectivity profiles revealed by partial correlation analysis, we compared the functional connectivity results of the three nucleus groups with their anatomical connectivity pattern in well-established tracing studies (Figure 4.7, results of tracing studies were respectively adopted from (Krettek and Price, 1977; Van Groen and Wyss, 1995; Vertes and Hoover, 2008)). In these tracing studies anterograde tracers were injected respectively in mediodorsal nucleus (part of MED, Figure 4.7a), paraventriclar nucleus (part of MTN, Figure 4.7b), and anterodorsal nucleus (part of ATN, Figure 4.7c) in rats. For each of all three nucleus groups, remarkable correspondence was observed between the functional connectivity pattern and the tracer destination from the injection site. These results collectively provided strong evidence validating partial correlation analysis in improving the spatial specificity of rsfMRI.

Discussion

In the present study we have investigated the patterns of thalamocortical connectivity in rodents by utilizing resting-state functional connectivity (Zhang et al., 2010b; Liang et al., 2012a). We found that the cortical connectivity from separate thalamic nuclei well agreed with the known thalamocortical anatomical connections in awake rats. In addition, the cortical connectivity for each thalamic nucleus was highly reproducible and more prominent at the awake condition relative to the anesthetized condition. Furthermore, greater spatial specificity of functional connectivity was obtained by partial correlation analysis in nucleus groups with high mutual connectivity, and

Figure 4.7. The spatial patterns of thalamocortical connectivity showed great agreement with the corresponding anatomical connectivity patterns identified in literature tracing studies. Left panels are functional connectivity map obtained by partial correlation analysis. Right panels are adopted from tracing studies with the injections sites originating from mediodorsal nucleus (part of MED, Panel a), paraventriclar nucleus (part of MTN, Panel b), anterodorsal nucleus (part of ATN, Panel c), respectively, in the rat (Krettek and Price, 1977; Van Groen and Wyss, 1995; Vertes and Hoover, 2008). White dots or lines indicated labeled neurons in destination regions.

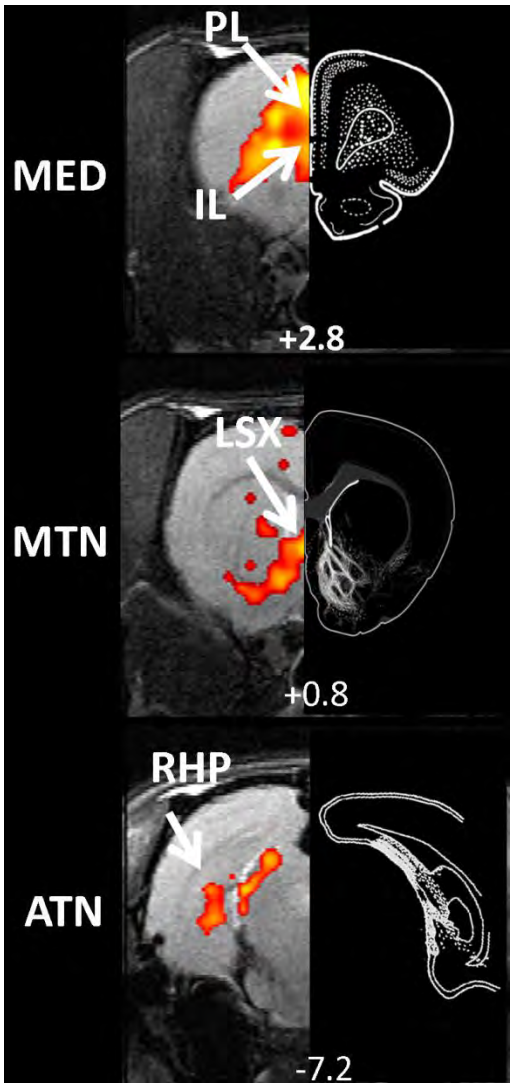
PL
MED
IL
+2.8
LSX
MTN
+0.8
RHP
ATN
-7.2

considerably improved spatial specificity was further validated by the high resemblance to the corresponding anatomical connectivity profiles identified in previous tracing studies (Krettek and Price, 1977; Van Groen and Wyss, 1995; Vertes and Hoover, 2008). To our best knowledge, it is the first study that simultaneously mapped multiple distinct thalamocortical networks in the rat brain.

The significance of the present study is in two folds. First, the excellent consistency between the cortical functional connectivity profiles for multiple thalamic nuclei and the known thalamocortical connectional relationship has provided very important evidence supporting the measurement of resting-state functional connectivity in awake rat brain. This establishment of this approach can significantly extend the applicability of rsfMRI research in numerous animal models which currently remains tremendously underexplored. Second, the present study demonstrated the feasibility of simultaneously mapping multiple thalamocortical networks in the rat brain. This ability makes it possible to further non-invasively investigate the function, neuroplasticity and mutual interactions of thalamocortical networks.

Robust functional connectivity was observed between thalamic nucleus groups subserving sensory-motor functions and their corresponding cortices (i.e., LG was connected with visual cortex, MG was connected with the auditory cortex and VENT was connected with motor/somatosensory cortices). The anatomical circuitries of these first-order thalamic nuclei are relatively simple as they all project to their corresponding sensory and motor cortices with little overlap. For example, axons of LG project to layer 4 of the primary visual cortex through excitatory synapses (Sherman, 2005). Accordingly, the observed functional connectivity of sensory-motor related thalamic nucleus groups all

had quite distinct connectivity profiles that well agreed with their respective anatomical connectivity patterns. Nevertheless, it is still worth to note that even for sensory-motor related thalamic nuclei, significant overlaps in their cortical connectivity were still observed. Overlaps in the connectivity maps in the sensory-motor related thalamic seeds, though not as significant as polymodal association cortex-related nuclei, can be induced by several factors including the partial volume effect and indirect cortico-coritical connectivity. At the rsfMRI spatial resolution of the present study (0.5x0.5x1mm3), when calculating the reference time course of a thalamic nucleus (see Materials and Methods), it is virtually impossible to avoid the partial volume effect from its neighboring nuclei. This partial volume effect can induce overlapping cortical connectivity between sensory-motor related nuclei. In addition, indirect cortico-cortical connectivity can also cause overlaps in cortical connectivity between sensory-motor related nuclei.

Thalamic nucleus groups related to higher-order polymodal functions also showed significant connections with various cortical regions (Figure 4.3). LAT had obvious functional connections with somatosensory, motor, insular and cingulate regions. This connectivity pattern was consistent with its anatomical connectivity profile (Paxinos, 2004). In addition, MED, MTN and ATN all showed robust connectivity with prefrontal regions (Figure 4.3b, c, d). Notably, when full correlation analysis was used to assess functional connectivity, the connectional profiles of MED, MTN and ATN did not appear much difference in their specific connectivity. This situation can be attributed to the indirect connectivity mediated through strong mutual connectivity among these three nucleus groups. It was previously shown that the thalamus had strong inter-nucleus correlations in resting-state activities (Zhang et al., 2010b). In the present study, these

three thalamic nucleus groups also showed considerably stronger connectivity among themselves than with other nucleus groups. Therefore, to examine that whether similar functional connectivity profiles of MED, MTN and ATN resulted from the mediating effects of inter-nucleus connections, partial correlation analysis was applied. This analysis method generated the functional connectivity map of one nucleus group by controlling for the resting-state activities of the other two nucleus groups. Our results clearly revealed distinct spatial patterns among the three nucleus groups. More interestingly, in the partial correlation maps, MED still showed robust functional connectivity with the prefrontal cortex, while this particular connectivity almost completely diminished in the connectivity maps of the other two seeds (Figure 4.6b, c). These results suggest that the prefrontal connectivity of MTN and ATN showed in full correlation maps were very likely mediated by MED. Anatomically, MED and the prefrontal cortex have robust and reciprocal connections (Paxinos, 2004). This connectional relationship revealed in tracing studies (Krettek and Price, 1977) also well corresponds to the functional connectivity pattern observed in the partial correlation map (Figure 4.7a). In addition, MTN consists of several small nucleus groups and has diverse afferent and efferent connections. Interestingly, part of efferent projections of MTN are in subcortical areas such as LSX (Vertes and Hoover, 2008). Again this result is consistent with the functional connectivity pattern revealed by partial correlation analysis (Figure 4.7b). With respect to ATN, two major nuclei of ATN, anterodorsal nucleus and anteroventral nucleus, both have projections in retrohippocampal regions (Van Groen and Wyss, 1995), which was also clearly revealed in the partial correlation map of ATN (Figure 4.7c). Taken together, these results strongly suggest that partial correlation

analysis can significantly improve the spatial specificity of rsfMRI while maintaining great sensitivity.

In addition to the well-established cortical connectivity patterns, we also observed prominent resting-state functional connectivity that was not extensively reported. For instance, strong connectivity between CPu and several thalamic nuclei was observed in the present study (Fig. 4.3), whereas the only anatomical connection reported was between CPu and parafasicular nucleus, a small region in dorsal thalamus (Cornwall and Phillipson, 1988). This discrepancy might indicate a previously overlooked connection, or it may originate from indirect connections between CPu and other cortical regions.

The major limitation of the current study is the relatively low spatial resolution of rsfMRI images. Thalamus is a highly heterogeneous brain region consisting of many small nuclei with both common and distinct anatomical connectivity. In the current study, thalamic nuclei were clustered into several groups (see Table 1 in SI) as seed regions due to the resolution limit of rsMRI. This limitation could potentially reduce the sensitivity and specificity of functional connectivity mapping due to the averaging of time courses of potentially heterogeneous voxels within one thalamic nucleus group. rsfMRI with higher spatial resolutions can be applied to more accurately delineate individual thalamic nucleus or even sub-nucleus in future studies. In addition, it should be noted that in the tracing studies cited in Figure 4.7 the injection sites were only a part of nucleus groups used as seed ROIs in the present study. Thus it may not be realistic to expect completely identical spatial patterns between the anatomical connectivity and functional connectivity.

In the past decade, rsfMRI has been shown to be a powerful tool to noninvasively probe dynamic communications between brain regions. Measuring resting-state functional connectivity in awake animals is an emerging technique that has the potential to substantially extend the applicability of rsfMRI in numerous preclinical animal models. Therefore, rigorously validating this approach is of critical importance. The thalamocortical networks are perhaps the most well studied neural networks in the brain. Given the well-known connectivity patterns, the thalamocortical networks provide an ideal model for validating the resting-state functional connectivity measurement in awake animals. Our results clearly indicated robust thalamo-cortical connectivity that is in excellent consistency with the known anatomical connectional relationship, and therefore provided strong evidence validating the approach of measuring rsfMRI in awake animals. More importantly, the current study further extended rsfMRI to establish a novel animal model of functional thalamocortical connectivity, and thus offered a tool for preclinical research of thalamus and thalamocortical connectivity. Given the vital importance of thalamocortical connectivity in brain functions such as consciousness, our resting-state animal model represents enormous opportunities of studying this functional connectivity at normal as well as pathological conditions.

Supplemental Information

SI Table 4.1. Anatomical definitions of thalamic groups.

LG

LGd	lateral geniculate complex dorsal part
LGv	lateral geniculate complex ventral part
LGvl	lateral geniculate complex ventral part lateral zone
LGvm	lateral geniculate complex ventral part medial zone

MG

MGd	medial geniculate complex dorsal part
MGv	medial geniculate complex ventral part
MGm	medial geniculate complex medial part

VENT

VAL	ventral anterio-lateral complex thalamus
VM	ventral medial nucleus thalamus
VPL	ventral posterolateral nucleus thalamus
VPLpc	ventral posterolateral nucleus thalamus parvicellular part
VPM	ventral posteromedial nucleus thalamus
VPMpc	ventral posteromedial nucleus thalamus parvicellular part
PP	peripeduncular nucleus
SPF	subparafascicular nucleus thalamus
SPFm	subparafascicular nucleus thalamus magnocellular part
SPFp	subparafascicular nucleus thalamus parvicellular part

MED

MD	mediodorsal nucleus thalamus
MDc	mediodorsal nucleus thalamus central part
MDl	mediodorsal nucleus thalamus lateral part
MDm	mediodorsal nucleus thalamus medial part

SMT	submedial nucleus thalamus
PR	perireuniens nucleus

MTN

IAM	interanteromedial nucleus thalamus
IMD	intermediodorsal nucleus thalamus
MID	midline nucline dorsal thalamus
RE	nucleus reuniens
RE1	nucleus reuniens
REa	nucleus reuniens rostral devision anterior part
REcd	nucleus reuniens caudal devision dorsal part
REcm	nucleus reuniens caudal devision medial part
REcp	nucleus reuniens caudal devision posterior part
REd	nucleus reuniens rostral devision dorsal part
REl	nucleus reuniens rostral devision lateral part
REm	nucleus reuniens rostral devision medial part
REv	nucleus reuniens rostral devision ventral part
PVT	paraventriclar nucleus thalamus
PT	parataenial nucleus

ATN

AM	anteromedial nucleus thalamus
AMc	anteromedial nucleus thalamus central part
AMd	anteromedial nucleus thalamus dorsal part
AMv	anteromedial nucleus thalamus ventral part
AV	anterioventral nucleus thalamus
LD	lateral dorsal nucleus thalamus

IAD	interanterodorsal nucleus thalamus
ATN	anterior nuclie dorsal thalamus

SI Figure 1. Summary of the known anatomical thalamocortical connectivity relationship. Afferent and efferent projections are both counted. Anatomical information is based on Swanson rat atlas and BAMS (http://brancusi1.usc.edu). Thalamic groups are colored as Fig. 1. AUD, auditory cortex. VIS, visual cortex. MO, motor cortex. SS, somatosensory cortex. LSX, lateral septal complex. VISC, visceral area. AI, agranular insular area. ACA, anterior cingulate cortex. RSP, retrosplenial cortex. IL, infralimbic cortex. PL, prelimbic cortex. ORB, orbital cotex. RHP, retrohippocampal area.

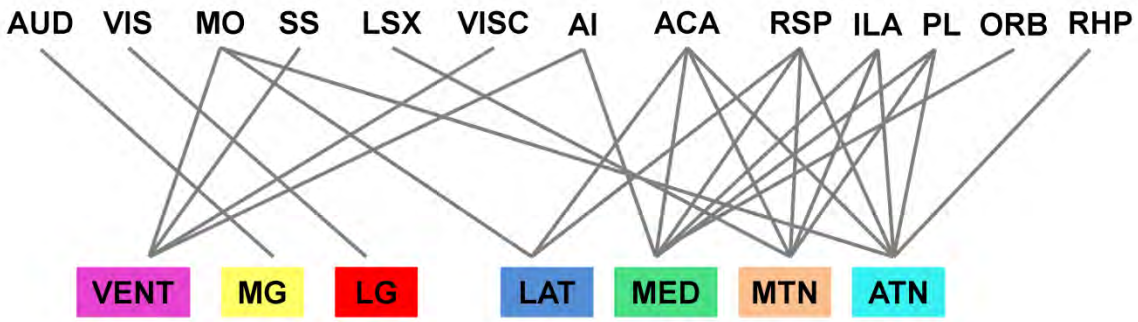
AUD
VIS
MO
SS
LSX
VISC
AI
ACA
RSP
ILA
PL
ORB
RHP
VENT
MG
LG
LAT
MED
MTN
ATN

SI Figure 2. Sagittal and axial views of the connectivity maps for all seven thalamic nuclei groups in awake rats.

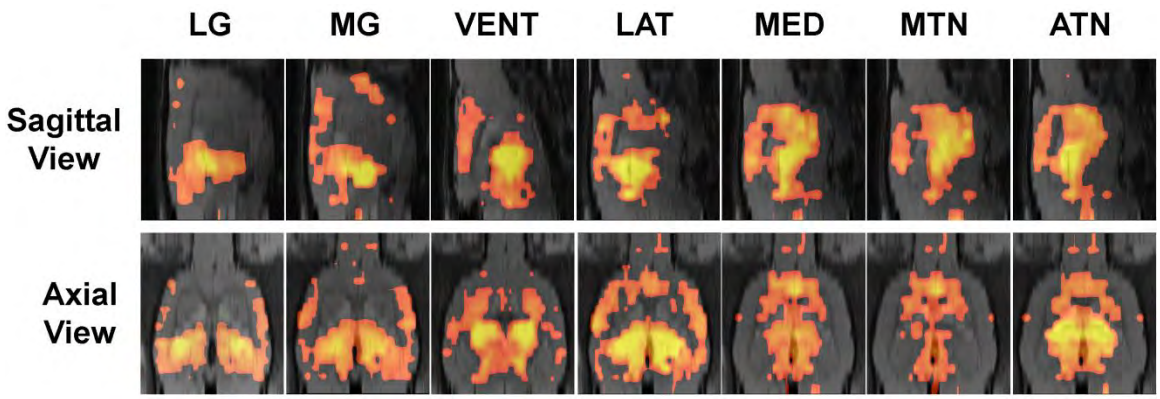
LG
MG
VENT
LAT
MED
MTN
ATN
Sagittal View
Axial View

SI Figure 4.3. The cortical connectivity patterns for all seven thalamic nuclei in the anesthetized rat.

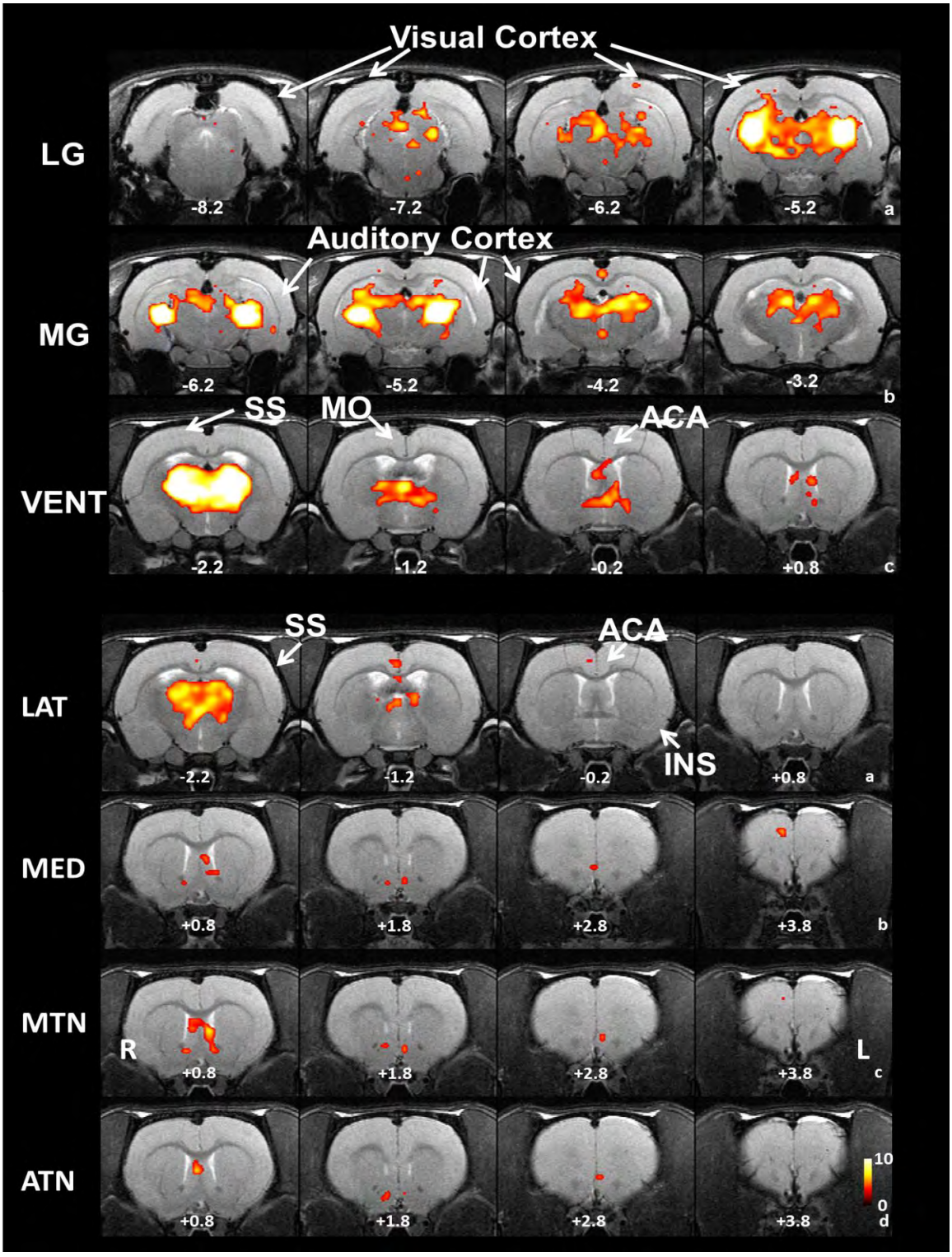
Visual Cortex
LG
-8.2
-7.2
-6.2
-5.2
a
Auditory Cortex
MG
-6.2
-5.2
-4.2
-3.2
b
SS
MO
ACA
VENT
-2.2
-1.2
-0.2
+0.8
c
SS
ACA
LAT
INS
-2.2
-1.2
-0.2
+0.8
a
MED
+0.8
+1.8
+2.8
+3.8
b
MTN
R
L
+0.8
+1.8
+2.8
+3.8
c
ATN
10
0
d
+0.8
+1.8
+2.8
+3.8

Acknowledgement:

We would like to thank Dr. Wei Huang for her technical support. This publication was made possible by the institutional fund from the University of Massachusetts Medical School.

CONCLUSION

The above studies have established a solid foundation for our understanding of large-scale functional neural networks in the awake rat brain using resting-state fMRI. Global organizing principles of functional neural networks were explored in Chapter I and II, revealing critical topological properties such as small-worldness and modularity as well as elementary functional units in the brain. Interestingly, those global properties remained intact even in the anesthetized state, although the global network was evidently reorganized at the local level. The comparison of connectional strength suggested a global but not uniform reduction from awake to anesthetized states, and the impact of anesthesia on the connectional strength was different for different brain regions. Importantly, the connectional strength was found not to be particularly decreased for long-distance connections. Those findings provide novel insights of the neural mechanism of anesthesia and consciousness. Resting-state fMRI was also utilized to study specific neural circuitries in Chapter III and IV. Chapter III examined the anticorrelated connectivity between infralimbic cortex and amygdala with various preprocessing methods, and Chapter IV further validate the resting-state fMRI by revealing nuclei specific thalamocortical connectivity.

These studies provide enormous future opportunities for both studying basic mechanism of resting-state functional connectivity and preclinical disease models with the awake rat resting-state fMRI. Coupled with other methods like calcium imaging, electrophysiology techniques and optogenetics, this imaging model has the unique strength for studying the largely unknown neural mechanism of resting-state functional connectivity, which is difficult or impossible to be conducted in human subjects.

Furthermore, as a widely used animal model in biomedical research, there are ample opportunities to study preclinical animal models with the awake rat resting-state fMRI. This type of studies will provide global insights into neural mechanisms of those disease models as well as bridge the gap between human imaging studies and basic preclinical research.

References:

Achard S, Salvador R, Whitcher B, Suckling J, Bullmore E (2006) A resilient, low-frequency, small-world human brain functional network with highly connected association cortical hubs. J Neurosci 26:63-72.

Albert NB, Robertson EM, Miall RC (2009) The resting human brain and motor learning. Curr Biol 19:1023-1027.

Alexander-Bloch AF, Gogtay N, Meunier D, Birn R, Clasen L, Lalonde F, Lenroot R, Giedd J, Bullmore ET (2010) Disrupted modularity and local connectivity of brain functional networks in childhood-onset schizophrenia. Front Syst Neurosci 4:147.

Alkire MT, Hudetz AG, Tononi G (2008) Consciousness and anesthesia. Science 322:876-880.

Allen EA, Damaraju E, Plis SM, Erhardt EB, Eichele T, Calhoun VD (2012) Tracking Whole-Brain Connectivity Dynamics in the Resting State. Cereb Cortex.

Allen EA, Erhardt EB, Damaraju E, Gruner W, Segall JM, Silva RF, Havlicek M, Rachakonda S, Fries J, Kalyanam R, Michael AM, Caprihan A, Turner JA, Eichele T, Adelsheim S, Bryan AD, Bustillo J, Clark VP, Feldstein Ewing SW, Filbey F, Ford CC, Hutchison K, Jung RE, Kiehl KA, Kodituwakku P, Komesu YM, Mayer AR, Pearlson GD, Phillips JP, Sadek JR, Stevens M, Teuscher U, Thoma RJ, Calhoun VD (2011) A baseline for the multivariate comparison of resting-state networks. Front Syst Neurosci 5:2.

Amano T, Unal CT, Pare D (2010) Synaptic correlates of fear extinction in the amygdala. Nat Neurosci 13:489-494.

Anderson JS, Druzgal TJ, Lopez-Larson M, Jeong EK, Desai K, Yurgelun-Todd D (2011) Network anticorrelations, global regression, and phase-shifted soft tissue correction. Hum Brain Mapp 32:919-934.

Bandettini PA, Wong EC, Hinks RS, Tikofsky RS, Hyde JS (1992) Time course EPI of human brain function during task activation. Magn Reson Med 25:390-397.

Bassett DS, Bullmore ET (2009) Human brain networks in health and disease. Curr Opin Neurol 22:340-347.

Becerra L, Pendse G, Chang PC, Bishop J, Borsook D (2011) Robust reproducible resting state networks in the awake rodent brain. PLoS One 6:e25701.

Beckmann CF, Smith SM (2005) Tensorial extensions of independent component analysis for multisubject FMRI analysis. Neuroimage 25:294-311.

Belliveau JW, Kennedy DN, Jr., McKinstry RC, Buchbinder BR, Weisskoff RM, Cohen MS, Vevea JM, Brady TJ, Rosen BR (1991) Functional mapping of the human visual cortex by magnetic resonance imaging. Science 254:716-719.

Berretta S, Pantazopoulos H, Caldera M, Pantazopoulos P, Pare D (2005) Infralimbic cortex activation increases c-Fos expression in intercalated neurons of the amygdala. Neuroscience 132:943-953.

Birn RM (2012) The role of physiological noise in resting-state functional connectivity. Neuroimage 62:864-870.

Birn RM, Diamond JB, Smith MA, Bandettini PA (2006) Separating respiratory-variation-related fluctuations from neuronal-activity-related fluctuations in fMRI. Neuroimage 31:1536-1548.

Biswal B, Bandettini PA, Jesmanowicz A, Hyde JS (1992) Time-frequency analysis of functional EPI time-course series. In: SMRM, 12the Annual Meeting, p 722. New York.

Biswal B, DeYoe EA, Jesmanowicz A, Hyde JS (1994) Removal of physiological fluctuations from functional MRI signals. In: SMR, 2nd Annual Meeting, p 653. San Francisco.

Biswal B, Yetkin FZ, Haughton VM, Hyde JS (1995) Functional connectivity in the motor cortex of resting human brain using echo-planar MRI. Magn Reson Med 34:537-541.

Biswal B, Hudetz AG, Yetkin FZ, Haughton VM, Hyde JS (1997a) Hypercapnia reversibly suppresses low-frequency fluctuations in the human motor cortex during rest using echo-planar MRI. J Cereb Blood Flow Metab 17:301-308.

Biswal BB (2012) Resting state fMRI: a personal history. Neuroimage 62:938-944.

Biswal BB, Van Kylen J, Hyde JS (1997b) Simultaneous assessment of flow and BOLD signals in resting-state functional connectivity maps. NMR Biomed 10:165-170.

Bloch F (1946) Nuclear Induction. Physical Review 70:460-474.

Boly M, Tshibanda L, Vanhaudenhuyse A, Noirhomme Q, Schnakers C, Ledoux D, Boveroux P, Garweg C, Lambermont B, Phillips C, Luxen A, Moonen G, Bassetti C, Maquet P, Laureys S (2009) Functional connectivity in the default network during resting state is preserved in a vegetative but not in a brain dead patient. Hum Brain Mapp 30:2393-2400.

Boveroux P, Vanhaudenhuyse A, Bruno MA, Noirhomme Q, Lauwick S, Luxen A, Degueldre C, Plenevaux A, Schnakers C, Phillips C, Brichant JF, Bonhomme V, Maquet P, Greicius MD, Laureys S, Boly M (2010) Breakdown of within- and between-network resting state functional magnetic resonance imaging connectivity during propofol-induced loss of consciousness. Anesthesiology 113:1038-1053.

Braun U, Plichta MM, Esslinger C, Sauer C, Haddad L, Grimm O, Mier D, Mohnke S, Heinz A, Erk S, Walter H, Seiferth N, Kirsch P, Meyer-Lindenberg A (2012) Test-retest reliability of resting-state connectivity network characteristics using fMRI and graph theoretical measures. Neuroimage 59:1404-1412.

Brown EN, Purdon PL, Van Dort CJ (2011) General anesthesia and altered states of arousal: a systems neuroscience analysis. Annu Rev Neurosci 34:601-628.

Buckner RL, Andrews-Hanna JR, Schacter DL (2008) The brain's default network: anatomy, function, and relevance to disease. Ann N Y Acad Sci 1124:1-38.

Bullmore E, Long C, Suckling J, Fadili J, Calvert G, Zelaya F, Carpenter TA, Brammer M (2001) Colored noise and computational inference in neurophysiological (fMRI) time series analysis: resampling methods in time and wavelet domains. Hum Brain Mapp 12:61-78.

Bullmore ET, Bassett DS (2010) Brain graphs: graphical models of the human brain connectome. Annu Rev Clin Psychol 7:113-140.

Buxton RB (2002) Introduction to Functional Magnetic Resonance Imaging: Cambridge University Press.

Buzsaki G, Draguhn A (2004) Neuronal oscillations in cortical networks. Science 304:1926-1929.

Calhoun VD, Adali T, Pearlson GD, Pekar JJ (2001) A method for making group inferences from functional MRI data using independent component analysis. Hum Brain Mapp 14:140-151.

Carp J (2011) Optimizing the order of operations for movement scrubbing: Comment on Power et al. Neuroimage.

Cauda F, Micon BM, Sacco K, Duca S, D'Agata F, Geminiani G, Canavero S (2009) Disrupted intrinsic functional connectivity in the vegetative state. J Neurol Neurosurg Psychiatry 80:429-431.

Chang C, Glover GH (2009a) Effects of model-based physiological noise correction on default mode network anti-correlations and correlations. Neuroimage 47:1448-1459.

Chang C, Glover GH (2009b) Relationship between respiration, end-tidal CO2, and BOLD signals in resting-state fMRI. Neuroimage 47:1381-1393.

Chang C, Glover GH (2010) Time-frequency dynamics of resting-state brain connectivity measured with fMRI. Neuroimage 50:81-98.

Cinelli AR, Ferreyra-Moyano H, Barragan E (1987) Reciprocal functional connections of the olfactory bulbs and other olfactory related areas with the prefrontal cortex. Brain Res Bull 19:651-661.

Ciuciu P, Varoquaux G, Abry P, Sadaghiani S, Kleinschmidt A (2013) Scale-Free and Multifractal Time Dynamics of fMRI Signals during Rest and Task. Front Physiol 3:186.

Cornwall J, Phillipson OT (1988) Afferent projections to the parafascicular thalamic nucleus of the rat, as shown by the retrograde transport of wheat germ agglutinin. Brain Res Bull 20:139-150.

Craddock RC, James GA, Holtzheimer PE, 3rd, Hu XP, Mayberg HS (2012) A whole brain fMRI atlas generated via spatially constrained spectral clustering. Hum Brain Mapp 33:1914-1928.

Deshpande G, Kerssens C, Sebel PS, Hu X (2010) Altered local coherence in the default mode network due to sevoflurane anesthesia. Brain Res 1318:110-121.

Dolleman-Van Der Weel MJ, Witter MP (1996) Projections from the nucleus reuniens thalami to the entorhinal cortex, hippocampal field CA1, and the subiculum in the rat arise from different populations of neurons. J Comp Neurol 364:637-650.

Erhardt EB, Rachakonda S, Bedrick EJ, Allen EA, Adali T, Calhoun VD (2010) Comparison of multi-subject ICA methods for analysis of fMRI data. Hum Brain Mapp 32:2075-2095.

Ferris CF, Febo M, Luo F, Schmidt K, Brevard M, Harder JA, Kulkarni P, Messenger T, King JA (2006) Functional magnetic resonance imaging in conscious animals: a new tool in behavioural neuroscience research. J Neuroendocrinol 18:307-318.

Forman SD, Cohen JD, Fitzgerald M, Eddy WF, Mintun MA, Noll DC (1995) Improved assessment of significant activation in functional magnetic resonance imaging (fMRI): use of a cluster-size threshold. Magn Reson Med 33:636-647.

Fox MD, Raichle ME (2007) Spontaneous fluctuations in brain activity observed with functional magnetic resonance imaging. Nat Rev Neurosci 8:700-711.

Fox MD, Zhang D, Snyder AZ, Raichle ME (2009) The global signal and observed anticorrelated resting state brain networks. J Neurophysiol 101:3270-3283.

Fox MD, Snyder AZ, Vincent JL, Corbetta M, Van Essen DC, Raichle ME (2005) The human brain is intrinsically organized into dynamic, anticorrelated functional networks. Proc Natl Acad Sci U S A 102:9673-9678.

Fox PT, Raichle ME (1986) Focal physiological uncoupling of cerebral blood flow and oxidative metabolism during somatosensory stimulation in human subjects. Proc Natl Acad Sci U S A 83:1140-1144.

Glover GH, Li TQ, Ress D (2000) Image-based method for retrospective correction of physiological motion effects in fMRI: RETROICOR. Magn Reson Med 44:162-167.

Good BH, de Montjoye YA, Clauset A (2010) Performance of modularity maximization in practical contexts. Phys Rev E Stat Nonlin Soft Matter Phys 81:046106.

Greicius MD, Krasnow B, Reiss AL, Menon V (2003) Functional connectivity in the resting brain: a network analysis of the default mode hypothesis. Proc Natl Acad Sci U S A 100:253-258.

Greicius MD, Flores BH, Menon V, Glover GH, Solvason HB, Kenna H, Reiss AL, Schatzberg AF (2007) Resting-state functional connectivity in major depression: abnormally increased contributions from subgenual cingulate cortex and thalamus. Biol Psychiatry 62:429-437.

Grinsted A, Moore JC, Jevrejeva S (2004) Application of the cross wavelet transform and wavelet coherence to geophysical time series. Nonlin Processes Geophys 11:561-566.

Guillery RW, Sherman SM (2002) Thalamic relay functions and their role in corticocortical communication: generalizations from the visual system. Neuron 33:163-175.

Hajos M, Richards CD, Szekely AD, Sharp T (1998) An electrophysiological and neuroanatomical study of the medial prefrontal cortical projection to the midbrain raphe nuclei in the rat. Neuroscience 87:95-108.

Hampson M, Peterson BS, Skudlarski P, Gatenby JC, Gore JC (2002) Detection of functional connectivity using temporal correlations in MR images. Hum Brain Mapp 15:247-262.

Hampson M, Driesen N, Roth JK, Gore JC, Constable RT (2010) Functional connectivity between task-positive and task-negative brain areas and its relation to working memory performance. Magn Reson Imaging 28:1051-1057.

Handwerker DA, Roopchansingh V, Gonzalez-Castillo J, Bandettini PA (2012) Periodic changes in fMRI connectivity. Neuroimage 63:1712-1719.

Haynes JD, Deichmann R, Rees G (2005) Eye-specific effects of binocular rivalry in the human lateral geniculate nucleus. Nature 438:496-499.

He BJ (2011) Scale-free properties of the functional magnetic resonance imaging signal during rest and task. J Neurosci 31:13786-13795.

Henry J, Petrides M, St-Laurent M, Sziklas V (2004) Spatial conditional associative learning: effects of thalamo-hippocampal disconnection in rats. Neuroreport 15:2427-2431.

Herman P, Sanganahalli BG, Hyder F, Eke A (2011) Fractal analysis of spontaneous fluctuations of the BOLD signal in rat brain. Neuroimage 58:1060-1069.

Hilgetag CC, Burns GA, O'Neill MA, Scannell JW, Young MP (2000) Anatomical connectivity defines the organization of clusters of cortical areas in the macaque monkey and the cat. Philos Trans R Soc Lond B Biol Sci 355:91-110.

Horovitz SG, Braun AR, Carr WS, Picchioni D, Balkin TJ, Fukunaga M, Duyn JH (2009) Decoupling of the brain's default mode network during deep sleep. Proc Natl Acad Sci U S A 106:11376-11381.

Hu X, Le TH, Parrish T, Erhard P (1995) Retrospective estimation and correction of physiological fluctuation in functional MRI. Magn Reson Med 34:201-212.

Hutchison RM, Mirsattari SM, Jones CK, Gati JS, Leung LS (2010) Functional networks in the anesthetized rat brain revealed by independent component analysis of resting-state FMRI. J Neurophysiol 103:3398-3406.

Hutchison RM, Womelsdorf T, Gati JS, Everling S, Menon RS (2012a) Resting-state networks show dynamic functional connectivity in awake humans and anesthetized macaques. Hum Brain Mapp.

Hutchison RM, Gallivan JP, Culham JC, Gati JS, Menon RS, Everling S (2012b) Functional connectivity of the frontal eye fields in humans and macaque monkeys investigated with resting-state fMRI. J Neurophysiol 107:2463-2474.

Hutchison RM, Womelsdorf T, Gati JS, Leung LS, Menon RS, Everling S (2012c) Resting-state connectivity identifies distinct functional networks in macaque cingulate cortex. Cereb Cortex 22:1294-1308.

Hyvarinen A, Oja E (2000) Independent component analysis: algorithms and applications. Neural Netw 13:411-430.

Jezzard P, LeBihan D, Cuenod D, Pannier L, Prinster A, Turner R (1992) An investigation of the contribution of physiological noise in human functional MRI studies at 1.5 Tesla and 4 Tesla. In: SMRM, 12th Annual Meeting, p 1392. New York.

Jones EG (2001) The thalamic matrix and thalamocortical synchrony. Trends Neurosci 24:595-601.

Jones EG (2007) The Thalamus, 2 Edition: Cambridge University Press.

Kalthoff D, Po C, Wiedermann D, Hoehn M (2013) Reliability and spatial specificity of rat brain sensorimotor functional connectivity networks are superior under sedation compared with general anesthesia. NMR Biomed.

Kalthoff D, Seehafer JU, Po C, Wiedermann D, Hoehn M (2011) Functional connectivity in the rat at 11.7T: Impact of physiological noise in resting state fMRI. Neuroimage 54:2828-2839.

Kannurpatti SS, Biswal BB, Kim YR, Rosen BR (2008) Spatio-temporal characteristics of low-frequency BOLD signal fluctuations in isoflurane-anesthetized rat brain. Neuroimage 40:1738-1747.

Keilholz SD, Magnuson ME, Pan WJ, Willis M, Thompson GJ (2012) Dynamic properties of functional connectivity in the rodent. Brain Connect 3:31-40.

Kelly AM, Uddin LQ, Biswal BB, Castellanos FX, Milham MP (2008) Competition between functional brain networks mediates behavioral variability. Neuroimage 39:527-537.

Kennedy DP, Redcay E, Courchesne E (2006) Failing to deactivate: resting functional abnormalities in autism. Proc Natl Acad Sci U S A 103:8275-8280.

King JA, Garelick TS, Brevard ME, Chen W, Messenger TL, Duong TQ, Ferris CF (2005) Procedure for minimizing stress for fMRI studies in conscious rats. J Neurosci Methods 148:154-160.

Kojima T, Onoe H, Hikosaka K, Tsutsui K, Tsukada H, Watanabe M (2009) Default mode of brain activity demonstrated by positron emission tomography imaging in awake monkeys: higher rest-related than working memory-related activity in medial cortical areas. J Neurosci 29:14463-14471.

Krettek JE, Price JL (1977) The cortical projections of the mediodorsal nucleus and adjacent thalamic nuclei in the rat. J Comp Neurol 171:157-191.

Kwong KK, Belliveau JW, Chesler DA, Goldberg IE, Weisskoff RM, Poncelet BP, Kennedy DN, Hoppel BE, Cohen MS, Turner R, et al. (1992) Dynamic magnetic resonance imaging of human brain activity during primary sensory stimulation. Proc Natl Acad Sci U S A 89:5675-5679.

Laufs H, Krakow K, Sterzer P, Eger E, Beyerle A, Salek-Haddadi A, Kleinschmidt A (2003) Electroencephalographic signatures of attentional and cognitive default modes in spontaneous brain activity fluctuations at rest. Proc Natl Acad Sci U S A 100:11053-11058.

Laureys S, Schiff ND (2011) Coma and consciousness: Paradigms (re)framed by neuroimaging. Neuroimage.

Lauterbur PC (1973) Image Formation by Induced Local Interactions: Examples Employing Nuclear Magnetic Resonance. Nature 242:190-191.

LeDoux JE (2000) Emotion circuits in the brain. Annu Rev Neurosci 23:155-184.

Lee U, Oh G, Kim S, Noh G, Choi B, Mashour GA (2010) Brain networks maintain a scale-free organization across consciousness, anesthesia, and recovery: evidence for adaptive reconfiguration. Anesthesiology 113:1081-1091.

Lena I, Parrot S, Deschaux O, Muffat-Joly S, Sauvinet V, Renaud B, Suaud-Chagny MF, Gottesmann C (2005) Variations in extracellular levels of dopamine, noradrenaline, glutamate, and aspartate across the sleep--wake cycle in the medial prefrontal cortex and nucleus accumbens of freely moving rats. J Neurosci Res 81:891-899.

Leopold DA, Murayama Y, Logothetis NK (2003) Very slow activity fluctuations in monkey visual cortex: implications for functional brain imaging. Cereb Cortex 13:422-433.

Liang Z, King J, Zhang N (2011) Uncovering intrinsic connectional architecture of functional networks in awake rat brain. J Neurosci 31:3776-3783.

Liang Z, King J, Zhang N (2012a) Anticorrelated resting-state functional connectivity in awake rat brain. Neuroimage 59:1190-1199.

Liang Z, King J, Zhang N (2012b) Intrinsic organization of the anesthetized brain. J Neurosci 32:10183-10191.

Lichtman JW, Livet J, Sanes JR (2008) A technicolour approach to the connectome. Nat Rev Neurosci 9:417-422.

Likhtik E, Pelletier JG, Paz R, Pare D (2005) Prefrontal control of the amygdala. J Neurosci 25:7429-7437.

Liu D, Yan C, Ren J, Yao L, Kiviniemi VJ, Zang Y (2010) Using coherence to measure regional homogeneity of resting-state FMRI signal. Front Syst Neurosci 4:24.

Liu X, Zhu XH, Zhang Y, Chen W (2011) Neural origin of spontaneous hemodynamic fluctuations in rats under burst-suppression anesthesia condition. Cereb Cortex 21:374-384.

Liu Y, Liang M, Zhou Y, He Y, Hao Y, Song M, Yu C, Liu H, Liu Z, Jiang T (2008) Disrupted small-world networks in schizophrenia. Brain 131:945-961.

Logothetis NK, Murayama Y, Augath M, Steffen T, Werner J, Oeltermann A (2009) How not to study spontaneous activity. Neuroimage 45:1080-1089.

Lowe MJ, Mock BJ, Sorenson JA (1998) Functional connectivity in single and multislice echoplanar imaging using resting-state fluctuations. Neuroimage 7:119-132.

Lu H, Zou Q, Gu H, Raichle ME, Stein EA, Yang Y (2012) Rat brains also have a default mode network. Proc Natl Acad Sci U S A 109:3979-3984.

Lu H, Zuo Y, Gu H, Waltz JA, Zhan W, Scholl CA, Rea W, Yang Y, Stein EA (2007) Synchronized delta oscillations correlate with the resting-state functional MRI signal. Proc Natl Acad Sci U S A 104:18265-18269.

Ma J, Leung LS (2006) Limbic system participates in mediating the effects of general anesthetics. Neuropsychopharmacology 31:1177-1192.

Ma J, Shen B, Stewart LS, Herrick IA, Leung LS (2002) The septohippocampal system participates in general anesthesia. J Neurosci 22:RC200.

Majeed W, Magnuson M, Keilholz SD (2009) Spatiotemporal dynamics of low frequency fluctuations in BOLD fMRI of the rat. J Magn Reson Imaging 30:384-393.

Mantini D, Perrucci MG, Del Gratta C, Romani GL, Corbetta M (2007) Electrophysiological signatures of resting state networks in the human brain. Proc Natl Acad Sci U S A 104:13170-13175.

Mantini D, Corbetta M, Romani GL, Orban GA, Vanduffel W (2013) Evolutionarily Novel Functional Networks in the Human Brain? J Neurosci 33:3259-3275.

Mantini D, Gerits A, Nelissen K, Durand JB, Joly O, Simone L, Sawamura H, Wardak C, Orban GA, Buckner RL, Vanduffel W (2011) Default mode of brain function in monkeys. J Neurosci 31:12954-12962.

Martuzzi R, Ramani R, Qiu M, Rajeevan N, Constable RT (2010) Functional connectivity and alterations in baseline brain state in humans. Neuroimage 49:823-834.

Massimini M, Ferrarelli F, Huber R, Esser SK, Singh H, Tononi G (2005) Breakdown of cortical effective connectivity during sleep. Science 309:2228-2232.

McDonald AJ (1998) Cortical pathways to the mammalian amygdala. Prog Neurobiol 55:257-332.

McKeown MJ, Makeig S, Brown GG, Jung TP, Kindermann SS, Bell AJ, Sejnowski TJ (1998) Analysis of fMRI data by blind separation into independent spatial components. Hum Brain Mapp 6:160-188.

Meunier D, Lambiotte R, Bullmore ET (2010) Modular and hierarchically modular organization of brain networks. Front Neurosci 4:200.

Meunier D, Lambiotte R, Fornito A, Ersche KD, Bullmore ET (2009) Hierarchical modularity in human brain functional networks. Front Neuroinform 3:37.

Mikula S, Binding J, Denk W (2012) Staining and embedding the whole mouse brain for electron microscopy. Nat Methods 9:1198-1201.

Moeller S, Nallasamy N, Tsao DY, Freiwald WA (2009) Functional connectivity of the macaque brain across stimulus and arousal states. J Neurosci 29:5897-5909.

Murphy K, Birn RM, Handwerker DA, Jones TB, Bandettini PA (2009) The impact of global signal regression on resting state correlations: are anti-correlated networks introduced? Neuroimage 44:893-905.

Nallasamy N, Tsao DY (2011) Functional connectivity in the brain: effects of anesthesia. Neuroscientist 17:94-106.

Newman ME (2006) Modularity and community structure in networks. Proc Natl Acad Sci U S A 103:8577-8582.

Newman ME (2010) Networks: An Introduction: Oxford University Press.

Nichols TE, Holmes AP (2002) Nonparametric permutation tests for functional neuroimaging: a primer with examples. Hum Brain Mapp 15:1-25.

Nir Y, Fisch L, Mukamel R, Gelbard-Sagiv H, Arieli A, Fried I, Malach R (2007) Coupling between neuronal firing rate, gamma LFP, and BOLD fMRI is related to interneuronal correlations. Curr Biol 17:1275-1285.

O'Connor DH, Fukui MM, Pinsk MA, Kastner S (2002) Attention modulates responses in the human lateral geniculate nucleus. Nat Neurosci 5:1203-1209.

O'Toole AJ, Jiang F, Abdi H, Penard N, Dunlop JP, Parent MA (2007) Theoretical, statistical, and practical perspectives on pattern-based classification approaches to the analysis of functional neuroimaging data. J Cogn Neurosci 19:1735-1752.

Ogawa S (2012) Finding the BOLD effect in brain images. Neuroimage 62:608-609.

Ogawa S, Lee TM, Nayak AS, Glynn P (1990a) Oxygenation-sensitive contrast in magnetic resonance image of rodent brain at high magnetic fields. Magn Reson Med 14:68-78.

Ogawa S, Lee TM, Kay AR, Tank DW (1990b) Brain magnetic resonance imaging with contrast dependent on blood oxygenation. Proc Natl Acad Sci U S A 87:9868-9872.

Ogawa S, Tank DW, Menon R, Ellermann JM, Kim SG, Merkle H, Ugurbil K (1992) Intrinsic signal changes accompanying sensory stimulation: functional brain mapping with magnetic resonance imaging. Proc Natl Acad Sci U S A 89:5951-5955.

Pan WJ, Thompson G, Magnuson M, Majeed W, Jaeger D, Keilholz S (2011) Broadband local field potentials correlate with spontaneous fluctuations in functional magnetic resonance imaging signals in the rat somatosensory cortex under isoflurane anesthesia. Brain Connect 1:119-131.

Pape HC, Pare D (2010) Plastic synaptic networks of the amygdala for the acquisition, expression, and extinction of conditioned fear. Physiol Rev 90:419-463.

Pare D, Smith Y (1993) The intercalated cell masses project to the central and medial nuclei of the amygdala in cats. Neuroscience 57:1077-1090.

Paul G. Barash BFC, Robert K. Stoelting, Michael Cahalan, M. Christine Stock (2009) Clinical Anesthesia, 6 Edition: Lippincott Williams & Wilkins.

Pauling L, Coryell CD (1936) The Magnetic Properties and Structure of Hemoglobin, Oxyhemoglobin and Carbonmonoxyhemoglobin. Proc Natl Acad Sci U S A 22:210-216.

Pawela CP, Biswal BB, Hudetz AG, Li R, Jones SR, Cho YR, Matloub HS, Hyde JS (2010) Interhemispheric neuroplasticity following limb deafferentation detected by resting-

state functional connectivity magnetic resonance imaging (fcMRI) and functional magnetic resonance imaging (fMRI). Neuroimage 49:2467-2478.

Pawela CP, Biswal BB, Cho YR, Kao DS, Li R, Jones SR, Schulte ML, Matloub HS, Hudetz AG, Hyde JS (2008) Resting-state functional connectivity of the rat brain. Magn Reson Med 59:1021-1029.

Paxinos G (2004) The Rat Nervous System: Elsevier.

Peltier SJ, Kerssens C, Hamann SB, Sebel PS, Byas-Smith M, Hu X (2005) Functional connectivity changes with concentration of sevoflurane anesthesia. Neuroreport 16:285-288.

Phelps EA, LeDoux JE (2005) Contributions of the amygdala to emotion processing: from animal models to human behavior. Neuron 48:175-187.

Phelps EA, Delgado MR, Nearing KI, LeDoux JE (2004) Extinction learning in humans: role of the amygdala and vmPFC. Neuron 43:897-905.

Poulet JF, Fernandez LM, Crochet S, Petersen CC (2012) Thalamic control of cortical states. Nat Neurosci 15:370-372.

Power JD, Barnes KA, Snyder AZ, Schlaggar BL, Petersen SE (2012) Spurious but systematic correlations in functional connectivity MRI networks arise from subject motion. Neuroimage 59:2142-2154.

Power JD, Cohen AL, Nelson SM, Wig GS, Barnes KA, Church JA, Vogel AC, Laumann TO, Miezin FM, Schlaggar BL, Petersen SE (2011) Functional network organization of the human brain. Neuron 72:665-678.

Purcell EM, Torrey HC, Pound RV (1946) Resonance Absorption by Nuclear Magnetic Moments in a Solid. Physical Review 69:37-38.

Quigley M, Cordes D, Turski P, Moritz C, Haughton V, Seth R, Meyerand ME (2003) Role of the corpus callosum in functional connectivity. AJNR Am J Neuroradiol 24:208-212.

Quirk GJ, Gehlert DR (2003) Inhibition of the amygdala: key to pathological states? Ann N Y Acad Sci 985:263-272.

Quirk GJ, Likhtik E, Pelletier JG, Pare D (2003) Stimulation of medial prefrontal cortex decreases the responsiveness of central amygdala output neurons. J Neurosci 23:8800-8807.

Raichle ME, Snyder AZ (2007) A default mode of brain function: a brief history of an evolving idea. Neuroimage 37:1083-1090; discussion 1097-1089.

Raichle ME, MacLeod AM, Snyder AZ, Powers WJ, Gusnard DA, Shulman GL (2001) A default mode of brain function. Proc Natl Acad Sci U S A 98:676-682.

Rilling JK, Barks SK, Parr LA, Preuss TM, Faber TL, Pagnoni G, Bremner JD, Votaw JR (2007) A comparison of resting-state brain activity in humans and chimpanzees. Proc Natl Acad Sci U S A 104:17146-17151.

Rosenkranz JA, Grace AA (2001) Dopamine attenuates prefrontal cortical suppression of sensory inputs to the basolateral amygdala of rats. J Neurosci 21:4090-4103.

Rubinov M, Sporns O (2010) Complex network measures of brain connectivity: uses and interpretations. Neuroimage 52:1059-1069.

Rubinov M, Sporns O (2011) Weight-conserving characterization of complex functional brain networks. Neuroimage 56:2068-2079.

Russchen FT (1982a) Amygdalopetal projections in the cat. II. Subcortical afferent connections. A study with retrograde tracing techniques. J Comp Neurol 207:157-176.

Russchen FT (1982b) Amygdalopetal projections in the cat. I. Cortical afferent connections. A study with retrograde and anterograde tracing techniques. J Comp Neurol 206:159-179.

Saalmann YB, Kastner S (2009) Gain control in the visual thalamus during perception and cognition. Curr Opin Neurobiol 19:408-414.

Salvador R, Suckling J, Coleman MR, Pickard JD, Menon D, Bullmore E (2005) Neurophysiological architecture of functional magnetic resonance images of human brain. Cereb Cortex 15:1332-1342.

Satterthwaite TD, Wolf DH, Loughead J, Ruparel K, Elliott MA, Hakonarson H, Gur RC, Gur RE (2012) Impact of in-scanner head motion on multiple measures of functional connectivity: Relevance for studies of neurodevelopment in youth. Neuroimage.

Satterthwaite TD, Elliott MA, Gerraty RT, Ruparel K, Loughead J, Calkins ME, Eickhoff SB, Hakonarson H, Gur RC, Gur RE, Wolf DH (2013) An improved framework for confound regression and filtering for control of motion artifact in the preprocessing of resting-state functional connectivity data. Neuroimage 64:240-256.

Scheeringa R, Bastiaansen MC, Petersson KM, Oostenveld R, Norris DG, Hagoort P (2008) Frontal theta EEG activity correlates negatively with the default mode network in resting state. Int J Psychophysiol 67:242-251.

Schmid MC, Mrowka SW, Turchi J, Saunders RC, Wilke M, Peters AJ, Ye FQ, Leopold DA (2010) Blindsight depends on the lateral geniculate nucleus. Nature 466:373-377.

Scholvinck ML, Maier A, Ye FQ, Duyn JH, Leopold DA (2010) Neural basis of global resting-state fMRI activity. Proc Natl Acad Sci U S A 107:10238-10243.

Schwarz AJ, Gozzi A, Bifone A (2009) Community structure in networks of functional connectivity: resolving functional organization in the rat brain with pharmacological MRI. Neuroimage 47:302-311.

Sesack SR, Deutch AY, Roth RH, Bunney BS (1989) Topographical organization of the efferent projections of the medial prefrontal cortex in the rat: an anterograde tract-tracing study with Phaseolus vulgaris leucoagglutinin. J Comp Neurol 290:213-242.

Shehzad Z, Kelly AM, Reiss PT, Gee DG, Gotimer K, Uddin LQ, Lee SH, Margulies DS, Roy AK, Biswal BB, Petkova E, Castellanos FX, Milham MP (2009) The resting brain: unconstrained yet reliable. Cereb Cortex 19:2209-2229.

Sherman SM (2005) Thalamic relays and cortical functioning. Prog Brain Res 149:107-126.

Shin LM, Orr SP, Carson MA, Rauch SL, Macklin ML, Lasko NB, Peters PM, Metzger LJ, Dougherty DD, Cannistraro PA, Alpert NM, Fischman AJ, Pitman RK (2004) Regional cerebral blood flow in the amygdala and medial prefrontal cortex during traumatic imagery in male and female Vietnam veterans with PTSD. Arch Gen Psychiatry 61:168-176.

Shmuel A, Leopold DA (2008) Neuronal correlates of spontaneous fluctuations in fMRI signals in monkey visual cortex: Implications for functional connectivity at rest. Hum Brain Mapp 29:751-761.

Smith SM, Miller KL, Salimi-Khorshidi G, Webster M, Beckmann CF, Nichols TE, Ramsey JD, Woolrich MW (2010) Network modelling methods for FMRI. Neuroimage 54:875-891.

Song S, Sjostrom PJ, Reigl M, Nelson S, Chklovskii DB (2005) Highly nonrandom features of synaptic connectivity in local cortical circuits. PLoS Biol 3:e68.

Stamatakis EA, Adapa RM, Absalom AR, Menon DK (2010) Changes in resting neural connectivity during propofol sedation. PLoS One 5:e14224.

Stevens WD, Hasher L, Chiew KS, Grady CL (2008) A neural mechanism underlying memory failure in older adults. J Neurosci 28:12820-12824.

Supekar K, Menon V, Rubin D, Musen M, Greicius MD (2008) Network analysis of intrinsic functional brain connectivity in Alzheimer's disease. PLoS Comput Biol 4:e1000100.

Swanson LW (2004) Brain Maps: Structure of the Rat Brain: Elsevier.

Thulborn KR, Waterton JC, Matthews PM, Radda GK (1982) Oxygenation dependence of the transverse relaxation time of water protons in whole blood at high field. Biochim Biophys Acta 714:265-270.

Tononi G (2008) Consciousness as integrated information: a provisional manifesto. Biol Bull 215:216-242.

Torrence C, Compo GP (1998) A Practical Guide to Wavelet Analysis. Bulletin of the American Meteorological Society 79:61-78.

Tzourio-Mazoyer N, Landeau B, Papathanassiou D, Crivello F, Etard O, Delcroix N, Mazoyer B, Joliot M (2002) Automated anatomical labeling of activations in SPM using a macroscopic anatomical parcellation of the MNI MRI single-subject brain. Neuroimage 15:273-289.

Upadhyay J, Baker SJ, Chandran P, Miller L, Lee Y, Marek GJ, Sakoglu U, Chin CL, Luo F, Fox GB, Day M (2011) Default-mode-like network activation in awake rodents. PLoS One 6:e27839.

Van den Aardweg JG, Karemaker JM (2002) Influence of chemoreflexes on respiratory variability in healthy subjects. Am J Respir Crit Care Med 165:1041-1047.

van den Heuvel M, Mandl R, Hulshoff Pol H (2008) Normalized cut group clustering of resting-state FMRI data. PLoS One 3:e2001.

Van Dijk KR, Sabuncu MR, Buckner RL (2012) The influence of head motion on intrinsic functional connectivity MRI. Neuroimage 59:431-438.

Van Groen T, Wyss JM (1995) Projections from the anterodorsal and anteroventral nucleus of the thalamus to the limbic cortex in the rat. J Comp Neurol 358:584-604.

Vanhaudenhuyse A, Noirhomme Q, Tshibanda LJ, Bruno MA, Boveroux P, Schnakers C, Soddu A, Perlbarg V, Ledoux D, Brichant JF, Moonen G, Maquet P, Greicius MD, Laureys S, Boly M (2010) Default network connectivity reflects the level of consciousness in non-communicative brain-damaged patients. Brain 133:161-171.

Vertes RP, Hoover WB (2008) Projections of the paraventricular and paratenial nuclei of the dorsal midline thalamus in the rat. J Comp Neurol 508:212-237.

Vertes RP, Hoover WB, Szigeti-Buck K, Leranth C (2007) Nucleus reuniens of the midline thalamus: link between the medial prefrontal cortex and the hippocampus. Brain Res Bull 71:601-609.

Vincent JL, Patel GH, Fox MD, Snyder AZ, Baker JT, Van Essen DC, Zempel JM, Snyder LH, Corbetta M, Raichle ME (2007) Intrinsic functional architecture in the anaesthetized monkey brain. Nature 447:83-86.

Vogels TP, Rajan K, Abbott LF (2005) Neural network dynamics. Annu Rev Neurosci 28:357-376.

Wang J, Wang L, Zang Y, Yang H, Tang H, Gong Q, Chen Z, Zhu C, He Y (2009) Parcellation-dependent small-world brain functional networks: a resting-state fMRI study. Hum Brain Mapp 30:1511-1523.

Wang K, van Meer MP, van der Marel K, van der Toorn A, Xu L, Liu Y, Viergever MA, Jiang T, Dijkhuizen RM (2010) Temporal scaling properties and spatial synchronization of spontaneous blood oxygenation level-dependent (BOLD) signal fluctuations in rat sensorimotor network at different levels of isoflurane anesthesia. NMR Biomed 24:61-67.

Wang L, Saalmann YB, Pinsk MA, Arcaro MJ, Kastner S (2012) Electrophysiological low-frequency coherence and cross-frequency coupling contribute to BOLD connectivity. Neuron 76:1010-1020.

Watts DJ, Strogatz SH (1998) Collective dynamics of 'small-world' networks. Nature 393:440-442.

Weisskoff R, Baker J, Belliveau J, TL Davis TL, Kwong KK, Cohen MS, Rosen BR (1992) Power spectrum analysis of functionally-weighted MR data: what's in the noise? In: SMRM, 12th Annual Meeting, p 7. New York.

Welsh RC, Chen AC, Taylor SF (2010) Low-frequency BOLD fluctuations demonstrate altered thalamocortical connectivity in schizophrenia. Schizophr Bull 36:713-722.

White JG, Southgate E, Thomson JN, Brenner S (1986) The structure of the nervous system of the nematode Caenorhabditis elegans. Philos Trans R Soc Lond B Biol Sci 314:1-340.

Williams KA, Magnuson M, Majeed W, LaConte SM, Peltier SJ, Hu X, Keilholz SD (2010) Comparison of alpha-chloralose, medetomidine and isoflurane anesthesia for functional connectivity mapping in the rat. Magn Reson Imaging 28:995-1003.

Woodward ND, Karbasforoushan H, Heckers S (2012) Thalamocortical dysconnectivity in schizophrenia. Am J Psychiatry 169:1092-1099.

Wouterlood FG, Saldana E, Witter MP (1990) Projection from the nucleus reuniens thalami to the hippocampal region: light and electron microscopic tracing study in the rat with the anterograde tracer Phaseolus vulgaris-leucoagglutinin. J Comp Neurol 296:179-203.

Wunderlich K, Schneider KA, Kastner S (2005) Neural correlates of binocular rivalry in the human lateral geniculate nucleus. Nat Neurosci 8:1595-1602.

Zalesky A, Fornito A, Bullmore ET (2010a) Network-based statistic: identifying differences in brain networks. Neuroimage 53:1197-1207.

Zalesky A, Fornito A, Bullmore E (2012a) On the use of correlation as a measure of network connectivity. Neuroimage 60:2096-2106.

Zalesky A, Cocchi L, Fornito A, Murray MM, Bullmore E (2012b) Connectivity differences in brain networks. Neuroimage 60:1055-1062.

Zalesky A, Fornito A, Harding IH, Cocchi L, Yucel M, Pantelis C, Bullmore ET (2010b) Whole-brain anatomical networks: does the choice of nodes matter? Neuroimage 50:970-983.

Zang Y, Jiang T, Lu Y, He Y, Tian L (2004) Regional homogeneity approach to fMRI data analysis. Neuroimage 22:394-400.

Zang YF, He Y, Zhu CZ, Cao QJ, Sui MQ, Liang M, Tian LX, Jiang TZ, Wang YF (2007) Altered baseline brain activity in children with ADHD revealed by resting-state functional MRI. Brain Dev 29:83-91.

Zhang D, Snyder AZ, Shimony JS, Fox MD, Raichle ME (2010a) Noninvasive functional and structural connectivity mapping of the human thalamocortical system. Cereb Cortex 20:1187-1194.

Zhang D, Snyder AZ, Fox MD, Sansbury MW, Shimony JS, Raichle ME (2008) Intrinsic functional relations between human cerebral cortex and thalamus. J Neurophysiol 100:1740-1748.

Zhang J, Wang J, Wu Q, Kuang W, Huang X, He Y, Gong Q (2011) Disrupted brain connectivity networks in drug-naive, first-episode major depressive disorder. Biol Psychiatry 70:334-342.

Zhang N, Rane P, Huang W, Liang Z, Kennedy D, Frazier JA, King J (2010b) Mapping resting-state brain networks in conscious animals. J Neurosci Methods 189:186-196.

Zou QH, Zhu CZ, Yang Y, Zuo XN, Long XY, Cao QJ, Wang YF, Zang YF (2008) An improved approach to detection of amplitude of low-frequency fluctuation (ALFF) for resting-state fMRI: fractional ALFF. J Neurosci Methods 172:137-141.

Zuo XN, Kelly C, Adelstein JS, Klein DF, Castellanos FX, Milham MP (2010) Reliable intrinsic connectivity networks: test-retest evaluation using ICA and dual regression approach. Neuroimage 49:2163-2177.